Environmental Studies Revolving Funds

008 The Assessment of Marine Radars for the Detection of Ice and Icebergs

Canada

August 198

The Environmental Studies Revolving Funds are financed from special levies on the oil and gas industry and administered by the Canada Oil and Gas Lands Administration for the Minister of Energy, Mines and Resources, and by the Northern Affairs Program for the Minister of Indian Affairs and Northern Development.

Environmental Studies Revolving Funds
Report Series No. 008

August 1985

ASSESSMENT OF MARINE RADARS FOR THE DETECTION OF ICE AND ICEBERGS

Joseph P. Ryan
Michael Harvey
Andrew Kent

Viatec Resource Systems Inc.

The Scientific Adviser was Mr. M. Audette

The correct citation for this report is:

Ryan, J.P., M. Harvey, and A. Kent. 1985. Assessment of marine radars for the detection of ice and icebergs. Environmental Studies Revolving Funds Report No. 008. Ottawa. 127 p.

Published under the auspices
of the Environmental Studies
Revolving Funds
ISBN 0-920783-07-4

TABLE OF CONTENTS

TABLE OF CONTENTS

LIST OF TABLES

LIST OF FIGURES

ABBREVIATIONS

The following acronyms are used in the text:

A/D	Analogue to digital
CFAR	Constant false alarm rate
DR	Dynamic range
FTC	Fast time constant
GRL	Growler
MDD	Medium dry dock
MDO	Medium dome
MDS	Minimum detectable signal
MPI	Medium pinnacle
MTA	Medium tabular
MWD	Medium wedge
P_{fa}	Probability of false alarm
PPI	Plan position indicator
PRF	Pulse repetition frequency
SAR	Synthetic aperture radar
SDD	Small dry dock
SLAR	Side-looking airborne radar
STC	Sensitivity time control
SWD	Small wedge
SWH	Significant wave height

PARAMETERS

The following terms are used in the text and in equations:

C	Clutter power (Watts)
c	Speed of light (m/s)
F	Propagation factor
G	Antenna gain (dB)
h_d	Height of duct (m)
L	Radar losses
l	Duct stability length
N	Noise power (Watts)
n	Number of pulses per beamwidth
n_{sa}	Sea-air refractivity index
P_d	Probability of detection
P_{fa}	Probability of false alarm
P_r	Power received (Watts)
P_t	Peak transmitter power (Watts)
R	Range to iceberg (m)
S	Signal power (Watts)
T_{fa}	Time between false alarms
τ	Pulse length (microsec.)
σ	Radar cross-section (m2)
θ	Beamwidth (deg.)
λ	Radar wave length (m)

ACKNOWLEDGEMENTS

The author would like to acknowledge the assistance provided throughout the field trials by Greg Warbanski, Husky/Bow Valley. Husky/Bow Valley operators of the Sedco 706 drilling platform provided transportation and rig accommodation for field personnel. The assistance provided by Derek Strong of COGLA and Jacques Benoit of Mobil Oil are also greatly appreciated. Gaetan Danis and Maurice Audette served as scientific advisers for this study and their input has helped make it a success.

SUMMARY

In the winter of 1984 a comprehensive field program was undertaken to assess the iceberg detection capability of existing marine-type radars. The semi-submersible Sedco 706 drilling platform was selected for the trials. The Sedco 706 has four radar systems on board, two X-band (3 cm) and two S-band (10 cm), all manufactured by Racal-Decca of Britain. One pair of the X- and S-band systems comprise the Racal-Decca FI 2459 combined (S/X) system which uses antennas that are co-located and synchronized. The complete system with X- and S-band transmitter and receiver units is mounted on the top of the derrick at a height of 75 m. In addition, this system is equipped with low-noise receivers for increased sensitivity. The other X- and S-band systems are standard units with respective antenna heights of 45 and 35 m.

During the data-collection program, recordings of radar video signals were made for various icebergs, ships, and drilling rigs. These data were collected on an opportunity basis, as (for the most part) the Sedco 706 is a stationary platform. Iceberg data were obtained during various sea and meteorological conditions. The stability of the platform permitted the collection of data without the usual pitch and roll effects contained in most previous data sets. The presence of other drilling rigs in the vicinity provided stable reference targets for use in the assessment of environmental parameters on radar performance.

The raw video signals from each radar were digitized sequentially and stored on standard nine track computer tape. The video was digitized at two different sampling rates with a six-bit quantization. In addition, reference recordings of fixed targets were made on floppy disks with a high-speed digital oscilloscope.

The data collected has proven useful in identifying the effect of critical environmental conditions, such as ducting and subrefraction, as well as providing valuable information on sea clutter. The calibration of the radar system has permitted the calculation of iceberg radar cross-sections and a normalized radar cross-section for the ocean in a wide range of sea conditions. Five of the important findings follow.

a) The derrick-mounted S-band radar detected and tracked about four times as many icebergs as the

other systems, which was due, in part, to different levels of system performance.

b) On clear, cool days when ducting was shown to exist, this S-band radar typically detected medium icebergs in the range from 17 to 20 naut mi (31.5 to 37 km).

c) During foggy weather, calculation for the refractivity in the lower atmosphere almost always indicated subrefractive conditions. The detection ranges for medium icebergs during these conditions were typically less than 17 naut mi (31.5 km) and most frequently around 15 naut mi (27.8 km) for the S-band radar.

d) Comparison of calculated back-scatter coefficients for the sea surface for various sea conditions with published data shows good agreement over certain ranges of grazing angles (normally 0.5° to 1.0°) in the higher sea conditions. Measured values were consistently lower than the published data at other grazing angles.

e) Calculation of iceberg radar cross-sections indicate a general agreement between the collected data and the relationship proposed by Budinger (1960) linking the radar cross-section to the cross-sectional area.

RÉSUMÉ

On a entrepris durant l'hiver 1984 une étude approfondie pour évaluer l'efficacité des radars maritimes dans la détection des icebergs. On a choisi la plateforme de forage semi-submersible Sedco 706 pour effectuer ces essais. La Sedco 706 possède quatre systèmes de radar, deux X-band (3 cm) et deux S-band (10 cm); tous deux sont fabriqués en Grande-Bretagne par Racal-Decca. Une paire de radars des systèmes X- et S-band inclut le Racal-Decca FI 2459 combiné au système (S/X) qui utilise des antennes placées au même endroit et synchronisées. Le système complet, y compris le transmetteur et le receveur X- et S-band, est installé au sommet du derrick, à une hauteur de 75 m. De plus, ce système est équipé de receveurs à faible intérference pour augmenter sa sensiblité. Les autres systèmes X- et S-band sont des modèles standard aux antennes mesurant respectivement 45 et 35 m.

On a fait des enregistrements de signaux vidéo sur radar, pendant la période de ramassage des données, et ceci pour une variété d'emissions provenant d'icebergs, de vaisseaux et d'appareils de forage. Ces enregistrements se sont fait au fur et à mesure puisque la Sedco 706 est, la plupart du temps, une plateforme stationnaire. Les données concernant les icebergs ont été ramassées sous diverses conditions de mer et de météo. La stabilité de la plateforme a permis de ramasser les données sans les effets de roulis et de tangage que l'on trouvait dans la plupart des autres expériences. La présence d'autres plateformes de forage dans les environs a aussi donné des points de repère stables qui ont été utilisés dans l'évaluation des paramètres environnementaux sur le fonctionnement du radar.

Les signaux video recueillis sur chaque radar ont été digitalisés séquentiellement sur des bandes magnétiques standard neuf pistes d'ordinateur. Le signal vidéo a été digitalisé á deux niveaux d'échantillonage quantifié à six bits. De plus, on a fait des enregistrements-témoins de cibles fixes sur disques souples à l'aide d'un oscillloscope digital à haute vitesse.

Les données ainsi recueillies ont été extrêmement utiles non seulement pour identifier l'effet des conditions environnementales critiques telles que canalisation et infraréfraction mais aussi pour fournir de précieux renseignements sur la circulation maritime. Le

calibrage du système de radar a permis de calcul de la portée des radars pour détection d'icebergs et la portée des radars normalisés pour utilisation dans l'océan sous une grande variété de conditions maritimes. Voici une liste des cinq résultats les plus importants:

a) Le radar S-band monté sur le derrick a détecté et noté environ quatre fois plus d'icebergs que les autres systemes. Ceci est du en partie aux différents niveaux de performance des systèmes.

b) Par temps clair et sec, en présence de canalisation, ce radar S-band a détécté typiquement des icebergs de taille moyenne à une distance de 17 à 20 miles nautiques (31,5 à 37 kms).

c) Par temps brumeux, les calculs de réfractivité dans la basse atmosphère indiquaient presque toujours des conditions d'infraréfraction. Le rayon de détection pour les icebergs de taille moyenne dans ces conditions était typiquement moins de 17 miles nautiques (31,5 kms) et fréquemment aux environs de 15 miles nautiques (27,8 kms) dans le cas du radar S-band.

d) La comparaison des coefficients de rétrodiffusion calculés à la surface de l'eau sous diverses conditions maritimes avec les donnees déjà publiées, montre une certaine uniformité dans certains angles de mesurage (entre 0,5° et 1,0°) pendant les périodes de grosse mer. Les valeurs mesurées étaient régulièrement plus faibles que les résultats publiés d'autres angles de mesurage.

e) Le calcul de la portée du radar pour la surveillance des icebergs indique qu'il y a en général, accord entre les données ramassées et la relation que proposait Budinger (1960), liant la portée du radar à la surface étudiée.

1. INTRODUCTION

As the production stage for the Hibernia oil field draws nearer, the research related to solving the problems imposed by icebergs intensifies. A major concern is the detection of icebergs, especially the smaller sizes known as growlers and bergy bits. In the past, a number of methods have been proposed. These include airborne mapping radars, such as synthetic aperture radar (SAR) and side-looking airborne radar (SLAR), microwave marine radar, and visual and infrared systems. More recently, interest has been generated in the use of high frequency radar for this application. It is generally accepted that the implementation of an ice hazard detection system will include a variety of sensors, each optimized to perform to their maximum ability. In this way an integrated system will be obtained. The first step in the implementation of such a system is assessment of the capabilities of each individual sensor.

The major objective of this study was to provide a quantitative assessment of the iceberg detection capability of present marine radars, with particular emphasis on bergy bits and growlers. In order to provide this quantitative assessment of marine radar, it was necessary to mount a field program to investigate the effects of radar, environmental, and target parameters on detection. Similar projects also were undertaken by other groups to assess the capability of airborne SAR and SLAR systems.

The most notable experimental work on the detection of icebergs by radar was reported by Budinger (1960). Currie and Haykin (1984) provided a review of this work and also that of LePage and Milwright (1953), Cross and Lewis (1974), and Selwyn (1981). Another study concerning iceberg detection was carried out by Remotec Applications Inc. for Petro-Canada Exploration Inc. (1983).

Marine radars have proven useful for monitoring ship and iceberg movement in operational situations in both the Grand Banks and Labrador Sea areas. However, it is recognized that the use of marine radar for the detection of icebergs is subject to many limitations. These limitations include:

a) Radar horizon - similar to the visual sighting of an object, the height of the observer dictates the range to the horizon. Beyond the radar horizon the

detection of targets does not usually occur, except in the cases of superrefraction or ducting. The typical horizon for radars mounted on the derrick top of semi-submersible rigs is about 36 km and for those on support vessels it is about 14 km.

b) The system noise level - for the detection of targets within the radar horizon it is necessary that the signal power received from the target be greater than the system noise power level. The factors affecting the target signal power include the target shape, size, condition, range, propagation path characteristics, and system parameters.

c) Competing signals or clutter - in the presence of competing signals, such as sea and rain clutter, the target signal power must overcome these signals, as well as the system noise level, to be detected.

In the initial stages of the program an evaluation of the available systems was undertaken to assess their suitability for the field program portion of the study. Offshore drilling platforms were considered, as well as supply boats. It was concluded from this preliminary investigation that the semi-submersible Sedco 706 drilling platform was the most suitable for the field program because of the radar configuration available and the inherent stability of the platform. (See discussion of candidate platforms in Appendix 1.) The four radars installed on board are two using X-band and two using S-band frequencies. Two of the systems (one X and one S) comprise a dual band system with antennas located on the derrick top at a height of 75 m. The other X- and S-band units have antennas located above the main deck at heights of 45 and 35 m respectively.

The program as planned called for personnel to be located in the field throughout the entire ninety days (1 March 1984 to 20 May 1984); however, due to limited accommodation on board the Sedco 706, the ice observers who are stationed on board during this season were trained to operate the data collection equipment. This plan initially appeared to be satisfactory, however, when iceberg sightings became more frequent, it became clear that the ice observers were far too busy to operate the equipment. To rectify this problem, it was attempted to have Viatec personnel on board during the last month of the program. During this period an abundance of radar data was collected on twelve well-documented icebergs and four additional icebergs, bergy bits, and growlers.

As this quantity of data precluded a statistical analysis based on iceberg size or class, the analysis used the collected data with a detailed model of radar propagation to derive radar cross-sections for icebergs of various sizes. The performance evaluation of the radar for various environmental parameters has been carried out using other drilling platforms and support vessels as reference targets and iceberg targets when available. This type of analysis is preferable to a purely statistical analysis, as the resultant model may be used to predict detection ranges for icebergs of sizes different than those for which data is available.

The iceberg radar cross-sections calculated in this report are compared to the relationship derived by Budinger (1960) and, in general, a good agreement was found. No attempt is made in this report to perform a quantitative comparison with the other previous experiments, as for the most part the data sets were small and variable. It would be of more value to compare the smaller data sets, such as this one, to those having a greater statistical significance.

Several sources of ground-truthing were available for the field program. The MV Polaris V was used to obtain above-water photographs of icebergs in the vicinity of the Sedco 706, however, as this vessel was not always in the area, detailed data from this source are available for only three icebergs. A more complete data set has been obtained from Fenco Newfoundland Ltd. whose personnel were aboard the MV Polar Duke performing iceberg profiling and monitoring work for Husky/Bow Valley. This data set covers most of the icebergs for which radar data was collected and includes above-water photographs from four sides of the iceberg. Dimensional data has been derived from these photographs and compared with vessel ice reports and radio reports to the Sedco 706 during the data collection.

2. REVIEW OF MARINE RADARS

Marine radar has evolved through the years from playing a role primarily in military applications, to a more universal role with applications in fishing, shipping, and pleasure boating. The general ease of operation, relative simplicity in design, and low cost of these radars have enabled a large market to develop, however, since the early radar there have been few real advances in radar design. This would seem to be due to the technology and expense required to alter the format of the plan position indicator (PPI) type of display. This PPI display, while having many limitations with respect to dynamic range and ease of operation, is a very efficient way to display a large amount of amplitude data which is in a polar (range and bearing) form. Early processing techniques also have proved to be long-lasting, with very few innovations available in this area.

As in the past, it is expected that radar developments for the military are far in advance of those available in the marketplace. In recent years, research institutions such as university laboratories and private companies have been working on radar innovations and improvements which will greatly enhance radars' role in iceberg detection and management. Some historical radars, as well as present-day systems, are discussed in the following sections.

2.1 EARLY RADARS

Early radars were developed with the detection of ships and airplanes as a primary goal. For large ships and airplanes the detection process consists mainly of looking for target signals in noise, and detection is a function of the radar parameters. A target will be detected if there is a sufficient margin between the target return power and the system noise level. This detection process in gaussian noise is well understood with the work of North (1963) and Swerling (1957) being applicable to the radar detection problem.

The detection of targets in various forms of clutter became important when small ships and periscopes were sought in heavy seas and rain. One of the earliest types of clutter processing was that known as the constant false

alarm rate (CFAR) display technique. Croney (1956) demonstrates that a logarithmic amplifier followed by a differentiating circuit having a fast time constant (FTC) may be used to subtract the mean clutter level from the displayed video signal for a particular range interval. Further normalization of the video by use of sensitivity time control (STC) permits the operator to obtain an acceptable level of false alarms (i.e., when a clutter signal exceeds a certain threshold, it may be mistaken for a target) over the entire display. This type of operation requires a highly skilled operator.

Many radar manufacturers presently offer automatic clutter suppression circuits based on these and other CFAR techniques of removing the mean clutter level. The danger in using most these types of devices when the detection of icebergs in clutter is required, is that the small target return may be suppressed by the device and go undetected.

Most other radar parameters are essentially unchanged from early radars, except for technological advances in transmitters and receivers which have increased transmitter efficiency and receiver sensitivity, as well as improved system reliability.

2.2 EXISTING MARINE RADARS

There is very little difference between the radar specifications of the equipment presently manufactured by commercial radar companies. Table 2-1 from Ryan (1983) gives the features of the most commonly available systems. Some of the major innovations provided by these manufacturers are:

- Sperry Marine
  - dual polarization antenna (horizontal or circular);
- Racal-Decca
  - dual X- and S-band radar system with synchronized antennas and transmitters
  - A combiner unit for selectively combining video from both X- and S-band systems; and
- Japan Radio Company sea-ice radar
  - digital CFAR and STC
  - pulse-to-pulse averaging

TABLE 2-1

Radar specifications for commonly-available systems (after Ryan 1983).

	Raytheon		Japan Radio Co.		Sea Ice Radar	Furuno	Sperry		Racal-Decca	
Band	X	S	X	S	X	X	X	S	X	S
P_t(kW) λ (m) G(dB) θ(deg) RPM NF(dB)	25/50 0.032 30/9' 0.85 33 10	60 0.1 28/12' 1.85 33 10	25/50 0.032 32/9' 0.8 22 10	30/60 0.1 28/12' 1.9 22 10	40 .032 33/12' 0.5 15-20 6	25 .032 31/8' .95 24 10	25/50 0.032 31/9'L* 28/9'CP* 0.8 22 8.5 (4.5)	25 0.1 27/12' 1.9 22 9	25/75 0.032 32/19' 0.8 28 5.0	30 0.1 26/12' 2.0 28 4
τ(μsec) PRF B_n(MHz)	.06 .5 1.0 3600 1800 400 20 4		0.08 0.2 0.7 1.0 3000 2000 1000 750 20 3		0.7 750 3	.08 .6 1.0 3000 1500 800 12 2.6	0.07 0.25 1.2 4000 2000 500 17 3		0.05 .25 1.0 3300 1650 825 18 5	
Model	Pathfinder 3 and 10 cm.		JMA-825 JMA-850	JMA-830 JMA-860		FR-1211	MK-4016 *L = Lin. polar. *CP = Circ. polar.		2459 F/I	
Detection Range, R_o P_d = .75 pfa = 10^{-6}	16/20	32	21	30/36	31	19	Lin. CP. 25/31 14/17	23	29	31.5

- scan-to-scan averaging
- real-time processing and display in bright television format.

All these companies offer transmitters in the same power range, with Racal-Decca presently offering the maximum with a 75 kW model suitable for use in their dual band system. Similarly, all companies offer optional low-noise preamplifiers and automatic radar plotting aid units which provide some automatic target acquisation and tracking ability.

The most advanced system presently in use on the Grand Banks of Newfoundland is the Racal-Decca 2459 F/I radar. This system, which uses both synchronized X- and S-band antennas as well as transmitters, makes maximum use of the large frequency diversity between the X- and S-band radars by combining the video information from both receivers before displaying. This configuration has been shown to provide increased detection capability over single frequency systems (Williams 1980; 1981).

A sophisticated processing unit available for this application with Japan Radio Company's sea-ice radar. Although this unit was developed primarily for sea-ice applications, its clutter processing capability (i.e., scan-to-scan averaging) makes it directly applicable to the detection of icebergs in sea clutter. Croney (1966; 1975) has demonstrated the capability of scan-to-scan processing for the detection of small targets in sea clutter. This unit has been recently withdrawn from the market due to changing company priorities.

Other radar systems which have potential for improved iceberg detection are presently under development at McMaster University and McGill University. A review of the McMaster work is contained in Currie and Haykin (1984). The essential components of the McGill hardware were used as the basis of the radar recording system for this field program and its capabilities are discussed later in this report and in Appendix 2.

3. ICEBERG DETECTION -- A MODEL

The detection of icebergs with marine radar is a function of the ratio of the signal powers received from the target to the sum of the signals from noise (N) and clutter (C) sources or S/(N+C). The higher this ratio becomes, the greater the probability of detection will be. The factors which influence this ratio are radar parameters, prevailing environmental conditions, and target characteristics.

The large number of possible combinations of system and environmental parameters preclude the collection of radar data for every possible combination for each iceberg encountered. An effective method of dealing with this problem is to develop a model of the phenomena and to validate this model with experimental data. To this end a mathematical model has been assembled from the existing theory on radar propagation and scatter. A brief outline of the theory used in the model and appropriate references is contained in Appendix 3. The model takes into account most of the parameters which influence target detection, as listed below, and Fig. 3-1 is a sample output of the model using these typical input parameters:

- frequency band (X or S)
- transmitter power (Watts)
- antenna gain (dB)
- radar wavelength (m)
- receiver noise figure (dB)
- pulse repetition frequency (Hz)
- antenna rotation speed (r.p.m.)
- pulse length (microsec.)
- horizonal beamwidth (deg.)
- vertical beamwidth (deg.)
- receiver bandwidth (Hz)
- transmission line loss (dB)
- scanning loss (dB)
- additional losses (dB)
- receiving line loss (dB)
- antenna loss (dB)
- iceberg length (m)
- iceberg width (m)
- iceberg height (m)
- radar cross-section (m^2)
- meteorological condition (Vis or Rain)
- significant wave height (m)
- air temperature (°C)
- probability of false alarm (exponent)

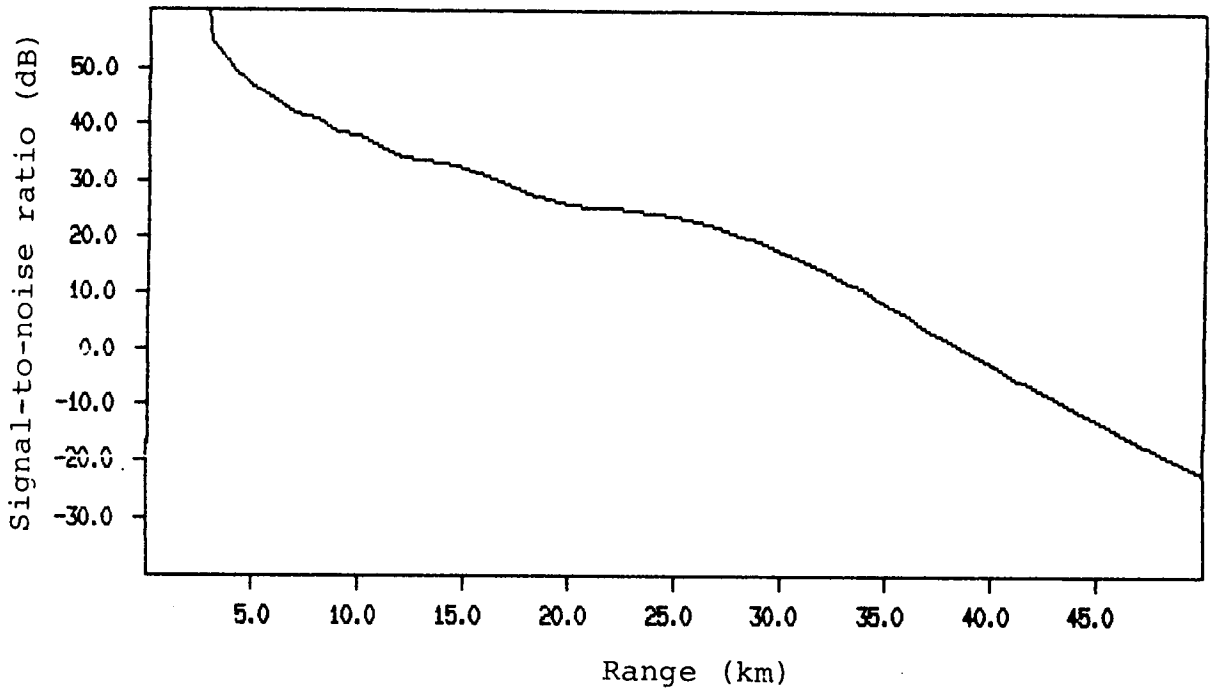

Fig. 3-1. Model output using parameters for a medium iceberg (T168).

- Swerling fluctuation case
- antenna height (m)
- target height (m)
- target base height (m)
- visibility (100,200,2000, or >2000 m.)

Fig. 3-1 gives the signal-to-noise ratio as a function of range for a medium iceberg using an S-band radar (parameters for the derrick-mounted S-band on the Sedco 706). The next section describes how this curve may be related to the operational detection process.

3.1 THE DETECTION PROCESS

The signals from both radar targets and background clutter (or noise sources) are not deterministic, that is, it is impossible to predict at any point in time what the exact value of either of these signals will be. The fluctuating nature of both the target and background signals is such that one must consider not the absolute, or fixed difference, between signal and background noise or clutter, but the average or expected difference. With a certain average value of S/(N+C) the target signal will exhibit a degree of visibility above the background. The greater this ratio, the more visible the target signal becomes, thereby increasing the certainty of the decision that a target is present. This leads to the treatment of the detection process as one involving the theory of probabilities. The detection probability, P_d, has the physical meaning that a target is expected to be observed to exceed some selected threshold P_d x 100 times in 100 antenna rotations (this is often referred to as a blip/scan ratio). For a P_d of 0.5, the target will be observed in 50 of 100 antenna revolutions. This definition of probability of detection is true only when each antenna rotation is considered independently. Associated with a given probability of detection, there will be usually a probability of a false alarm (P_{fa}). The probability of a false alarm decreases as the decision threshold is increased. The higher the threshold, the greater the S/(N+C) ratio needed to produce the same probability of detection. The curves in Fig. 3-2 from Skolnik (1970) illustrate this relationship.

In practice, the operator changes the threshold every time one of the display controls is altered (i.e., gain, FTC, STC). Increasing the gain decreases the

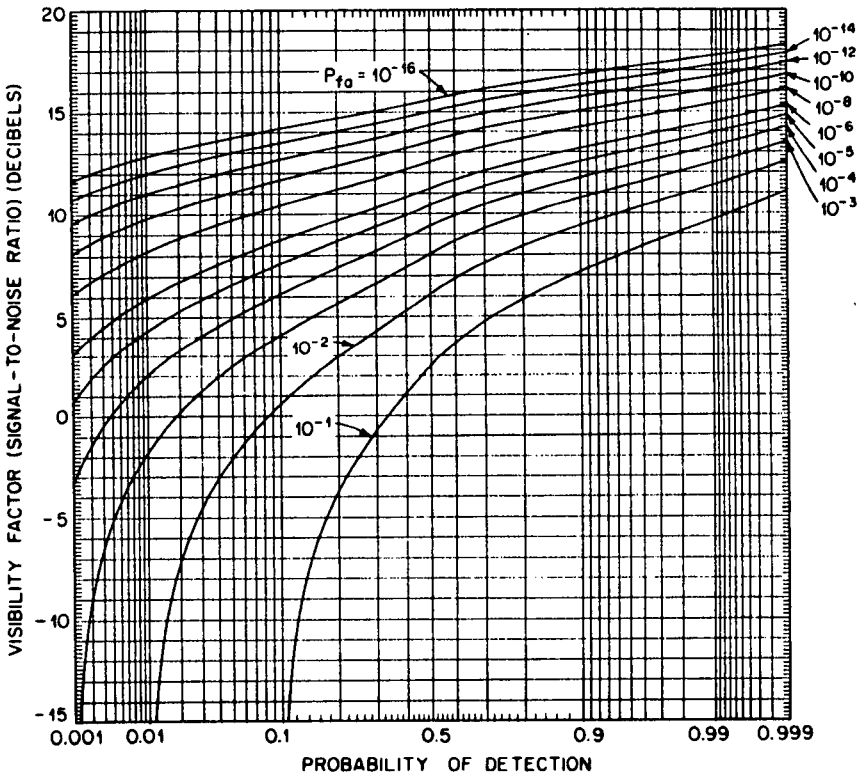

Fig. 3-2. Required signal-to-noise ratio (visibility factor) at the input terminals of a linear rectifier detector as a function of probability of detection for a single pulse, with the false alarm probability (P_{fa}) as a parameter. A non-fluctuating signal is assumed (after Skolnik 1970).

threshold, thereby allowing more noise and clutter to be displayed which results in an increased number of false alarms. The quote from Williams (1979),

> "Thus it is mandatory that a ship seriously wishing to detect growlers, or indeed any really small targets, must first display sea clutter out to the desired detection range if there is to be any chance at all of making a detection,"

is directly applicable to this discussion.

3.2 THE MODEL

When more than one radar pulse hits a target during the antenna dwell time on the target, a decrease in the required signal-to-noise (S/N) ratio for a specific probability of detection is obtained by integrating (summing) the return signals from consecutive pulses. Pulse-to-pulse integration occurs usually both in the display and in the operator's eye. This is a useful technique when the background signal is system noise, as the noise is not correlated from pulse-to-pulse. However, for the case of detection limited by sea clutter, very little gain is achieved in signal-to-clutter ratio improvement. The number of pulses per beamwidth, n, is given by

$$n = \frac{\theta \cdot PRF}{6 \cdot RPM} \qquad (3.1)$$

where

θ = antenna horizontal beamwidth (deg.)
PRF = pulse repetition frequency (Hz)
RPM = antenna rotation speed (r.p.m.)

In Fig. 3-3 a set of curves is presented for finding the required signal-to-noise ratio for n pulses integrated and a probability of detection of 0.75. Each curve in the figure represents a different probability of false alarm. For noise-limited detection the P_{fa} may be used to calculate the average time between false alarms, T_{fa}, from

$$T_{fa} = \frac{n\tau}{P_{fa}} \qquad (3.2)$$

where τ is the radar pulse length (or more accurately the reciprocal of the noise bandwidth of the receiver) and n

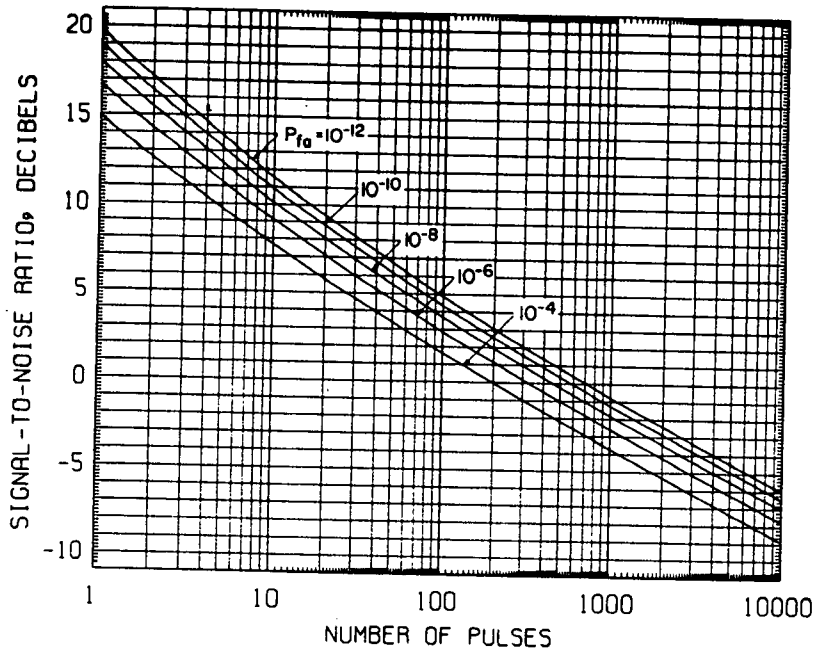

Fig. 3-3. Required signal-to-noise ratio for detection with noncoherent integration of pulses; square-law detector, Swerling Case 1 fluctuation, P_d = 0.75 (after Blake 1980).

is the number of pulses integrated. The curves in Fig. 3-3 are for a Swerling case 1 target fluctuation model. This model is chosen usually for slowly-moving objects at sea and assumes the target signal does not fluctuate from pulse-to-pulse.

From this figure a probability of detection of 0.75 (P_{fa} = 10-6) requires a signal-to-noise ratio of 16.8 dB for single pulse detection and one of 12 dB for a radar which integrates four pulses. A complete set of curves for probabilities of detection from 0.25 to 0.95 are presented in Appendix 4. These curves may be used with Fig. 3-1 to estimate the probability of detection for that iceberg at any range. The probabilities of detection presented in this report assume that the radar is used by a skilled operator.

4. COLLECTION OF DATA

4.1 FIELD PROGRAM

During the months of March, April and May of 1984 a data collection program was carried out using the existing radars on the semi-submersible Sedco 706 drilling platform to investigate iceberg detectability. In this period, radar data were recorded for 12 iceberg targets in a range of sea states and atmospheric conditions. The range of iceberg and environmental conditions data collected may be summarized as follows.

- Icebergs -

- smallest: T191 bergy bit 2 m x 2 m x 2 m (LxWxH)
- largest: T181 medium dome 82 m x 59 m x 26 m
- average size: medium
- total: 12

- Environmental data -

• significant wave height	0.9 to 4.6 m
• wind speed	2 to 43 knots
• visibility	0 to 15 naut mi
• air temperature	1 to 7°C
• sea temperature	0 to 4.6°
• dew point temperature	0 to 6°
• barometric pressure	998 to 1029 mb

The icebergs were classified in size using the WMO/AES classification which is given below.

Growler:

- height less than 1 m
- area usually about 20 m^2

Bergy bit:

- height 1-5 m
- area usually 100-300 m^2

Icebergs:

a) all types except tabular

small
- height 5-15 m
- length less than 60 m

medium
- height 15-45 m
- length 60-120 m

large
- height 45-75 m
- length 120-210 m

very large
- height greater than 75 m
- length greater than 210 m

b) tabular icebergs

small
- height less than 6 m
- length less than 90 m

medium
- height 6-15 m
- length 90-120 m

large
- height greater than 15 m
- length greater than 120 m

Sizes refer to above-water portion only. If the length and height fell into different categories, the smaller class was assigned.

The shape description used is summarized as follows.

Tabular:

- iceberg having a very flat or horizontal top and near-vertical sides, greater length/height ratio than other icebergs.

Blocky:

- massive iceberg usually having steep precipitous sides and angular features, may have horizontal or flat top.

Dome:

- iceberg having large smooth rounded top, very solid iceberg.

Pinnacle:

- iceberg with large central spire or pyramid of one or more spies dominating shape; less massive than a dome iceberg of similar dimensions.

Dry dock:

- iceberg eroded such that a large U-shaped slot is formed, with twin columns or pinnacles, slot extends into the water or close to it.

Wedge:

- iceberg having a flat sloping top and near vertical sides, one side higher than the other. The length/height ratio is usually higher.

The code (for example T191 or N1243) associated with each iceberg are the designations given by Fenco Newfoundland Ltd. (T code) and the offshore operators ice management system (N code).

4.2 RADAR SYSTEM DESCRIPTION

The Sedco 706 was selected primarily for the existing radars on board, which included two X-band and two S-band radars. One X-band and one S-band radar comprised the Racal-Decca F/I 2459 Dual Radar System. This system was located at the derrick top, at a height of 75 m, with the radar transceivers located directly under the antennas, keeping waveguide losses to a minimum. The other X-band and S-band radars were standard Decca models with antennas mounted at heights of 45 m and 35 m respectively. Table 4-1 lists the specifications and physical characteristics of the four radars. The primary data recording system consisted of a PDP $11/23^{+}$ microcomputer, a Kennedy nine-track tape drive, radar interface, and auxillary equipment. The recording was carried out under computer control with the operator required to enter target and environmental data and perform the switching between the radar interface unit and the four radars. In the final version of the collection procedure all the necessary switching could be carried out from a single panel in the chart room. The radar interface was capable of sampling the incoming radar video at either 1.5 MHz or 6.0 MHz with six-bit sample resolution. The analogue to digital conversion was

TABLE 4-1

System characteristics of the four radars on board the Sedco 706.

Characteristic	Experimental designation of radar			
	X1	S1	X2	S2
Frequency (MHz)	9410 ± 30	3050 ± 10	9410 ± 30	3050 ± 10
Transmitter peak power (kW)	18.5	27.0	11.5	25.0
Pulse length (s)	1.0a	0.25	0.05	
Pulse repetition frequency (Hz)	825[a]	1650	3300	
Receiver bandwidth (MHz)	5[a]		18	
Receiver noise figure (dB)	6.0	3.5	10.0	10.0
Horizontal beamwidth (3dB) (deg.)	0.8	2.0	0.8	2.0
Vertical beamwidth (3dB) (deg.)	20	30	15	25
Antenna gain (dB)	32	26	33	27
System losses (dB)	3	3	6	5
Physical antenna height (m)	75	75	45	35
Blind arc (deg. relative)	nil	nil	135-222	95-132
Number of pulses per beamwidth	3.67	9.17	3.67	9.17

[a]During the experimental program, data was collected only for these settings.

performed on the peak radar video within a sampling interval. This digital radar video for each sweep, or radial, is combined with a header word and written onto magnetic tape. The header word contains azimuth and digitizer status information. Having the azimuth information with each sweep of radar video was an asset during data analysis.

A back-up recording system consisting of an A-scope adaptor and a Nicolet 4094-2 digital oscilloscope also was used to record reference target data on floppy disks. Comparison of voltage levels recorded for the drill-rig Sedco 710 on the primary and back-up system, at about the same time and averaged over six antenna rotations, verified the system stability over the data collection program.

The system configuration, including the recording system, is given in Fig. 4-1. The radar video signals were taken from the output of the intermediate frequency stage of each of the four receivers before any video processing. These signals were all available in the vicinity of the chart room, beside the control room (bridge) where the recording equipment was set up. The radar interface required three-wire synchro data from the antenna to generate azimuth information, and as the existing systems used only two-wire bearing data, it was necessary to run cables to each of the antenna turning units from the chart room. At the same time additional cable was installed to permit the continuous monitoring of the transmitted power at the antenna inputs. It was intended that these cables would carry data from peak power sensors (HP 84811A), inserted in the waveguide using directional couplers (Fig. 4-2), to the power meter located in the chart room, however, because of ground differentials between the derrick top and the chart room, it was necessary to bring the power meter to the derrick top to measure the transmitter power.

The system calibration was carried out using two microwave signal generators (HP 8683B, HP 8684B) as illustrated in Fig. 4-3. The generator was placed as close to the antenna as possible so that waveguide losses would be taken into account. For each radar two sets of calibration data (input power versus output voltage) were taken, starting at the minimum detectable signal (MDS) measured in decibels below one milliWatt, dBm, and increasing in 5 dB steps to saturation, then decreasing back to the MDS for the long pulse setting. The average results are presented in Figs. A6-1 to A6-4, Appendix 6. Table 4-2 gives the measured MDS values for the four

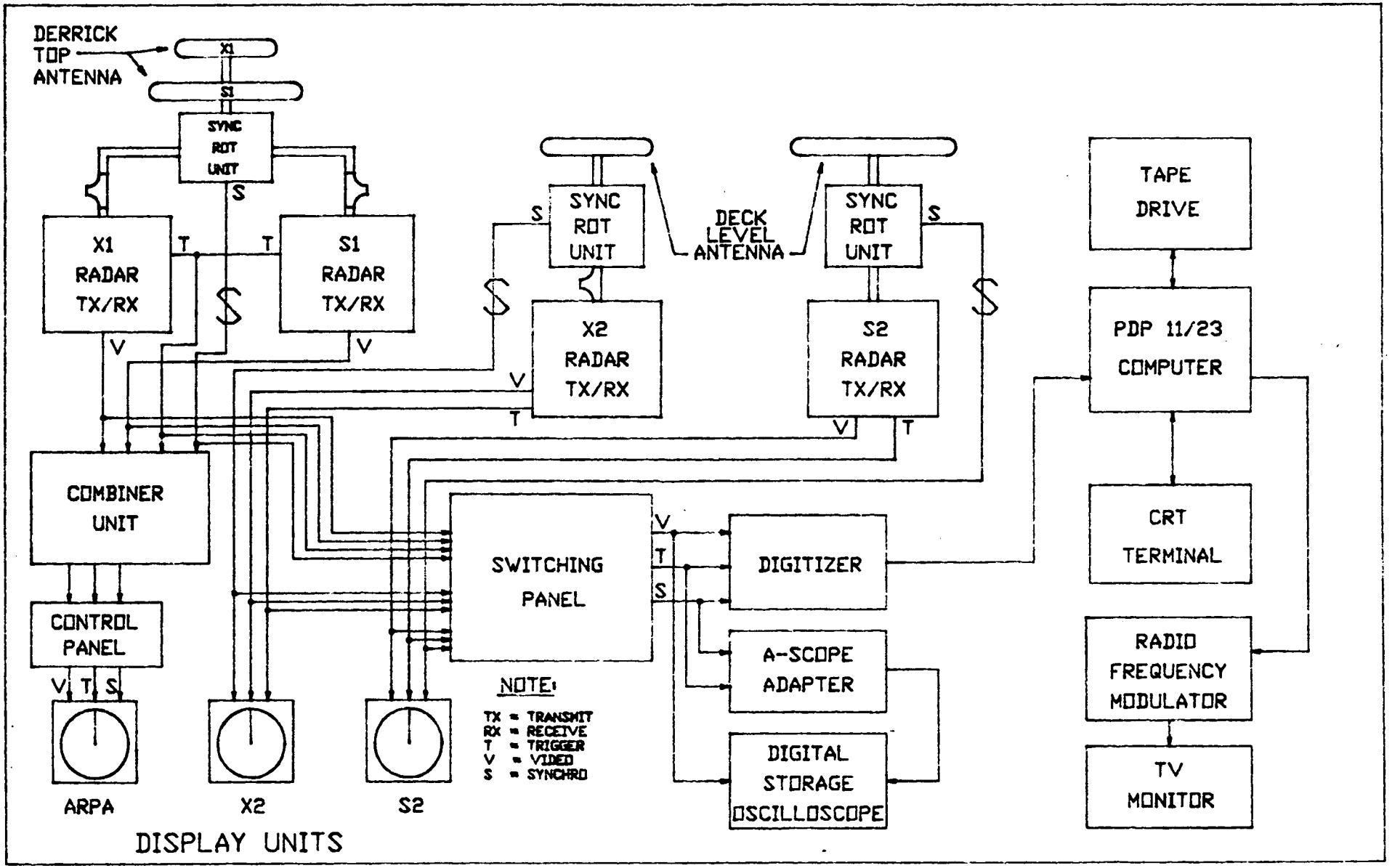

Fig. 4-1. System configuration and radar recording system.

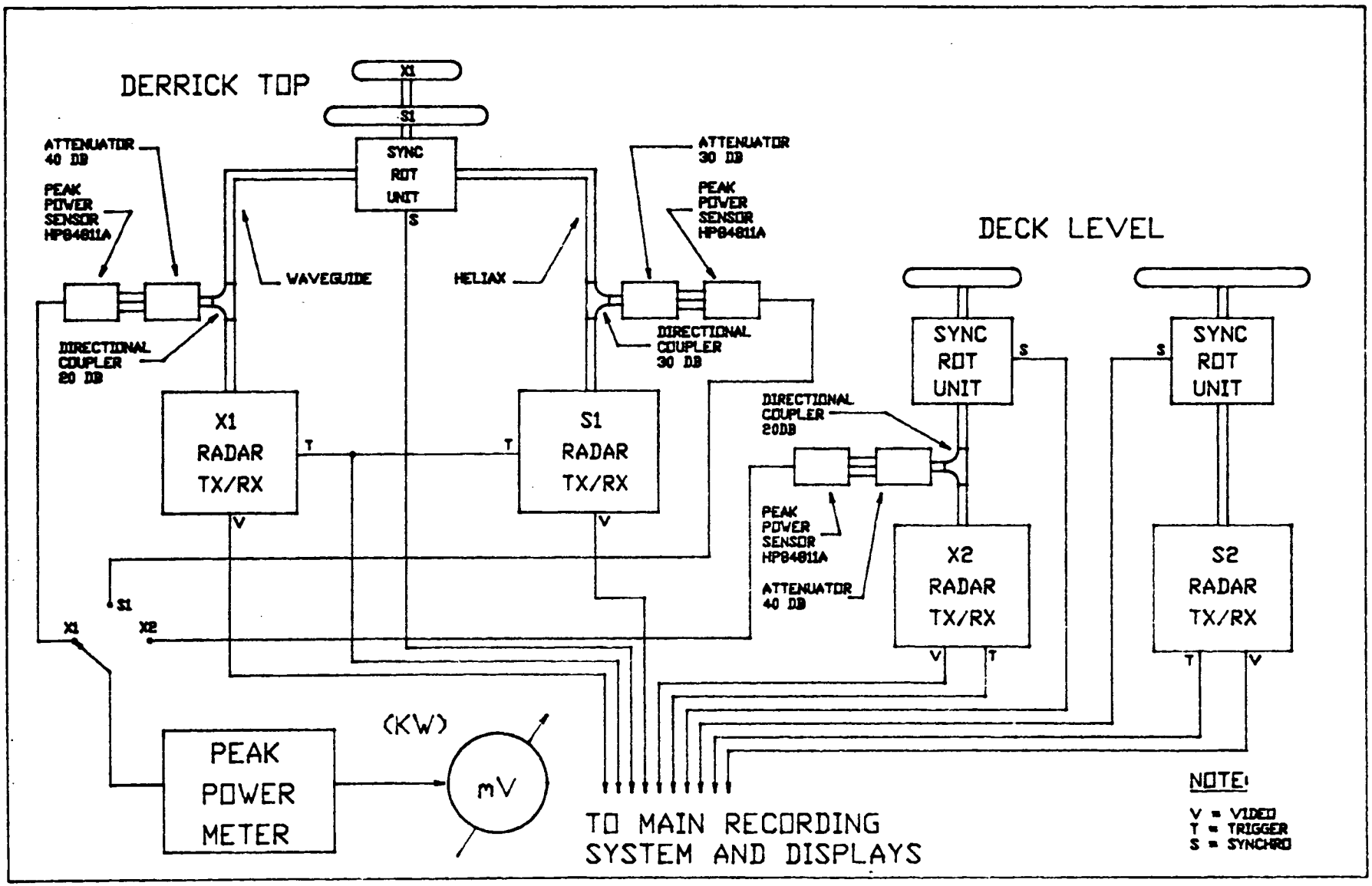

Fig. 4-2. Transmitter power measurement.

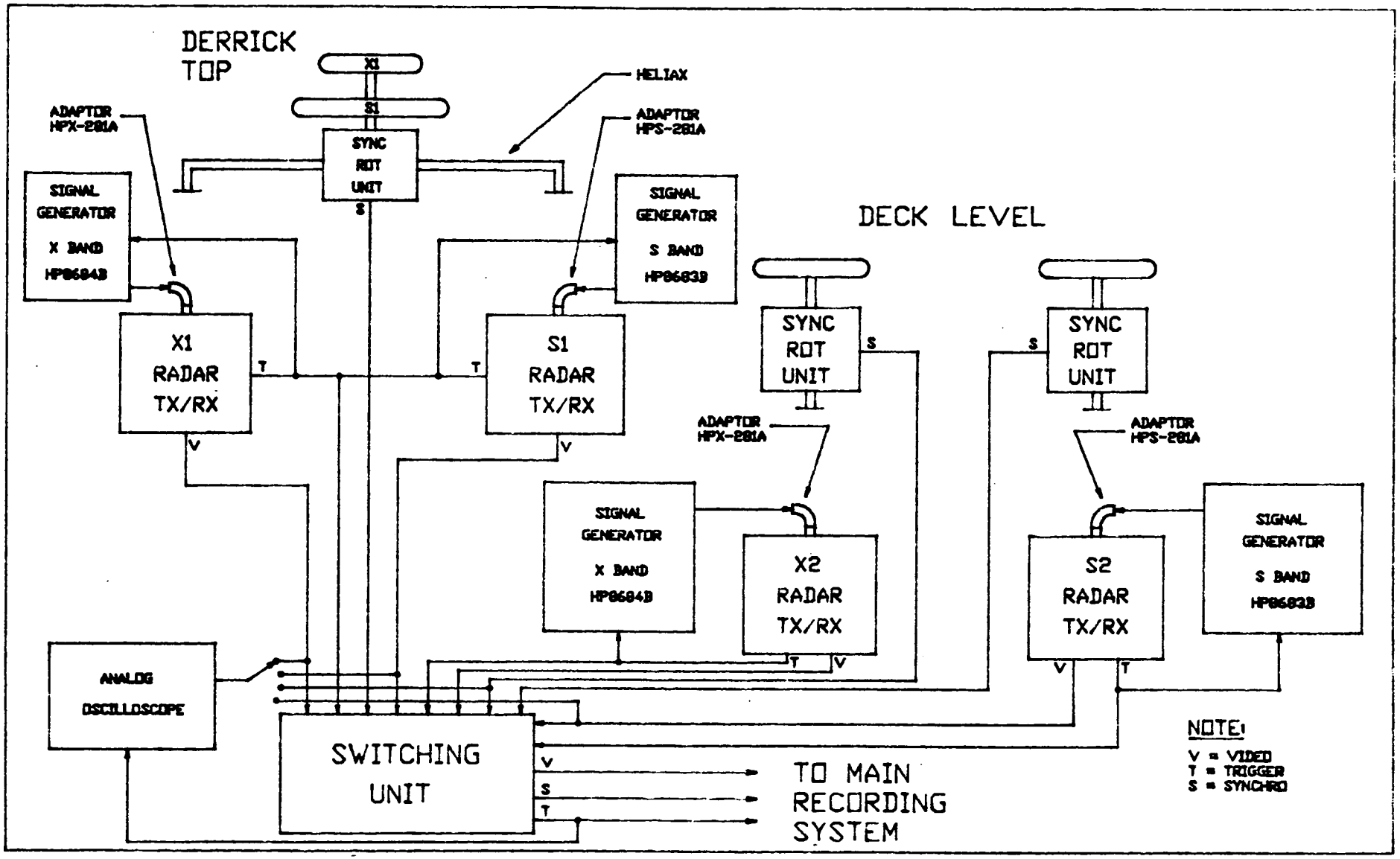

Fig. 4-3. System calibration.

systems. The poor MDS levels for S2 were caused by the measurement procedure. This radar used a special S-band coaxial waveguide with connection to the radar transmitter by Rhode-Swartz SNB1061 connectors. These could not be located so a crude calibration was undertaken by clamping a standard waveguide to N-type adaptor for S-band onto the transceiver input/output port. This adaptor was located to achieve maximum output from the receiver for a given input power level. For data analysis purposes the S-band calibration curve was shifted to line up with the calculated MDS. It is expected that the error introduced could be as much as 3 dB.

TABLE 4-2

Minimum detectable signal levels for each radar.

Minimum detectable signal (dBm)	Radar system X1	S1	X2	S2
Measured	-97.0	-103.0	-94.0	-80.0
Calculated	-99.0	-102.0	-95.0	-95.7

The calibration of the derrick-mounted units was the most comprehensive, as it was possible to connect the signal generators for both X- and S-bands directly to the waveguide at the antenna input/output ports, and at the same time to measure the output voltage at the radar interface input in the chart room.

The radar interface also was calibrated for input voltage versus output digital level. This plot is given in Appendix 6, Fig. A6-5.

It would have been desirable to calibrate the derrick-mounted receivers more than once, however, weather, as well as the availability of manpower (the calibration requires at least two personnel familiar with the equipment) impeded this. The stability of the returns from several reference targets recorded during the field program indicates that the complete system was stable within several dB.

The largest difference between recorded target signals was obtained with radar X1, from a support vessel

at 0.4 naut mi which gave a received power of -45 dBm, and from a bergy bit at 4.2 naut mi which gave a received power of -86 dBm. This difference indicates that the recording system covered 41 dB of the total system dynamic range, however, it was found that the characteristic curves of the receiver were not well matched with the characteristic curve of the radar interface in the lower signal range. This problem and other system limitations are discussed in Appendix 7. For more details on the platform selection, recording system selection, and system installation, the reader is referred to the Data Acquisition Plan Final Report prepared for this project and Appendices 1, 2 and 8.

5. DATA ANALYSIS AND RESULTS

The major objectives of this study were to investigate the environmental effects on propagation and detection and, as well, consider the relationship between the iceberg above-water size to its radar cross-section. As such it was necessary to first isolate any anomalous propagation periods. This was carried out by using quantitative measurements for steady targets in the area in conjunction with the prevailing environmental conditions. These environmental conditions were used as input to a model that calculates the refractive index near the ocean surface, thereby giving an indication of the type of propagation which may occur in the lower atmosphere. A description of this procedure and the results are given in Section 5.3.

Once propagation anomalies were identified, the calculation of the radar cross-section of each target was undertaken. These cross-sections are presented with reference to the propagation conditions present and are compared with the work of other investigators.

Although there were no visible iceberg targets in sea clutter, data from sea clutter was analysed for comparison with published data. Section 5.5 contains a comparison of ocean back-scatter coefficients calculated from the collected data for various sea conditions and grazing angles with the tabulated values of Nathanson (1969) and calculated values using the model of Sittrop (1977).

5.1 METHOD FOR ANALYSING RADAR DATA

The analysis of the digital radar data stored on magnetic tape was carried out using a PDP 11/23+ computer and hardware required to produce a 256 x 256 pixel colour display. The data of interest on each tape were identified from the information logged on the tape itself and from field log-books. The analysis considered all the iceberg targets and most of the support vessels and drilling rigs in the surveyed area. Using the calibration data of Appendix 6, the received power for all targets was calculated. This received power was then used with the radar model to calculate the target radar cross-section for two conditions: the case when the propagation factor,

F, is one (i.e., free space conditions) and the case when the F is calculated. The model also computed a predicted signal-to-noise ratio curve for the same target cross-section over the entire radar range. This curve was then used to estimate the detection range for each target. Further discussion on detection is provided in Section 6.

Several computer programs were written to assist in the data reduction. The first phase of the analysis consisted of target selection. Once the desired target was located, all the antenna scans on a particular tape for a particular radar were transferred to a computer disk for easy future access. This process usually entailed storing six 45-degree sectors of data representing six consecutive antenna rotations. Using the azimuth information with each record these six sectors were overlaid precisely and were averaged to produce one averaged sector. This sector of data was used with a program which can interactively alter display thresholds on a high resolution monitor enabling the operator to identify and quantify the peak digital value for each target. This digital value was converted to a voltage using the curve in Fig. A6-5 in Appendix 6 and then converted to a power value using the appropriate calibration curves in Figs. A6-1 - A6-4.

5.2 OBSERVATIONS ON POWER RECEIVED FROM TARGETS

The results of this analysis are contained in three tables. Table 5-1 documents the power received from all the icebergs for which data was collected. Table 5-2 contains all the support vessel data and Table 5-3 contains the support vessel data for the range from 8 to 10 naut mi only with the average and standard deviation of these data. The data on power received from the Sedco 710 is contained in Table 5-4. The following observations can be made from these tables:

a) The S1 radar outperformed the other radars for iceberg detection. This confirms the experience gained operationally.

b) The smallest recorded signal for each radar and the corresponding signal-to-noise ratio referred to the demodulator input are as follows:

	X1	S1	X2	S2
P_r (dBm)	-86	-98	-86	-88
S/N (dB)	11	5	8	8

TABLE 5-1

Power received at each radar from iceberg targets.

Iceberg code	Iceberg type	Above Water Size (M) L	W	H	Date (1984)	Range (naut mi)	Power received (dBm) X1	S1	X2	S2	Comment
T166[a]	MDD	90	80	26	10 May	21.6	-	-92.0	-86.0	-	IN TOW (N1243)[b]
T167	MPI	NA	NA	NA	28 Apr.	19.5	-	-90.0	-	-	
T168	MWD	75	59	20	28 Apr.	18.0	-	-90.0		-	N1242
					08 May	10.0	-	-90.0	-	-	
					08 May	8.9	-	-85.0	-78.0	-	
					08 May	8.9	-77.0	-82.0	-83.0	-	
					09 May	8.0	-	-83.0	-86.0	-	
					10 May	19.0	-	-84.0		-	
T175	MDO	96	54	15	08 May	10.2	-	-88.0	-	-	N1283
					08 May	10.5	-	-84.0	-77.5	-88.0	
					08 May	9.5	-	-90.0	-	-	
					09 May	8.6	-	-85.0	-86.0	-	
					10 May	18.3	-	-81.4	-	-	
T180	SDD	28	27	9	09 May	14.2	-	-	-	-	N1306
T181	MDD	98	73	22	09 May	14.0	-	-78.0	-	-	N1318
		82	59	23	10 May	17.0	-	-84.0	-	-	
T187	SDD	20	15	6	11 May	7.9	-	-88.0	-	-	
					12 May	13.3	-68.0	-74.0	-74.0	-84	IN TOW
					13 May	17.4	-	-92.0	-	-	
T188	MDD	30	25	20	11 May	7.5	-86.0	-80.5	-	-	
T191	GRL	2	2	2	12 May	4.2	-86.0	-93.4	-	-	
T195	SDD	NA	NA	NA	12 May	21.8	-	-93.4	-	-	
T196	MDD	38	38	12	13 May	21.6	-	-95.0	-	-	
T197	MDD	61	58	24	17 May	12.4	-	-84.0	-	-	
T198	SWD	33	25	6	12 May	18.0	-	-	-	-	N1376
1277	MTA	90	55	12	09 May	16.5	-	-85.0	-	-	
					10 May	11.0	-	-	-	-	IN TOW
					11 May	19.0	-	-	-	-	
					11 May	16.0	-	-	-	-	
					12 May	17.5	-	-80.5	-	-	
					13 May	16.1	-	-98.0	-	-	
NCC	GRL	3	2	.6	17 May	0.6	-	-	-	-	
NC	GRL	NA	NA	NA	08 May	2.5	-	-	-	-	

a T - Fenco code number. b N - Offshore operators code number. c NC - No code available.

TABLE 5-2

Power received at each radar from support vessels.

Tape No.	Date (1984)	Range (naut mi)	Power received (dBm) X1	S1	X2	S2	Comment
19A	28 Apr.	6.7	-63.0	-71.0	-69.0	-74.3	
		8.2	-68.0	-72.0	-73.0	-83.0	
20	08 May	9.7	-70.0	-72.5	-77.0	-	
		9.7	-76.6	-73.0	-78.0	-	
		11.9	-	-76.0	-79.0	-	
21	08 May	9.7	-	-69.0	-66.0	-	
22	08 May	3.9	-60.3	-68.0	-63.0	-66.0	
		8.3	-74.0	-74.0	-77.5	-	
24	08 May	3.4	ND[a]	ND	-70.0	-75.0	
		8.8	-78.5	-74.0	-71.2	-	
		9.2	-76.6	-73.0	-69.2	-83.0	
		9.6	-74.0	-73.6	-79.0	-	
		11.1	-86.0	-75.0	-76.0	-	
28	10 May	4.0	ND	-67.0	ND	-75.0	
		10.9	-80.0	-74.0	-69.2	-89.0	
		10.6	-	-80.0	-81.0	-	
		14.9	-	-70.0	-	-	
		21.5	-	-79.0	-79.0	-	
29	11 May	9.2	-70.0	-73.0	-79.0	-80.0	
		11.2	-69.0	-72.5	-70.0	-	
		15.5	-	-	-	-	
31	11 May	7.5	-67.6	-71.0	-	-	
32	12 May	2.0	-51.0	-67.5	-82.0	-73.0	
		3.7	-58.0	-66.0	-61.0	-76.0	Polar Duke
		12.2	-59.0	-71.0	-72.0	-74.0	
34	12 May	1.5	-47.5	-70.5	ND	ND	
		13.3	-67.0	-69.0	-68.5	-86.0	
		18.5	-66.0	-71.6	-	-	
		33.4	-80.0	-72.0	-	-	
		35.3	-73.0	-78.0	-	-	
36	13 May	8.0	-63.5	-67.0	-73.0	-86.0	
		10.0	-86.0	-78.0	-80.0	-	
		10.6	-65.5	-70.0	-72.0	-	
		16.1	-	-92.0	-	-	

TABLE 5-2 (Continued).

Tape No.	Date (1984)	Range (naut mi)	Power received (dBm) X1	S1	X2	S2	Comment
37	13 May	11.8	-67.0	-72.5	ND	ND	
39	15 May	17.0	-	-93.5	-	-	Polar Duke
41	16 May	10.8	-65.5	-75.0	-79.0	ND	
45	17 May	11.0	-	-75.0	-76.0	-	
		12.4	-76.6	-80.0	-83.0	-	
47	17 May	13.0	-58.0	-70.0	ND	-70.0	

[a] ND = no data.

TABLE 5-3

Mean received power from support vessels at a range of 8 to 10 nautical miles.

Tape No.	Date (1984)	Range (naut mi)	Power received (dBm) X1	S1	X2	S2
19A	28 Apr.	8.2	-68.0	-72.0	-73.0	-83.0
20	08 May	9.7	-70.0	-72.5	-77.0	-
20	08 May	9.7	-76.6	-73.0	-78.0	-
22	08 May	8.3	-74.0	-74.0	-77.5	-
24	08 May	8.8	-78.5	-74.0	-71.2	-
24	08 May	9.2	-76.6	-73.0	-69.2	-83.0
24	08 May	9.6	-74.0	-73.6	-79.0	-
29	11 May	9.2	-70.0	-73.0	-79.0	-80.0
36	13 May	8.0	-63.5	-67.0	-73.0	-86.0
36	13 May	10.0	-86.0	-78.0	-80.0	-
Mean			-73.72	-73.01	-75.69	-83.00
Standard Deviation			6.28	2.68	3.76	2.45

TABLE 5-4

Power received from the Sedco 710 drilling rig.

Tape No.	Date (1984)	Range (naut mi)	Power received (dBm) X1	S1	X2	S2
19A	28 Apr.	9.7	-60.0	-68.0	-66.0	-74.0
20	08 May	9.7	-57.0	-70.5	-67.0	-78.0
21	08 May	9.7	-	-69.0	-66.0	-
22	08 May	9.8	-55.0	-67.0	-66.0	-76.0
24	08 May	9.5	-66.0	-70.0	-65.0	-75.0
28	10 May	9.8	-58.0	-69.0	-63.0	-64.0
29	11 May	9.6	-49.0	-68.5	-66.5	-78.0
32	12 May	9.6	-54.0	-67.0	-63.5	-76.0
34	12 May	9.6	-47.0	-67.0	-63.0	-77.0
36	13 May	9.6	-51.0	-67.0	-66.0	-76.0
37	13 May	9.7	-51.0	-69.0	NDa	ND
41	16 May	9.7	-50.0	-68.3	-61.0	ND
45	17 May	9.6	-61.0	-70.0	-65.0	-77.0
47	17 May	9.7	-50.0	-67.0	ND	-64.5
Mean			-54.54	-68.33	-64.73	-74.14
Standard Deviation			5.60	1.30	1.86	5.03

[a] ND = no data.

c) S1 detected and measured seven icebergs at 18 naut mi and greater.

d) Enhanced detection occurred for several targets. The furthest range for an iceberg was 21.8 naut mi (for T195, a small dry dock) and the furthest range for a support vessel was 35 naut mi (i.e., beyond the normal radar horizon of 20.5 naut mi for a vessel).

e) There was little difference in medium range (8-10 naut mi) signal strength from support vessels for X1, S1, and X2, but the signal from S2 was lower by 8 dB.

f) For the Sedco 710 X1 outperformed all the other radars by at least 10 dB and X2 outperformed S1 by about 3 dB.

g) The received signal power from the Sedco 710 was very stable for S1 and X2 over a one-month period, with a standard deviation of less than 2 dB. The variation in received power from X1 and S2 was about the same at a 5 dB standard deviation.

h) As a variety of meteorology conditions occurred during this data collection period, the stability of signals received from the support vessels and drilling rig (as in Tables 5-3 and 5-4) indicates that propagation is not greatly affected out to a range of 8 to 10 naut mi (15.0 to 18.5 km). At greater ranges, however, propagation appears to be affected severely by prevailing meteorological conditions, which is documented further in the following subsection.

5.3 RADAR PROPAGATION

Perhaps the first documentation and discussion on radar propagation on the Grand Banks was presented by Budinger (1960). Budinger states that for the Grand Banks

> "subnormal radar propagation (i.e., reduced detection ranges) is the rule rather than the exception."

Further, he identifies the early spring and summer months, when southerly winds and fog are the most prevalent, as the time of the year when subnormal propagation occurs most frequently.

There are several propagation modes which may occur over the ocean surface. They include:

a) Standard propagation, when the refractive index of the atmosphere decreases with increasing height from the ocean, and the rate of decrease is less than 157 parts per million per kilometer. The effect of standard refraction is that radar waves are bent slightly around the curvature of the earth, making the radar horizon about 16% greater than the geometrical horizon.

b) Superrefraction, which occurs when the refractive index decreases with height more rapidly than for standard propagation. This rapid decrease causes the radar waves to bend downward more than usual, thereby trapping the radar energy. This mode is usually referred to as ducting and detection ranges beyond the radar horizon may be obtained. Cool, dry air over a cold ocean will often create this mode.

c) Subrefraction, which occurs when the refractive index increases with height. This inversion of the standard refractive index profile will cause upward bending of the radar waves away from the ocean surface. The strength, or severity, of the upward bending is a function of the gradient of the refractive index. The occurrence of warm, moist air over a cold ocean will usually induce this mode of propagation.

During the period of 17 April to 17 May environmental data was collected from the MV Polaris V and the Sedco 706 to help to evaluate the propagation conditions. The meteorological parameters were used with a model[1] to indicate the type of propagation that was occurring within 100 m of the ocean surface. A report by Rotherham (1978) details the method and its limitations. The model was intended for use in prediction of over-the-horizon radar propagation and detection by an

---

[1] The model was developed by Marconi Research Laboratories of GEC-Marconi Electronics Ltd., U.K. for the NATO Defence Research Group with support from the Admiralty Surface Weapons Establishment, see Appendix 9.

evaporation duct, however, it has been used here to derive the existing propagation conditions within the horizon.

The environmental parameters were input and the parameters of duct thickness (ocean surface to top of duct), stability length, and effective earth's radius were calculated following the stated procedure. Also available in the procedure is the sea-air refractivity difference, n_{sa}. For those days when meteorological measurements were made on the MV Polaris V and when radar data recordings took place on the Sedco 706, a set of propagation conditions have been derived. Table 5-5 presents a review of the environmental conditions, the duct height, and the sea-air refractivity difference. Rotherham (1978) states that when n_{sa} is negative, no duct is present and the lower atmosphere is subrefractive. As the duct height becomes very small, propagation conditions approach standard. The procedure thereby provides a convenient method of determining which of the three propagation modes possible is predominant. A list of limitations given by Rotherham (1978) are included at the end of Appendix 8, the most pertinent being that the theory does not take into account the possibility of the existence of elevated ducts. This situation does not appear to have been a problem during this experiment, as the propagation appears to be described adequately by the surface duct.

Qualitatively, the radars all performed much better on clear days, with typical maximum detection ranges for medium icebergs and support vessels being in the range of 17 to 22 naut mi. On days when heavy fog was present, maximum detection ranges were consistently shorter for all radars. The presence of the fog itself might cause some attenuation at X-band, however, it should not have affected the performance of S-band at all. Similar observations were made by Budinger (1960) and the following quantitative analysis would tend to confirm his assertion that these propagation anomalies were caused by the propagation conditions near the ocean.

During the experiment period the model analysis indicated that ducting occurred on 16 out of 26 days, or 61.5% of the time. Subrefraction occurred on 9 out of 26 days, or 34.6%, and there was one day where the propagation was standard. On 12 May the results are out of bounds for the validity of the model, however, if the wind speed was increased to 10 knots, the model indicated that a large surface duct of 30 m height would exist. This was probably the case on this day as the maximum

TABLE 5-5

Review of propagation conditions
for the period 17 April to 17 May 1984.

Date (1984)	Tape no.	Air temp. (oC)	Sea temp. (oC)	Dew point (oC)	Visibility (naut mi)	Wind speed (knots)	Duct height (m)	Sea-air refractivity (Δ N)
17 Apr.		1.7	1.4	0.5	1/2-1	11.0	2.15	+
18 Apr.		2.4	1.8	1.8	1/3-1/2	17.4	0.44	+
19 Apr.		0.6	1.3	0.4	5-11	17.7	0.90	+
20 Apr.		1.1	1.4	0.3	11-27	9.8	1.50	+
21 Apr.		1.6	1.6	0.9	1-2	5.7	1.10	+
22 Apr.		1.8	1.5	1.9	1/2-1	11.1	-	-.63
23 Apr.		0.5	1.0	0	1-2	31.0	1.16	+
24 Apr.		-0.6	0.4	-2.9	5-11	29.0	3.76	+
25 Apr.		-0.8	0.4	-2.8	11-27	14.0	2.88	+
26 Apr.		1.3	1.1	0.4	2-5	27.7	1.21	+
27 Apr.		3.0	2.1	2.2	1.2	28.0	0.30	+
28 Apr.	19A	2.0	1.2	2.0	Poor	24.0	-	-1.10
29 Apr.		1.0	1.0	1.0	1/3-1/2	13.0	0	+
08 May	20	2.0	0	1.0	8	30.0	-	.20
	22	2.0	1.8	1.0	6	30.0	1.40	+
	23	2.0	1.5	1.0	15	30.0	1.14	+
	24	1.0	1.5	0.0	10	30.0	1.96	+
09 May	27	4.0	1.5	0.0	15+	22.0	4.24	+
10 May	28	2.0	1.3	0.0	15+	11.0	3.47	+
11 May	29	2.0	1.5	4.0	8	43.0	-	-6.20
	30	5.0	2.2	5.0	0.5	42.0	-	-4.60
	31	4.0	2.0	4.0	9+	12.0	-	-3.10
12 May	32	4.0	2.0	4.0	12	14.0	-	-3.10
	34	7.0	3.8	4.0	12	2.0	a	
13 May	36	4.0	2.7	4.0	1/4	13.0	-	-2.10
14 May	38	5.0	3.1	5.0	0	25.0	-	-3.30
15 May	39	4.5	3.6	5.0	0	30.0	-	-2.95
	40	5.0	3.3	5.0	1/8	30.0	-	-2.95
16 May	41	6.0	3.9	6.0	1/8	34.0	-	-3.94
	42	5.8	4.6	6.0	1/8	43.0	-	-2.91
	43	5.8	4.6	6.0	1/8	43.0	-	-2.91
17 May	44	6.0	4.2	6.0	0	38.0	-	-3.42
	45	6.0	3.9	6.0	1/8-1/4	37.0	-	-3.94

a Not valid; if wind speed = 10 knots, duct was 30 m.

detection ranges for both support vessels and icebergs were achieved: two different support vessels were recorded at 33 and 35 naut mi and two icebergs (T195, a small dry dock and T196, a medium dry dock) were recorded at ranges of 21.8 and 21.6 naut mi, respectively. These ranges were all beyond the usual radar horizon of 20.5 naut mi for a derrick-mounted radar sensing a 10 m-high target. Of the 12 recordings of icebergs beyond 17 naut mi (Table 5-1) six were detected in periods of ducting and six were detected in periods when subrefractive or standard conditions existed. However, during ducting conditions all medium-size icebergs within 19 naut mi of the rig were detected with the derrick-mounted S-band radar, while there were 16 instances of medium-size icebergs not detected at ranges from 16 naut mi and greater during subrefractive conditions.

It would appear from the analysis that even though the S-band antenna is mounted high above the ocean it is able to take advantage of ducting conditions for targets at ranges of 11 naut mi and greater. At the longer ranges the incidence angle of the radar waves with the duct would be sufficiently small to allow penetration into the duct and for the reflected energy to escape from the duct and return to the radar to permit detection. During ducting conditions data for medium-size icebergs were recorded frequently in the range from 18 to 22 naut mi. During subrefractive conditions these ranges were less by 3 to 4 naut mi.

5.4 RADAR CROSS-SECTIONS OF ICEBERGS, SUPPORT VESSELS AND DRILLING RIGS

It is desirable to estimate the radar cross-section of the target in order to find some all-encompassing relationship between the actual target size and its effective echoing area. Two procedures have been used to estimate this cross-section. The radar cross-section, σ, in square meters, is given by the equation

$$\sigma = \frac{P_r R^4 (4\pi)^3 L}{P_t G^2 \lambda^2 F^4} \qquad (5.1)$$

where P_r = power received in Watts
R = range to iceberg in meters
L = system losses
P_t = peak transmitter power in Watts
G = antenna gain
λ = radar wavelength in meters
F = propagation factor.

Using this equation with the target received power from Tables 5-1 to 5-4 and the radar parameters from Table 4-1 the radar cross-section for any of these targets may be calculated. When F = 1, the calculation neglects the influence of the earth's curvature and sea conditions on the received power and, hence, may not yield accurate results especially in the far range where the range does not follow an R^{-4} dependency. To rectify this, another set of radar cross-sections were calculated using the propagation factor, F, given by the model of Appendix 3. These cross-sections reflect the influence of the spherical earth and its roughness on the received power.

Table 5-6 presents both of these cross-sections for each iceberg and each radar. From this table there appears to be some relationship between the iceberg size and its radar cross-section, although there are some large anomalies in the cross-section calculation, especially for longer ranges. These may be directly attributable to the propagation conditions which existed. Comparison of the data of Table 5-6 with Table 5-5 reveals that in most of the instances when an abnormally large cross-section (compared to the iceberg's physical size) was calculated, for ranges greater than 11 naut mi, there was evidence of surface ducting. It is possible for the cross-section to be small and ducting to exist, however, from the fact that some of these targets were beyond the usual radar horizon, one can conclude that ducting caused extended propagation and, hence, the radar cross-section calculation predicted an excessively large cross-section. It is difficult to estimate the actual amount by which the cross-section has been enhanced, however, rough estimates using targets T175 and T187 indicated an increase in cross-section of about 15 to 25 dB for a surface duct greater than 3 m. This may be supported by a comparison of the return power levels for support vessels on tapes 28 and 34, to those levels when ducting was not occurring (i.e., tapes 20, 21, and 36 to 45). The free space radar cross-sections for all the radars except S2 (the S-band with deck level antenna) are plotted in Fig. 5-1 as a function of their average cross-sectional area. For iceberg shape refer to the

TABLE 5-6

Radar cross-sections for icebergs determined by the four radars on board the Sedco 706.

Iceberg Code	Area (m^2)	Range (naut mi)	Radar cross-section (m^2) X1 F=1[a]	X1 F[b]	S1 F=1[a]	S1 F[b]	X2 F=1[a]	X2 F[b]	S2 F=1[a]	S2 F[b]
T166	2210	21.6	-	-	106.0	945.0	546.0	10894.0	-	-
T167	NA[c]	19.5	-	-	112.0	885.0	-	-	-	-
T168	1340	18.0	-	-	81.0	290.0	-	-	-	-
		10.0	-	-	7.7	8.0	-	-	-	-
		8.9	-	-	15.3	15.0	99.0	30.0	-	-
		8.9	87.0	49.0	29.0	28.0	31.0	14.0	-	-
		8.0	-	-	15.8	16.0	10.3	5.0	-	-
		19.0	-	-	400.0	1830.0	-	-	-	-
T175	1125	10.2	-	-	13.2	6.1		-	-	-
		10.5	12.8	44.0	37.3	15.4	215.0	NA	12.8	44.0
		9.5	-	-	6.3	4.3	-	-	-	-
		8.6	-	-	12.7	11.0	-	-	-	-
		18.3	-	-	626.0	4870.0	-	-	-	-
T181	1881	14.0	-	-	256.0	256.0	-	-	-	-
	1622	17.0	-	-	256.0	256.0	-	-	-	-
T187	105	7.9	-	-	4.8	2.7	-	-	-	-
		13.3	3444.0	2812.0	960.0	28117.0	1243.0	3155.0	82.5	79245.0
		17.4	-	-	45.0	7924.0	-	-	-	-
T188	550	7.5	-	-	21.7	16.3	5.5	2.8	-	-
T191	4	4.2	0.5	0.9	0.1	0.1	-	-	-	-
T195	NA	21.8	-	-	80.0	183269.0	-	-	-	-
T196	466	21.6	-	-	53.0	14937.0	-	-	-	-
T197	1440	12.4	-	-	72.5	72.5	-	-	-	-
1277	870	16.5	-	-	180.0	1430.0	-	-	-	-
		17.5	-	-	645.0	142979.0	-	-	-	-
		16.1	-	-	8.2	902.0	-	-	-	-

[a] Column F=1 gives the radar cross-section when the propagation factor is 1.
[b] Column F gives the radar cross-section for a calculated propagation factor.
[c] Not available.

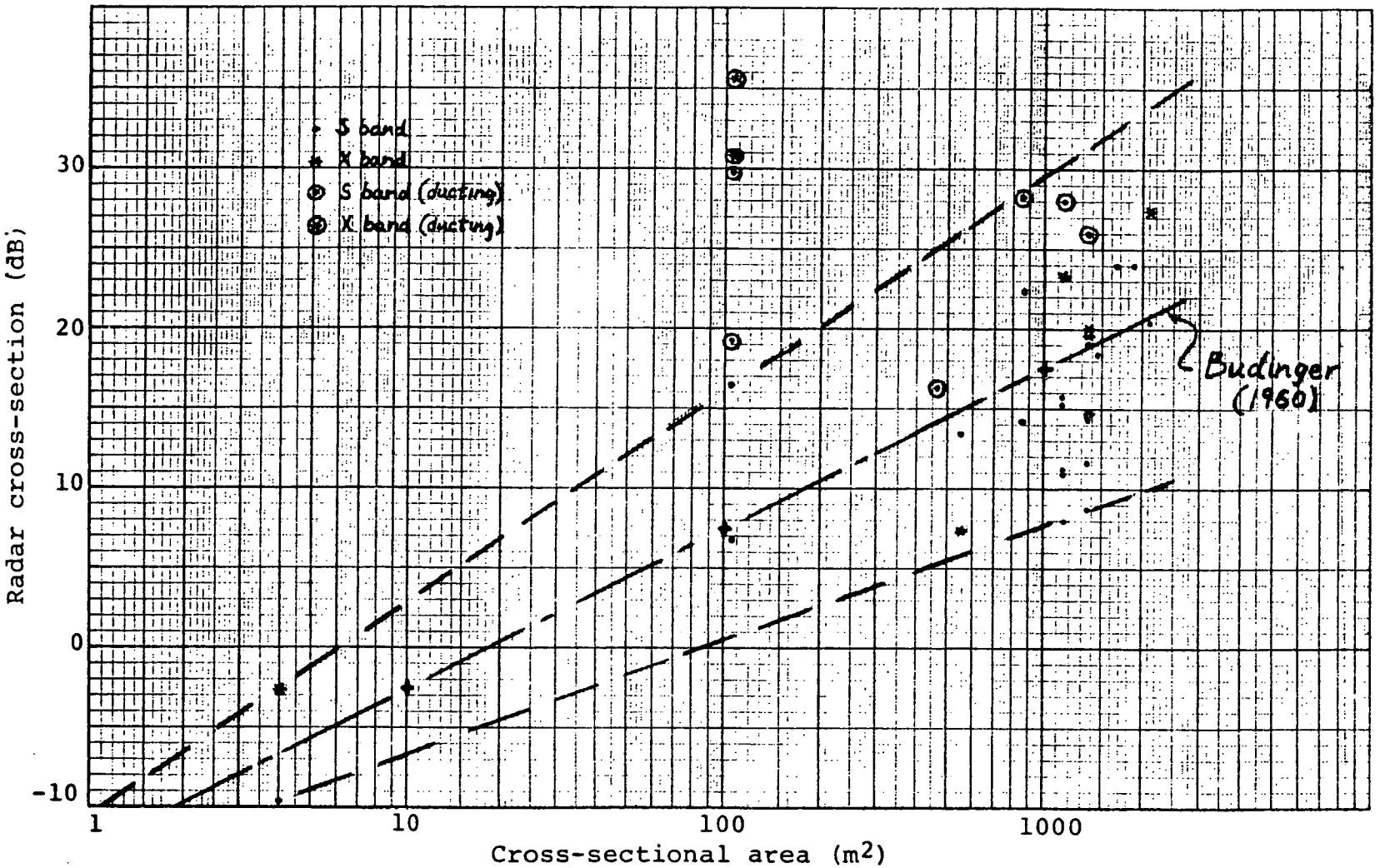

Fig. 5-1. Radar cross-section of icebergs, as a function of cross-sectional area.

iceberg photographs in Appendix 5. The circled data points are for occasions when ducting was occurring, the other points are for days of standard or subrefractive conditions. Plotted in this figure also is the relationship between cross-sectional area and radar cross-section derived by Budinger (1960). Budinger related the radar cross-section to the physical area by the coefficient 0.056. Unfortunately, there was not enough field data on small icebergs to fill in the lower portion of the graph, however, if the smallest growler having a 4 m^2 physical size is used as a lower reference, and the outer bounds of the data for non-ducting conditions are connected with dotted lines, a general trend agreeing with the Budinger relationship is demonstrated.

Table 5-7 presents calculated cross-section values for support vessels at a range of 8 to 10 naut mi and the semi-submersible Sedco 710 drilling platform. These cross-sections were calculated using equation 5.1 and data from Tables 5-3 and 5-4. Fig. 5-2 compares the general shape and dimensions of these targets.

TABLE 5-7

The average radar cross-sections
for support vesssels (at 8 to 10 naut mi)
and the Sedco 710.

	Radar cross-section (m^2)			
	X1	S1	X2	S2
Support vessels	146	234	192	22
Sedco 710	21614	1002	2973	226

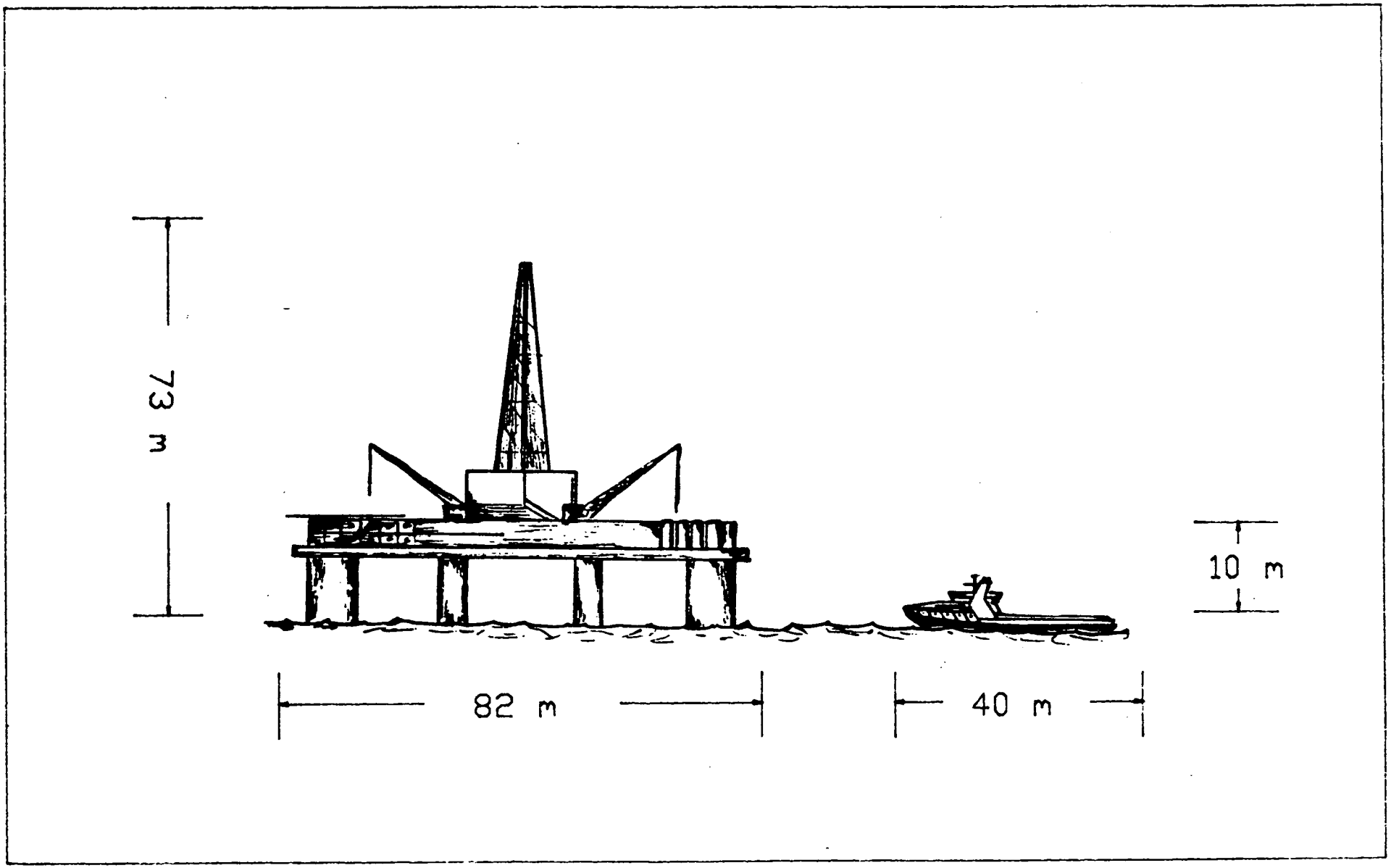

Fig. 5-2. Comparison of cross-section area of typical semi-submersible platforms and support vessels.

5.5 SEA CLUTTER

Since the radar data set contained only two small ice targets in sea clutter, neither of which could be separated from their background (i.e., detected) in the field or in the analysis, the following discussion presents some of the data on sea clutter itself for comparison with published values of other studies. This comparison is useful from the point of view of evaluating the applicability of existing sea clutter models to a rig-based radar in the Hibernia area.

To estimate the back-scatter coefficient from the collected data, it was necessary to find the average power level for specific sea conditions and grazing angles. The average of five or six consecutive antenna rotations was calculated from the digital data. As expected, the clutter peaks smoothed out considerably. This processed data was then thresholded to find the range for a specific average power level. As the averaged clutter was still not perfectly smooth, some error is to be expected in using this method, as a decision must be made as to the range that the given threshold was exceeded. The error in range estimation is not expected to be greater than half a nautical mile.

The measured digital levels were converted to received power using the procedure for target data and then the normalized radar cross-section (back-scatter coefficient) was calculated for a propagation factor, F, of 1.0. The sea clutter measurements showed a marked dependence on wind speed, with maximum clutter occurring on a fully-developed sea (i.e., sea state developed proportional to the wind speed present). The back-scatter coefficients for the different sea states were calculated and a comparison between these values and those given by Nathanson (1969) showed good correspondence in some cases of sea states and grazing angles and poor correspondence for others. These discrepancies could not be explained from the limited analysis of sea clutter carried out. It is expected that a more detailed analysis of the clutter will reveal a better-defined relationship to the Nathanson data. It was found in many cases that the trend in most of the sea clutter data was as expected. The antennas mounted higher on the derrick top gave greater amounts of clutter, with X-band giving the most clutter.

In the following ten figures (Figs. 5-3 to 5-12) a sample of the sea clutter back-scatter coefficients

plotted as a function of grazing angle are compared to data from Nathanson (1969) and Sittrop (1977). These curves are all for upwind directions for the derrick-mounted radars. Data was collected for all wind directions, however, it was only possible to provide this preliminary analysis within the present study. As such, it establishes the usefulness of the data base. All the data presented were recorded in long pulse mode (one microsecond pulse length).

For the most part the S-band data agrees fairly well with Nathanson's for higher wind speeds and significant wave heights (SWH) (see Figs. 5-3, 5-5, and 5-9), however for low grazing angles (i.e., less than 0.5 deg.), Nathanson's values are consistently higher and for medium grazing angles (i.e, from 0.5 to 1.0 deg.) Nathanson's values are consistently lower. X-band shows much lower back-scatter values compared to Nathanson for all wind speeds and significant wave heights. These values may be questionable considering the doubtful performance of this radar, even though they are, for the most part, greater than those for S-band. The X-band data shows the best agreement with Nathanson for high wind speeds. Figs. 5-6 and 5-12 demonstrate this agreement for grazing angles near 1.0 deg. Also plotted in Fig. 5-12 is the model of Sittrop (1977), which predicted larger values than those which were measured.

In conclusion, for the calculation of signal-to-clutter ratios for rig-mounted radars, the use of the Nathanson data may give pessimistic detection ranges. Using Nathanson's back-scatter coefficient for S-band, the signal-to-clutter ratio is given by

$$S/C = \frac{\sigma_t}{\sigma_c} \qquad (5.2)$$

where σ_t is the target cross-section and σ_c is the clutter cross-section. The latter is given by

$$\sigma_c = \frac{c\tau}{2R\theta}$$

where c = speed of light (m/s)
τ = pulse length (s)
R = range (m)
θ = beamwidth (deg. or radius).

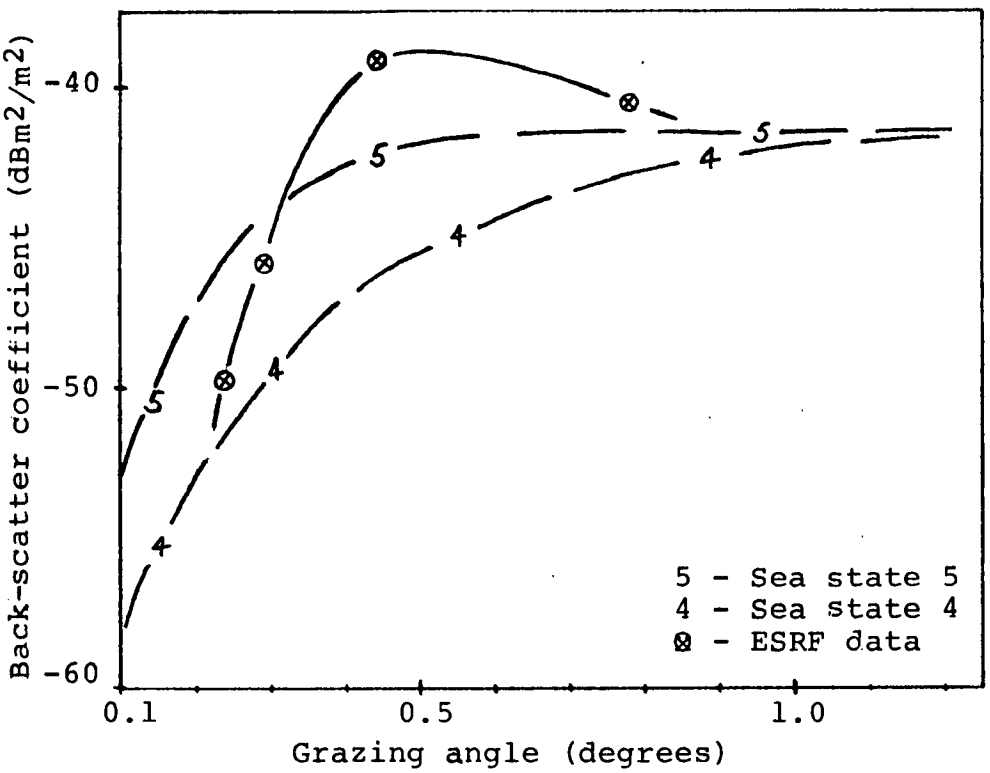

Fig. 5-3. Comparison of measured ocean back-scatter coefficients at S-band, for a significant wave height of 4.6 m and a wind speed of 30 knots, with values from Nathanson (1969) for sea states 4 and 5.

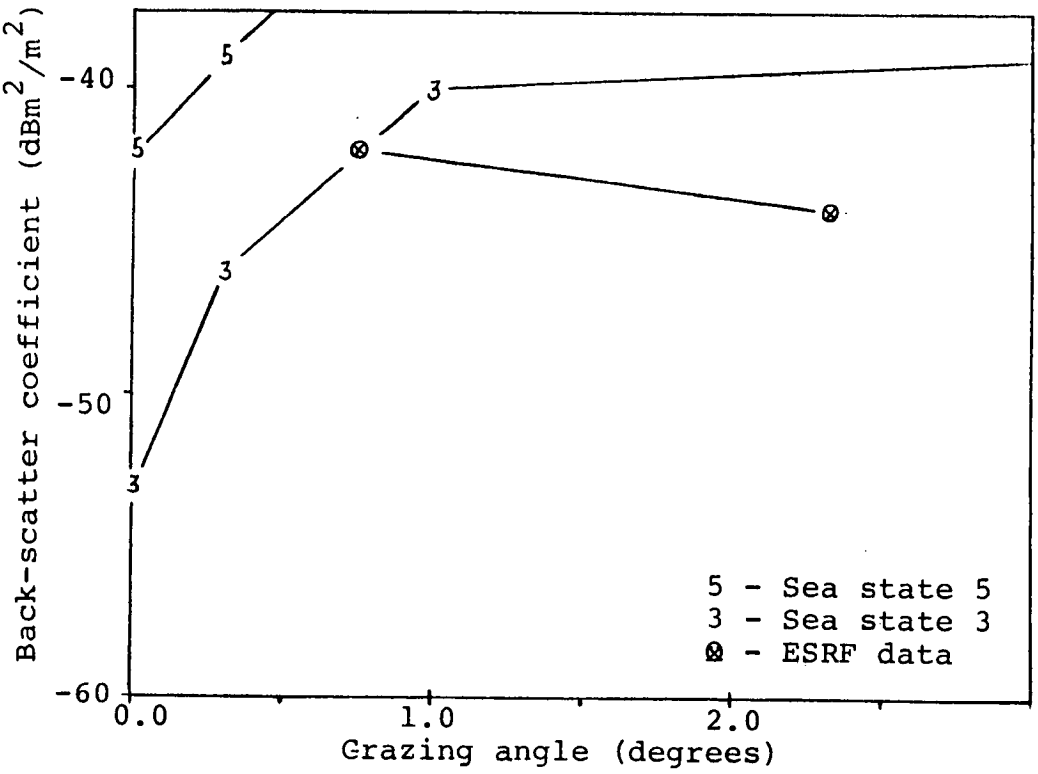

Fig. 5-4. Comparison of measured ocean back-scatter coefficients at X-band, as in Fig. 5-3, with values from Nathanson (1969) for sea states 3 and 5.

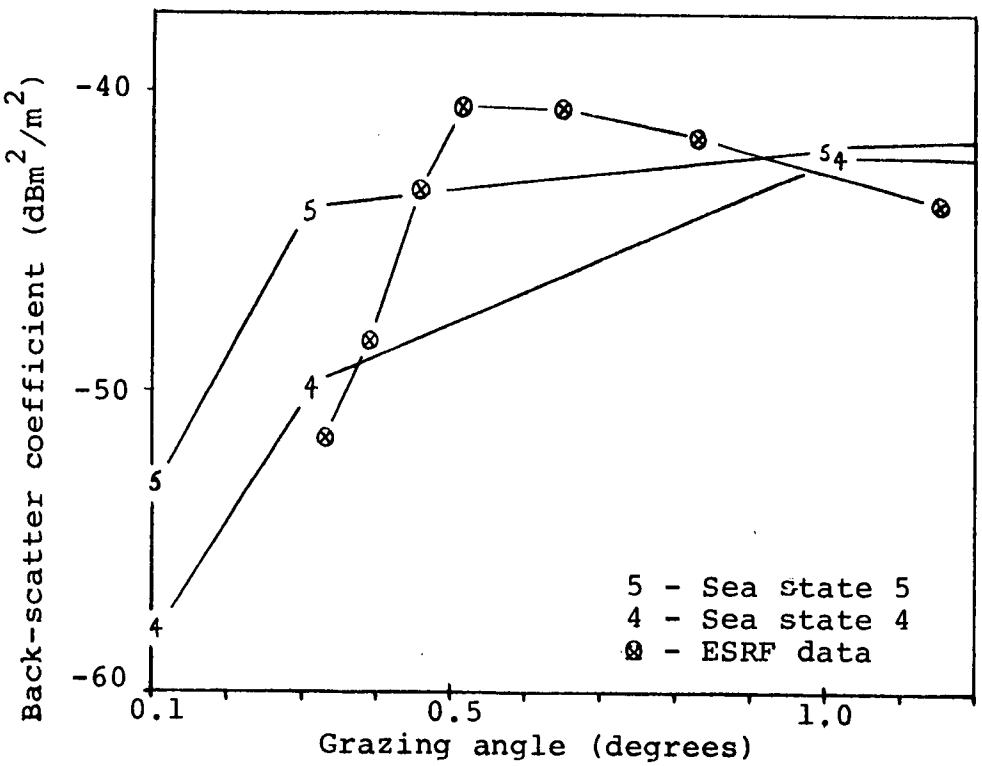

Fig. 5-5. Comparison of measured ocean back-scatter coefficients at S-band, for a significant wave height of 1.9 m and a wind speed of 43 knots, with values from Nathanson (1969) for sea states 4 and 5.

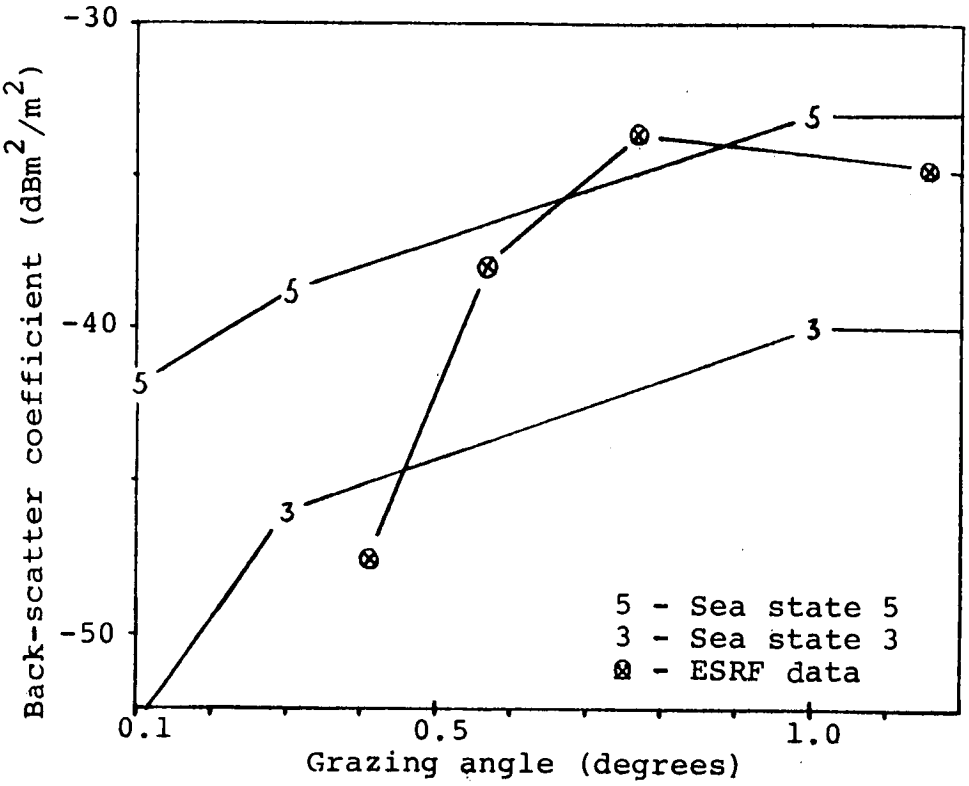

Fig. 5-6. Comparison of measured ocean back-scatter coefficients at X-band, as in Fig. 5-5, with values from Nathanson (1969) for sea states 3 and 5.

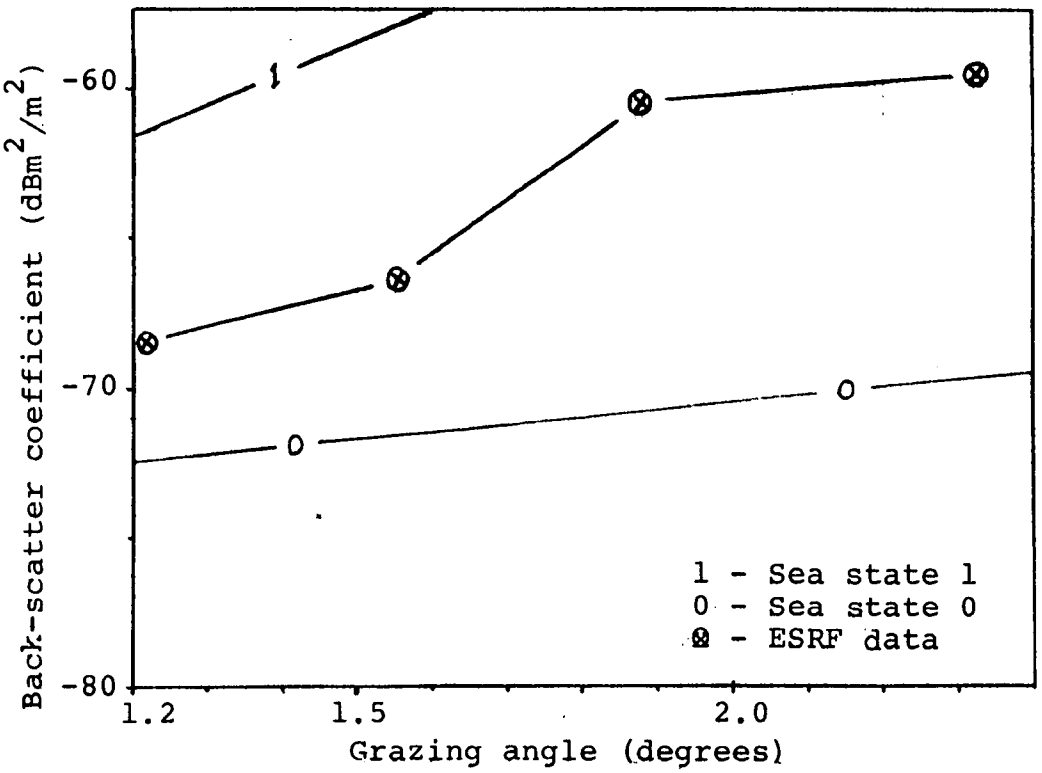

Fig. 5-7. Comparison of measured ocean back-scatter coefficients at S-band, for a significant wave height of 1.2 m and a wind speed of 30 knots, with values from Nathanson (1969) for sea states 0 and 1.

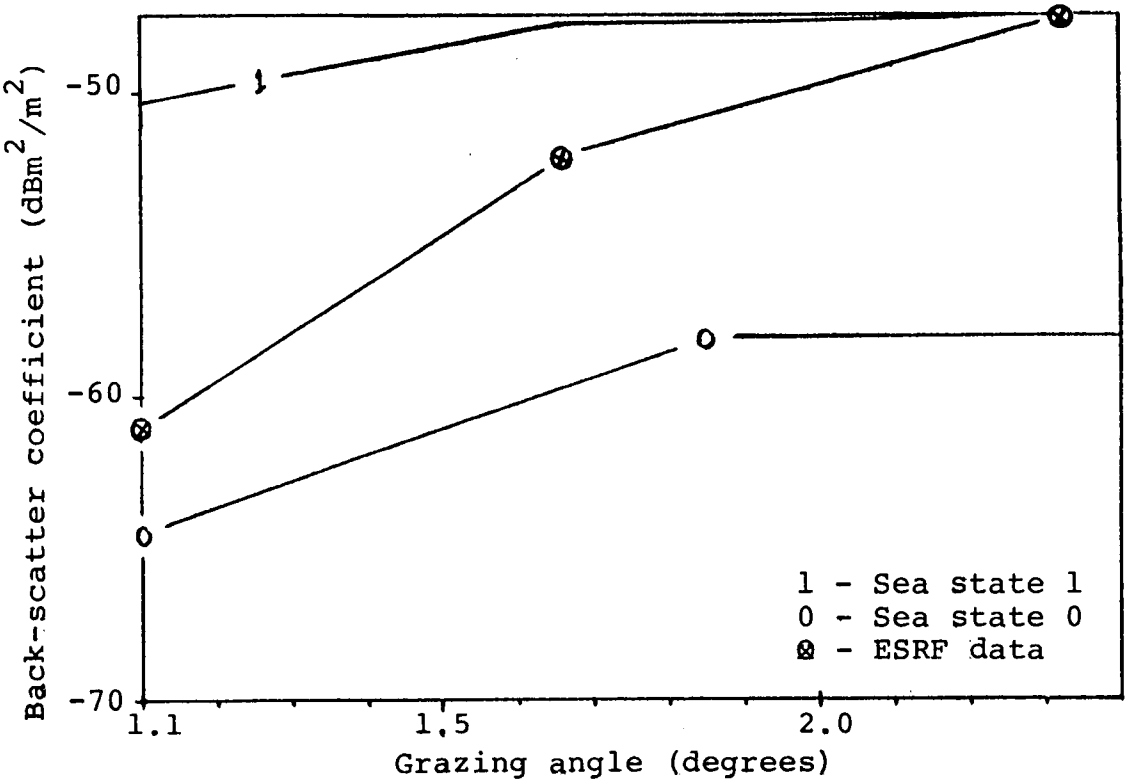

Fig. 5-8. Comparison of measured ocean back-scatter coefficients at X-band, as in Fig. 5-7, with values from Nathanson (1969) for sea states 0 and 1.

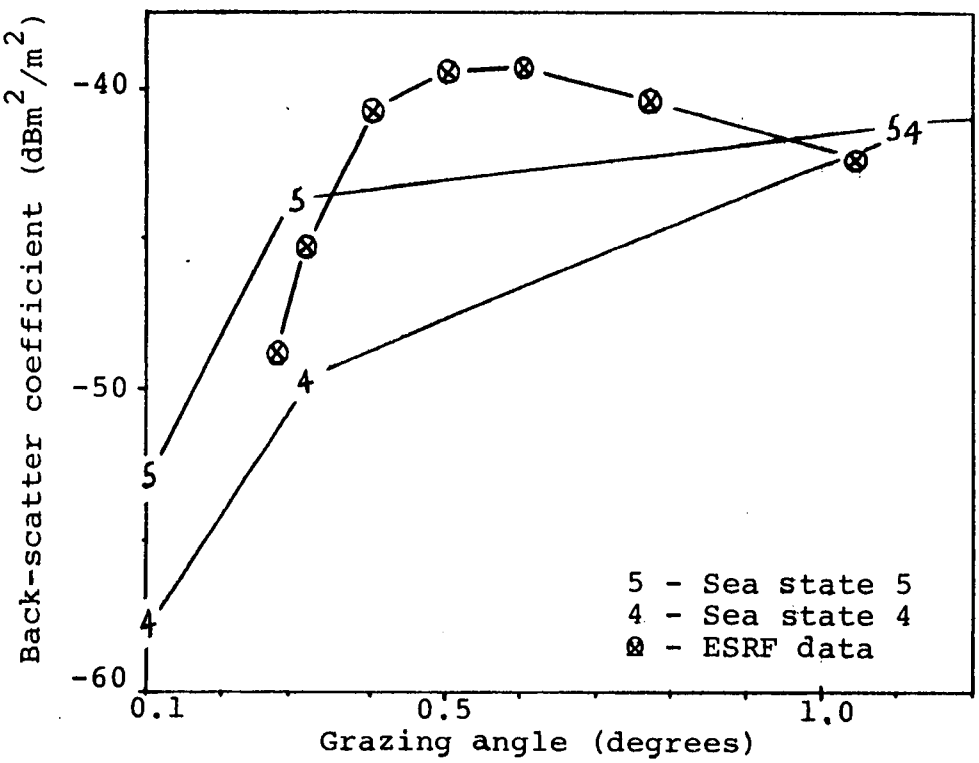

Fig. 5-9. Comparison of measured ocean back-scatter coefficients at S-band, for a significant wave height of 3.4 m and a wind speed of 30 knots, with values from Nathanson (1969) for sea states 4 and 5.

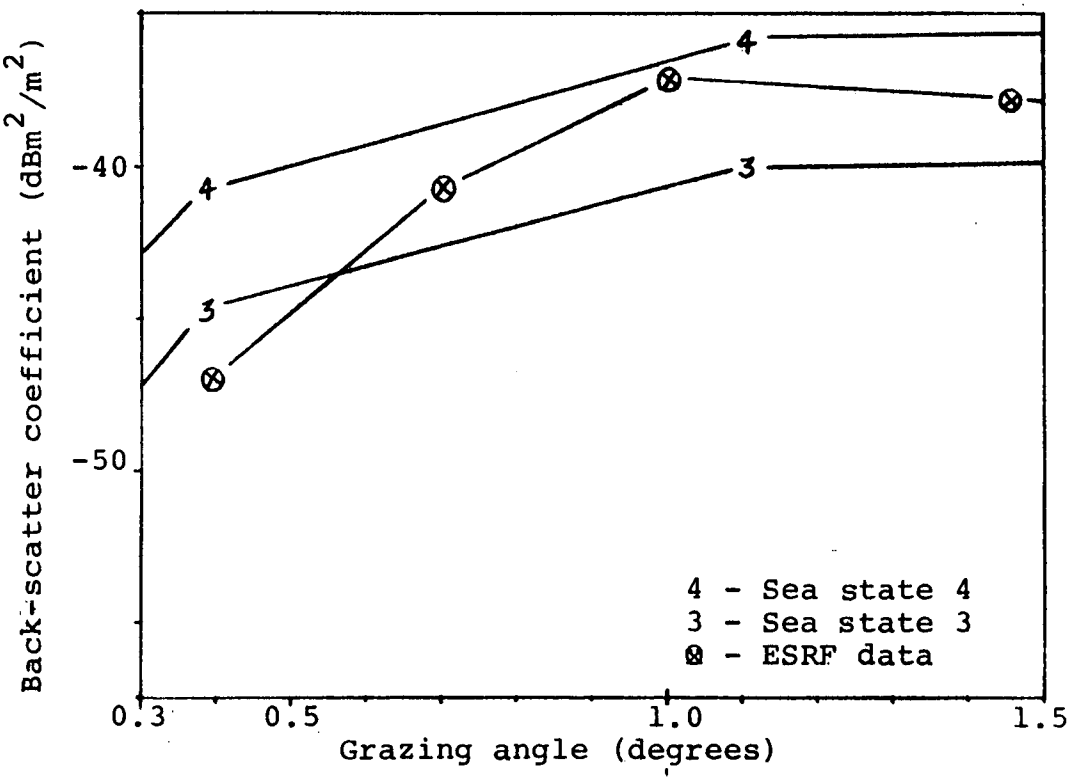

Fig. 5-10. Comparison of measured ocean back-scatter coefficients at X-band, as in Fig. 5-9, with values from Nathanson (1969) for sea states 3 and 4.

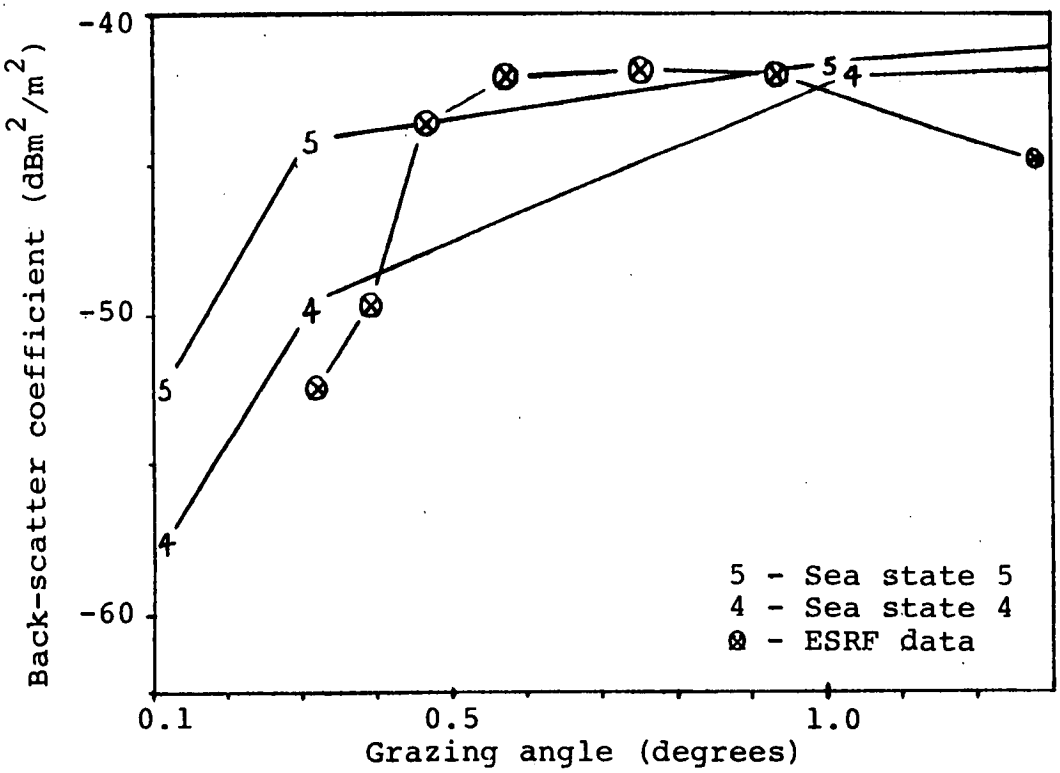

Fig. 5-11. Comparison of measured ocean back-scatter coefficients at S-band, for a significant wave height of 2.6 m and a wind speed of 37 knots, with values from Nathanson (1969) for sea states 4 and 5.

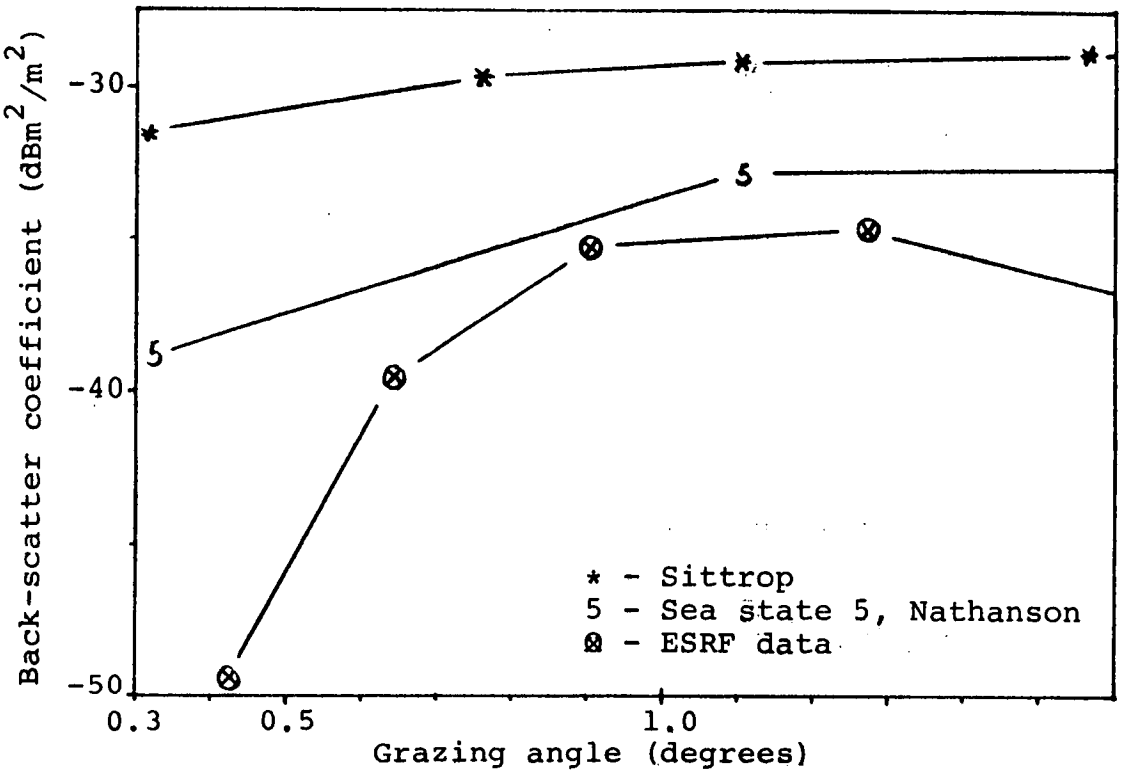

Fig. 5-12. Comparison of measured ocean back-scatter coefficients at X-band, as in Fig. 5-11, with values from Nathanson (1969) for sea state 5 and values from Sittrop (1977) for a 37 knot wind.

For the growler T191 at a range of 4.2 naut mi, SWH of 1.6 m, and wind speed of 14 knots (corresponding to sea state 3), with 0.11 m^2 cross-section (from Table 5-6), equation 5.2 predicted an undetectable S/C ratio of -0.7 dB for a one microsecond pulse.

During the analysis it was found that the sea clutter around this target was below the receiver noise level and the signal-to-noise ratio was found to be 9.6 dB, which in practice enabled fairly reliable detection (this point is discussed in the next section).

It is, therefore, concluded that while the Nathanson (and other similar) data is useful over certain ranges (usually around a one-degree grazing angle, approximately 2.3 naut mi for derrick-mounted radars), it is necessary to investigate the back-scatter coefficients for smaller grazing angles further. It is possible that the field data set collected did not reflect the "average" situation which the Nathanson data was intended to depict. In order to predict the detection ranges for small ice hazards in sea clutter effectively, all parameters which affect sea condition should be taken into account, including wind speed, duration, and direction.

5.6 ENVIRONMENTAL CONDITIONS

As discussed in Section 5.3, the major effect the environmental conditions had on propagation was the generation of ducting and subrefractive conditions in the lower atmosphere. There were no instances observed or recorded when rain influenced detection, and it would appear from the steadiness of the rig and support vessel data that even the heaviest fog does not effect received power significantly. Therefore, in these situations subrefraction is more of a problem than attenuation. Table 5-8 contains the environmental conditions for each tape and date.

TABLE 5-8

Meteorological and ocean conditions during the field program.

Date (1984)	Tape no.	SWH (m)	WS (knot)	WD (°rel.)	VIS (naut mi)	AT (°C)	ST (°C)	DPT (°C)	BP (mb)	Period (sec)
28 Apr.	19A	2.2	24	100	Poor	2.0	1.2	2	1017.9	-
08 May	20	4.6	30	328	8.0	2.0	0.0	1	998.0	-
08 May	21	3.5	28	280	>5.0	1.8	1.6	-	1001.2	6.0
08 May	22	3.0	30	345	6.0	2.0	1.8	1	1004.8	7.0
08 May	23	3.4	30	335	10.0	2.0	1.5	1	1010.4	6.7
09 May	24	3.4	30	335	10.0	2.0	1.5	1	1010.4	6.7
09 May	25	3.1	30	335	10.0	1.0	1.5	0	1012.5	6.5
09 May	27	2.4	22	350	15+	4.0	1.5	0	1017.0	6.0
10 May	28	2.7	11	355	15+	2.0	1.3	0	1021.5	7.0
11 May	29	1.9	43	254	8.0	2.0	1.5	4	1019.0	5.7
11 May	30	2.5	42	252	.5	5.0	2.2	5	1018.0	6.0
11 May	31	2.2	12	330	9.0	4.0	2.0	4	1021.7	6.8
12 May	32	1.6	14	330	12.0	4.0	2.0	4	1023.0	6.5
12 May	34	1.4	2	145	12.0	7.0	3.8	4	1029.5	7.4
12 May	36	0.9	13	243	0.3	4.0	2.7	4	1030.0	8.0
04 May	38	1.1	25	273	0	5.0	3.1	5	1029.2	9.6
15 May	39	1.2	30	263	0	4.5	3.6	5	1028.0	8.0
15 May	40	1.1	30	275	0	5.0	3.3	5	1026.5	6.1
16 May	41	1.2	34	253	1/8	6.0	3.9	6	1022.1	6.6
16 May	42	1.6	43	250	1/8	5.8	4.6	6	1021.4	5.0
16 May	43	1.6	43	250	1/8	5.8	4.6	6	1021.4	5.0
17 May	44	2.0	38	253	0	6.0	4.2	6	1020.9	7.0
17 May	45	2.6	37	250	1/8-1/4	6.0	3.9	6	1023.5	7.2

SWH = significant wave height
WS = wind speed
WD = wind direction
VIS = visibility
AT = air temperature
ST = sea temperature
DPT = dew point temperature
BP = barometric pressure

6. PROBABILITY OF DETECTION

The received power values for icebergs, support vessels and drill-rig targets were converted to a signal-to-noise (S/N) ratio, referred to the demodulator (detector) input, by taking the difference between the received power and the measured MDS. This signal-to-noise ratio may then be used with Figs. A4-1 - A4-5 to find the probability of detection (P_d) for a particular probability of a false alarm (the exact procedure was described in the subsection on the detection process). Alternatively, the radar cross-sections of the targets may be used with the radar model to plot the signal-to-noise ratio as a function of range.

For example, the bergy bit, T191, at a range of 4.2 naut mi (7.8 km) gave a received signal of 86 dBm for radar X1 which corresponded to a signal-to-noise ratio of 11 dB at the detector input (MDS = 97 dBm). This S/N is given for single pulse detection. For more than one pulse a scanning loss of 1.5 dB must be used, giving an effective S/N over n pulses of 9.5 dB. For n = 3.7 (see Table 4-1 for X1) and $P_{fa} = 10^{-6}$, the probability of detection of this target was 0.5 (from Fig. A4-2). This same target with radar S1 had a S/N ratio of 9.6 dB, however, as n = 9.2 for S1 and the effective S/N for n pulses is 8.1 dB (i.e., 9.6 dB minus 1.5 dB scanning loss) the probability of detection would be 0.70 (Figs. A4-2 and A4-3).

Using the calculated radar cross-sections of targets for the X1 and S1 radars, and the model input parameters as given, a plot of S/N ratio as a function of range was obtained using the radar model. The results, which do not take ducting into account, are presented in Figs. 6-1 and 6-2. The S/N ratios for both of these curves at 7.8 km correspond to the those values given above. These two plots can be used to find the maximum range of detection. This was accomplished by deciding on an acceptable P_d and probability of false alarm, P_{fa} (usually 10^{-6}), and by using Figs. A4-1 to A4-5 to find the required S/N ratio.

If, for example, the range is required where the P_d for S1 reaches .5, Fig. A4-2 gives a required S/N of 5.5 dB for 9.2 pulses ($P_{fa} = 10^{-6}$), and adding the previously-mentioned scanning loss of 1.5 dB, gives a total of 7 dB for the required S/N ratio. This corresponds

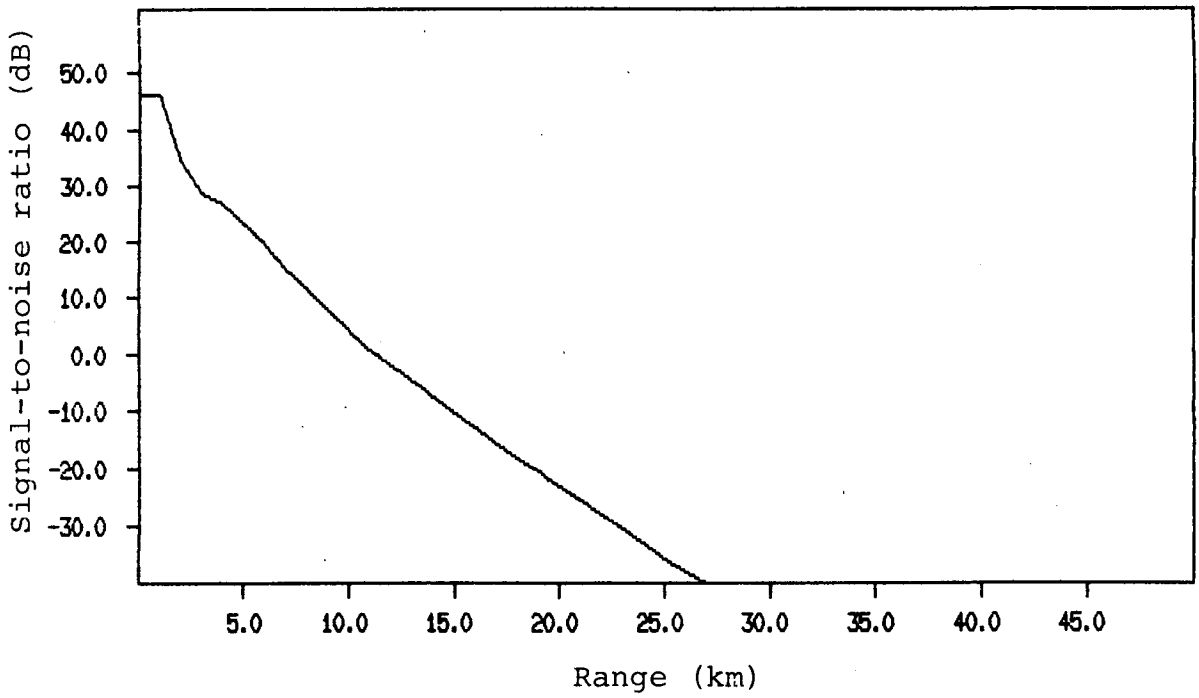

'S'	Frequency band
27000.0	Transmitter power (Watts)
26.	Antenna gain (dB)
.1	Radar wavelength (m)
3.5	Receiver noise figure (dB)
825.	Pulse repetition frequency (Hz)
30.	Antenna rotation speed (r.p.m.)
1.0	Pulse length (microsec.)
2.0	Horizonal beamwidth (deg.)
30.0	Vertical beamwidth (deg.)
5.E6	Receiver bandwidth (Hz)
.5	Transmission line loss (dB)
.0	Scanning loss (dB)
1.0	Additional losses (dB)
.5	Receiving line loss (dB)
1.0	Antenna loss (dB)
2	Iceberg length (m)
2	Iceberg width (m)
2	Iceberg height (m)
0.11	Radar cross-section (m2)
'VIS'	Meteorological condition
1.6	Significant wave height (m)
0.0	Air temperature (°C)
6	Probability of false alarm (exponent)
1	Swerling fluctuation case
75.0	Antenna height (m)
2.0	Target height (m)
.1	Target base height (m)
20000.	Visibility (m).

Fig. 6-1. Model Output for a bergy bit (T191) using the derrick-mounted S-band radar, S1.

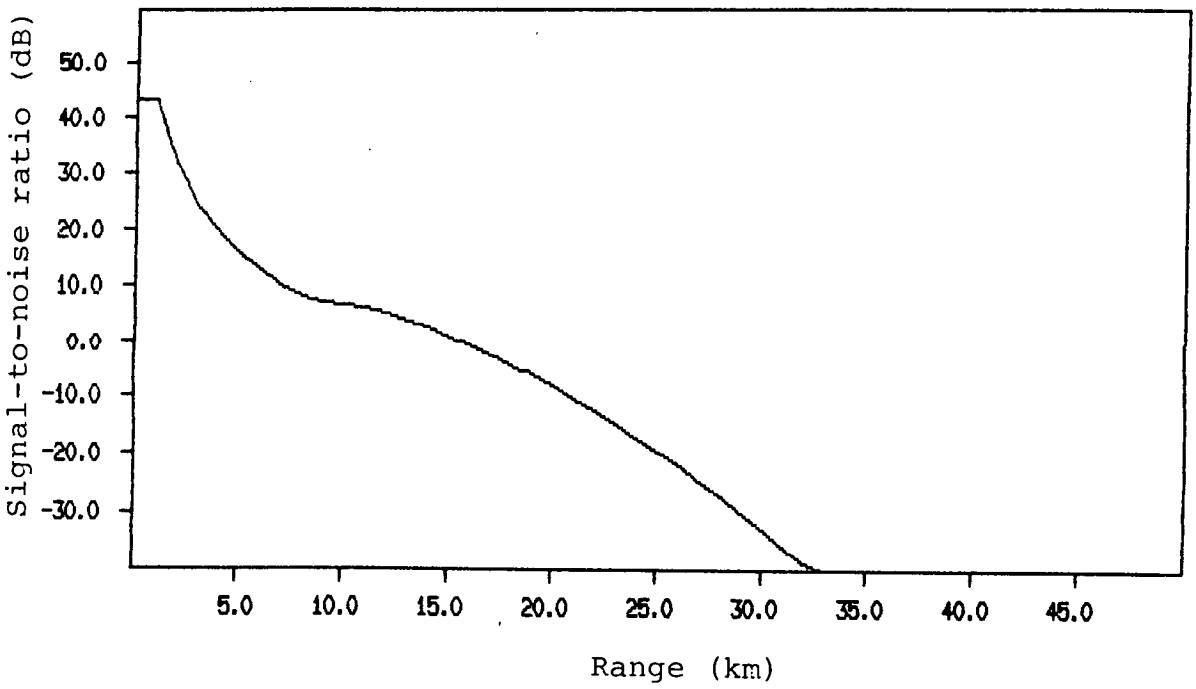

'X'	Frequency band
18500.	Transmitter power (Watts)
32.	Antenna gain (dB)
.032	Radar wavelength (m)
6.0	Receiver noise figure (dB)
825.	Pulse repetition frequency (Hz)
30.	Antenna rotation speed (r.p.m.)
1.0	Pulse length (microsec.)
0.8	Horizonal beamwidth (deg.)
25.0	Vertical beamwidth (Deg.)
5.E6	Receiver bandwidth (Hz)
.5	Transmission line loss (dB)
.0	Scanning loss (dB)
1.0	Additional losses (dB)
.5	Receiving line loss (dB)
1.0	Antenna loss (dB)
2	Iceberg length (m)
2	Iceberg width (m)
2	Iceberg height (m)
0.11	Radar cross-section (m^2)
'VIS'	Meteorological condition
1.6	Significant wave height (m)
0.0	Air temperature (°C)
6	Probability of false alarm (exponent)
1	Swerling fluctuation case
75.0	Antenna height (m)
2.0	Target height (m)
.1	Target base height (m)
20000.	Visibility (m).

Fig. 6-2. Model output for a bergy bit (T191) using the derrick-mounted X-band radar, X1.

to a detection range of 13.5 km (7.3 naut mi). Similarly for a detection probability of 0.9, the detection ranges for both X1 and S1 will be 5.5 km (2.9 naut mi).

Although the model takes into account the significant wave height when the data was recorded (in this case SWH = 1.6 m), this discussion was based on using the signal-to-noise ratio as opposed to the signal-to-clutter ratio. This method was chosen, primarily, because the use of tabular sea clutter values appear to overestimate the sea values.

Tables 6-1 to 6-4 present the probabilities of detection for each iceberg target recorded by the four radars. The methods previously outlined were used to calculate the 0.5 and the 0.9 probability of detection ranges for the environmental conditions. The iceberg parameters were given previously in Table 5-1. The probability of detection ranges are shown graphically in Fig. 6-3 for the derrick-mounted S-band radar.

Comparison of the detection ranges in these four tables confirms again that the derrick-mounted S-band radar outperformed the other radars. From Table 6-1, the model predicted typical detection ranges for medium icebergs (under non-ducting conditions) to be 13.5 to 16.7 naut mi. This conclusion was reached by considering the stability of the radar data for support vessels and drilling rig under all the environmental conditions experienced. Out to 11 naut mi the returns were stable, beyond this range propagation was variable and varied more with increasing range. This variability was demonstrated by the abnormally large radar cross-sections of iceberg targets in Section 5.4. Therefore, using only radar cross-sections for icebergs within the stable range (i.e., less than 11 naut mi) the prediction of detection range for non-ducting situations can be determined. Using these predicted ranges to indicate the existence of a surface duct for medium icebergs revealed that the ducting model predicted the presence of a duct correctly about 85% of the time (i.e., it was proposed that detection beyond about 17 naut mi range for a medium iceberg was due to ducting).

There was not enough field data to form conclusions about the probability of detection of smaller icebergs, however, for bergy bits and growlers maximum detection ranges of less than 11 naut mi are expected and these probably would be unaffected by such propagation phenomena.

TABLE 6-1

Probability of detection and detection range for icebergs using the derrick-mounted S-band radar, S1.

Iceberg								
		Size (M)					Detection range (naut mi)	
Code	Type	L	W	H	Range (naut mi)	P_d(pfa)[a]	P_d(.5)[b]	P_d(.9)[b]
T166	MDD	90	80	26	21.6	.75(-12)	22.4	20.0
T167	MPI				19.5	.75(-10)	20.0	18.7
T168	MWD	75	59	20	18.0	.75(-10)	19.7	17.5
					10.0	.75(-10)	15.0	8.9
					8.9	.90(-12)	15.4	9.2
					8.9	.95(-12)	16.5	14.3
					8.0	.95(-10)	15.4	9.2
					19.0	.90(-6)	22.0	19.4
T175	MDO	96	54	15	10.2	.90(-6)	13.9	10.1
					10.5	.95(-6)	13.4	12.4
					9.5	.75(-10)	13.5	8.1
					8.6	.95(-6)	15.1	11.6
					18.3	.95(-12)	21.9	19.4
T181	MDD	98	73	22	14.0	.95(-12)	20.4	17.8
					17.0	.95(-6)	20.4	17.8
T187	SDD	20	15	6	7.9	.90(-6)	10.3	7.9
					13.3	.95(-12)	20.0	17.5
					17.4	.75(-6)	18.5	16.5
T188	MDD	30	25	20	7.5	.95(-12)	16.7	13.0
T191	GRL	2	2	2	4.2	.75(-5)	4.6	3.4
T195	SDD				21.8	.75(-5)	22.7	20.0
T196	MDD	38	38	12	21.6	.50(-12)	24.6	19.7
T197	MDD	61	58	24	12.4	.95(-6)	19.2	16.6
1277	MTA	90	55	12	16.5	.95(-6)	19.2	17.3
					17.5	.95(-12)	24.3	22.4
					16.1	.25(-8)	15.1	13.4

[a] The exponent for the probability of a false alarm.
[b] The probability of a false alarm is 10^{-6} for P_d(.5) and P_d(.9) columns.

TABLE 6-2

Probability of detection and detection range for icebergs using the derrick-mounted X-band radar, X1.

Iceberg								
		Size (M)					Detection range (naut mi)	
Code	Type	L	W	H	Range (naut mi)	P_d(pfa)[a]	P_d(.5)[b]	P_d(.9)[b]
T166	MDD	90	80	26	21.6	-	19.4	13.0
T168	MWD	75	59	20	8.9	0.90(-8)	17.0	9.9
T187	SDD	20	15	6	13.3	7.95(-12)	19.2	17.8
T188	MDD	30	25	20	7.5	0.50(-8)	8.8	4.9
T191	GRL	2	2	2	4.2	0.50(-8)	4.9	2.7

[a] The exponent for the probability of a false alarm.
[b] The probability of a false alarm is 10^{-6} for P_d(.5) and P_d(.9) columns.

TABLE 6-3

Probability of detection and detection range for icebergs using the deck-mounted S-Band Radar, S2.

Iceberg								
		Size (M)					Detection range (naut mi)	
Code	Type	L	W	H	Range (naut mi)	P_d(pfa)[a]	P_d(.5)[b]	P_d(.9)[b]
T175	MDO	96	54	15	10.5	.50(-8)	10.8	9.2
T187	SDD	20	15	6	13.3	.50(-10)	14.6	12.7

[a] The exponent for the probability of a false alarm.
[b] The probability of a false alarm is 10^{-6} for P_d(.5) and P_d(.9) columns.

TABLE 6-4

Probability of detection and detection range for icebergs using the deck-mounted X-band radar, X2.

Iceberg								
		Size (M)					Detection range (naut mi)	
Code	Type	L	W	H	Range (naut mi)	P_d(pfa)[a]	P_d(.5)[b]	P_d(.9)[b]
T166	MDD	90	80	26	21.6	0.25	21.0	19.4
T168	MWD	75	59	20	8.9	.75(-8)	12.4	7.5
					8.9	.50(-8)	9.6	5.1
					8.0	.25(-8)	7.0	4.0
T175	MDO	96	54	15	10.5	.75(-12)	NA	NA
T187	SDD	20	15	6	13.3	.95	19.3	13.5

[a] The exponent for the probability of a false alarm.
[b] The probability of a false alarm is 10^{-6} for P_d(.5) and P_d(.9) columns.

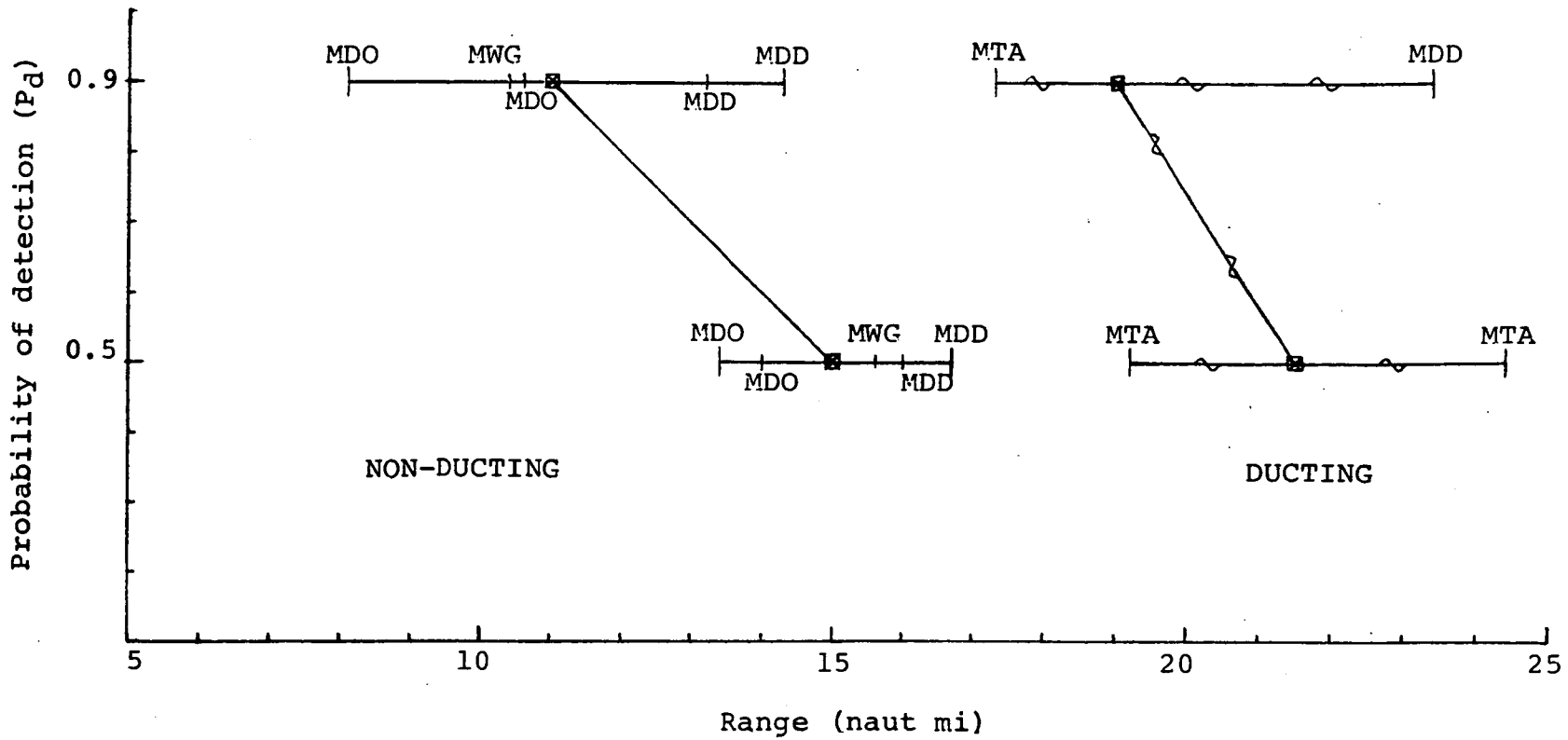

Fig. 6-3. Detection range for medium icebergs using a derrick-mounted S-band radar, for ducting and non-ducting conditions.

7. CONCLUSIONS

The study was undertaken to assess the iceberg detection capability of existing marine radars. Despite equipment failures and logistical problems, a comprehensive field evaluation was successfully completed. Radar data for icebergs, support vessels, and drilling rigs were collected from the semi-submersible Sedco 706 drilling rig for two radar frequencies (3050 and 9410 MHz) and at derrick top and deck antenna heights in a variety of environmental conditions. This data identified certain environmental effects which affected detectability, such as ducting and subrefraction, and provided valuable information on sea clutter. The calibration of the radar systems permitted the calculation of iceberg radar cross-sections and a normalized radar cross-section for the the ocean in a wide range of sea conditions.

The derrick-mounted S-band radar detected and tracked four times as many icebergs as the X-band radar at the same height and the X- and S-band radars with antennas at 35 and 45 m. This large performance margin was due to some extent to the poor condition of the other radars. The two lower deck level radars had not been recently serviced and performance deficiences were identified. The derrick-mounted X-band radar experienced magnetron and receiver front-end problems. A mismatch between the front-end low noise preamplifier and the intermediate frequency stage is suspected. This conclusion was reached after ruling out propagation effects and considering the radar's performance in detecting large and small targets. The unit continuously outperformed all other radars when detecting the Sedco 710 drilling rig, indicating the receiver's ability to lock on to the carrier frequency when the signal is large. The same was true for vessel targets close to the radar. The deck-mounted S-band radar demonstrated the worst performance.

Ducting or superrefraction was responsible for the maximum detection ranges during the experiment. On one occasion support vessels were detected at a range of 35 naut mi and a small iceberg was detected at a range of 22 naut mi, both of which were well beyond the usual radar horizon. Clear, cool days usually provided ducting conditions, with typical detection ranges for medium icebergs, using the derrick-mounted S-band radar, of from 17 to 20 naut mi. During foggy weather, calculations for the refractivity in the lower atmosphere almost always

indicated that subrefractive conditions existed. In periods of subrefraction, the detection ranges for support vessels using the derrick-mounted S-band radar were observed to decrease to 17 to 18 naut mi from a usual range of 20 to 22 naut mi. The X-band radar on the derrick top usually detected support vessels and icebergs at ranges of several miles less than the S-band radar. The detection of medium icebergs during subrefractive conditions was limited to less than 17 naut mi. From the data analysis it was evident that anomalous propagation is one of the major factors influencing iceberg detection beyond 10 naut mi. Furthermore, the worst or shortest detection ranges occurred in periods of heavy fog. These results are similar to the findings of Budinger (1960).

Although no data was obtained for detectable targets in sea clutter, there were two reports of growlers at 0.6 and 2.5 naut mi from the Sedco 706, which were not detected because of sea clutter returns. While these two instances serve presently to remind one of what these radar systems are incapable of detecting, it is hoped that these data may be used in future work to assess processing techniques for iceberg detection in sea clutter.

The comparison of the normalized radar cross-section (back-scatter coefficient) for the ocean derived from the collected data with published values and models revealed that the sea clutter problem needs further analysis. Agreement between these sets of data was very good in some cases and very poor in others. It is suspected that this may be due to the average nature of the published values and models. It is, therefore, necessary to assess and modify existing sea clutter models and compare in detail with data collected from rig and ship-based radars operating in the Hibernia area. This will ensure that reliable iceberg detection models are available for operational risk assessment.

The calculated values of iceberg radar cross-section were compared to the icebergs' average cross-sectional area. While there were not sufficient icebergs to draw any specific conclusions, it is interesting to note that the maximum deviation from the relationship presented by Budinger (1960) is 10 dB, with 67% of the data falling within 5 dB of Budinger's values.

8. RECOMMENDATIONS

Major improvements in the reliability of marine radars presently in use for iceberg detection may be achieved by both the implementation of effective equipment maintenance and performance monitoring procedures, hardware improvements, and the incorporation of signal processing techniques to increase the signal-to-clutter and signal-to-noise ratios.

8.1 EQUIPMENT MAINTENANCE

The Racal-Decca dual X- and S-band radar system on board the Sedco 706 is still the most sophisticated radar system in use on the Grand Banks for iceberg monitoring. By combining the video signals from both frequencies, target fading may be decreased, providing far more reliable detection and continuity of monitoring. Unfortunately, in the 1984 field program, this system never demonstrated this capability. Although the detection capability of the S-band unit was exceptional, the X-band performed very poorly and it is believed that this unit was malfunctioning.

It would seem to be of little value to propose new systems or techniques to improve iceberg detection when presently-used equipment is not maintained on a routine basis. In addition the equipment must be used effectively by the operators: they should be informed of the systems' capabilities and limitations, such that they maximize the detection capability of the existing system. This is particularly true for detection in sea clutter situations. For operational iceberg detection it is recommended that:

a) Regular equipment maintenance be performed.

b) In conjunction with the maintenance, a performance evaluation of the system should be carried out on a regular basis. This could be as simple as having a support vessel receed from the rig until its radar return is no longer received by each of the radars. Although this would not provide quantitative information on radar performance, it would indicate when a particular radar was malfunctioning and which radar was performing best.

c) That operators of the equipment must be trained in the basic principles of iceberg detection, in different environmental conditions. This training should include the limitations and capabilities of specific pieces of hardware, such as automatic target acquisition and tracking systems.

8.2 HARDWARE IMPROVEMENT

Since the installed marine radars are quite advanced the only suggested improvement would be to increase the transmitter power, although this is not expected to improve the long-range detection of larger icebergs significantly, or the detection of smaller icebergs in sea clutter. The other alternative is to redesign the radar hardware to provide additional detection capability. The ongoing work at the Communications Research Laboratory, McMaster University, is addressing this problem.

8.3 SIGNAL PROCESSING

There are other proven techniques for improving target detection that are not being used, which have resulted from advances in computer technology and digital signal processing. Several improvements that will increase detection capability include:

a) Implementation of real-time radar data processing to provide pulse-to-pulse and scan-to-scan processing including:

- averaging
- correlation
- filtering.

b) Combine data for more than two radars. Presently the dual band system combines the data in real time but by introducing a small delay, it would be possible to synchronize three or four radars digitally. This would be advantageous as the lower elevation radars could provide detection close to the rig (since sea clutter is less for lower antennas) and the derrick-mounted radars would provide long-range coverage. It is expected that

this height, as well as frequency diversity would provide more reliable detection and tracking of icebergs.

8.4 FUTURE STUDIES

The present assessment of marine radar for iceberg detection is far from complete. Although the number of icebergs recorded in the experiment was not large, the quality of the radar data has proved to be good. The detection ranges achieved regularly from the Sedco 706 exceed the detection ranges which would be expected from other vessels. The following recommendations are directed towards the future work for the evaluation of marine radars for iceberg detection:

a) An ongoing program to acquire a iceberg radar cross-section data base for icebergs in the Hibernia area should be implemented. Icebergs on the Grand Banks are older, smoother, and, in general, more difficult to detect with radar than less weathered icebergs further north.

b) Investigate the present data set for the dependence of sea clutter on wind speed, wind direction, and significant wave height. This analysis would help to choose suitable clutter models for use in the analysis of rig-based radar systems. The development of an analytical model for sea clutter would aid in optimizing radar system design and operational considerations (i.e., antenna height, etc.).

c) Collect, on a continuous basis, the meteorological parameters required to calculate evaporation duct parameters. This would develop a long-term propagation guide for operational use.

d) Undertake a data collection program to obtain radar data for small ice targets in sea clutter.

e) Investigate data processing techniques that show promise for increasing signal-to-noise and signal-to-clutter ratios.

f) Investigate automatic target detection methods which are applicable to this problem.

APPENDIX 1

Discussion of Candidate Platforms

APPENDIX 1
DISCUSSION OF CANDIDATE PLATFORMS

The field program phase of the study to assess the detection capability of standard marine radar may be carried out on either an offshore drilling platform or a workboat. Each of these platforms offer distinct advantages and disadvantages. The main advantage of using a workboat over a stationary drilling platform is that comprehensive iceberg detection versus range experiments may be carried out. The derivation of this type of statistic from a stationary platform will depend greatly on the behavior of the particular target (i.e. advancing towards the rig or receding from the rig).

The other major advantage of the workboat is also related to its mobility in that it would be possible to pursue targets rather than wait for them to come within radar range. Unfortunately, the mobility of the workboat also causes problems. These include mainly radar platform instability. In calm seas this may not pose much of a problem, however, in rough seas when accurate data is most desired, the pitch, roll, yaw and heave of the workboat will introduce severe distortions in the radar data set. These types of distortions are virtually impossible to remove from the data, thereby making derivation of the statistics on iceberg detection versus sea state highly unreliable. In addition, at times when data should be collected (i.e. severe environmental conditions), the workboat may be required to perform its normal operational duties. Finally, most of these workboats offer only dual radar systems as opposed to the systems employed on the drilling platforms, most of which have four radars. The advantage of the four radar system is that at least two antenna heights for each frequency (X-band and S-band) may be used to collect data for iceberg detection versus antenna height statistics.

Therefore, to provide the highest probability of success, it is recommended that a drilling platform be employed for the field program.

There are presently four drilling platforms operating on the Grand Banks. They include the Zapata Ugland, the Sedco 706, the John Shaw and the West Venture. The Zapata Ugland will soon finish its contract to Mobil Oil Ltd. and is not expected to return to the Grand Banks area. The Sedco 710 which is presently in Marystown, Newfoundland, may be a considered candidate platform, however, its winter drilling site is unknown (possibly Scotia Shelf). The Bow Drill 3 presently being constructed in Saint John, New Brunswick, may possibly join the Sedco 706, the John Shaw and the West Venture. At the end of this appendix the specifications of the

radar systems on each of these rigs are given. Table A1 contains a summary of these specifications. Of the five candidate platforms, the John Shaw, the Sedco 706 and the Sedco 710 all have four radars while the other platforms have three.

The West Venture uses the sophisticated Racal-Decca combined S and X band systems, however, only one additional X-band system is available on board. The two X-band systems have only 4 meters difference in antenna heights making comparisons of detection versus antenna height difficult.

The Bow Drill 3 also has only three radar systems, however, there is good height diversity on the S-band systems and the high power X-band system utilizes a switchable circular/horizontal polarization antenna. There are certainly merits in utilizing this system to verify the operational ability of the circular polarization to reject rain echos and, hence, improve the signal to clutter ratio in the presence of rain. Although this is not a direct requirement of this study, it certainly concerns the detection capability of existing marine radar. At the time of the writing of this report only approximate information on the antenna location could be obtained. From discussions with Sperry and the Saint John Marine Consultants it was identified that the X-band CP/HH antenna and an S-band antenna would be located part way up the derrick at about 60 meters height and the remaining S-band antenna on the transformer house at about 35 meters. All the radar equipment on the Bow Drill 3 is manufactured by Sperry Marine.

The Sedco 710 has four standard Decca radars on board interswitched through a Decca ARPA (Automatic Radar Plotting Aid) unit. There is very little height difference among the radar antennas and their positions are such that overlapping coverage for the four systems is not favourable for near-simultaneous data collection with all four radars.

On the John Shaw, there are three X-band radars and one S-band radar. One of the X-band radars and the S-band radar comprise the Racal-Decca combined S/X band system. This system is mounted on the derrick top for complete 360° coverage. The other two X-band systems are virtually identical and their antennas are located at the same height. Moreover, even considering the coverage of both of these X-band radars, there is still a large blind sector that neither can see (i.e. 35°-140°). This system would not be suitable for this program.

The remaining candidate platform, the Sedco 706, also has the Racal-Decca Combined S and X band System with the dual antenna mounted on the derrick top for 360° coverage. The other two radars are S and an X band systems with antennas

TABLE A-1

Oil rig radar specification summary.

Rig	Radar					Special Features
	Power (kw)	Frequency Band	Antenna Height (meters)	Make	Coverage (degrees)	
John Shaw	25	X	24	Raytheon	195-35	*Note 1
	25	X	24	Furuno	140-320	
	30	S	85	Decca	360	
	25	X	85	Decca	360	
Sedco 706	25	X	36	Decca	320	*Note 1
	30	S	33	Decca	300	
	25	X	85	Decca	360	
	30	S	85	Decca	360	
West Venture	25	X	36	Decca	340	*Note 1
	25	X	40	Decca	335	
	25	S	40	Decca	335	
Sedco 710	25	X	49	Decca	NA	
	30	S	49	Decca	NA	
	25	X	43	Decca	NA	
	30	S	43	Decca	NA	
Bow Drill 3	30	S	60	Sperry	NA	*Note 2
	50	X	60	Sperry	NA	
	30	S	35	Sperry	NA	

Note: 1. Racal-Decca Combined S/X System.

2. High power X-band has switchable horizontal or circular polarization.

mounted at about 33 meters and 36 meters respectively. The two X-band and two S-band antennas offer the best antenna height diversity of any of the considered platforms. In addition, the blind arc of the two lower radars is significantly smaller than for the John Shaw. The location of the transmitter and receiver with respect to the antennas on the combined S/X system is also favorable for radar transmitted power measurement and radar system calibration (i.e. approximately only 3 meters of wave guide between transmitter and antenna).

From these considerations, it is recommended that the Sedco 706 be considered the most preferable platform to perform the experiment. The Bow Drill 3 should be considered as the second choice. Although this rig has only one X-band radar, the circular polarization feature warrants consideration. Also, the height diversity between the two S-band systems is quite good.

Mobil

WEST VENTURE

Owner:	MOBIL
Model:	DECCA 2459 F/I A.R.P.A.
Radar Frequency:	F 3040-3060 I 9380-9440
Polarization:	HORIZONTAL BOTH
Peak Power:	F/30KW I/25W
Pulse length:	.05, .25, 1u SEC
PRF:	3300, 1650, 825
Antenna Gain:	F-26 db I-32db
Antenna Vert Beam Width:	F-38 deg i-20 Deg
Antenna Horz. Beam Width:	F-2 Deg I-0.8 Deg
Antenna Height:	130 FT. APPROX.
Antenna Rotation:	22 RPM
Rx noise factor:	F4DB I-7db
Signal Processing:	A.R.P.A.
Antenna Location:	20 Feet above Helideck Fwd mounted Decca 2459 Blind arc 25 deg astern.

Interswitched with

Owner:	MOBIL
Model:	DECCA RM 1229 C
Radar Frequency:	9380-9440 MHz
Polarization:	HORIZTONAL
Peak Power:	25 K.W.
Pulse Length:	0.5, .25, 1 u sec.
PRF:	3300, 1650, 825
Antenna Gain:	30 db.
Antenna Vert Beam Width:	20 Deg.
Antenna Horz Beam Width:	1.2 Deg
Antenna Height:	120 FEET
Antenna Rotation:	28 RPM
RX noise factor:	BETTER 10 db

Mobil

Signal Processing:	CLEAR SCAN V.P.I.
Display:	12 Inch.
Antenna Location:	20 FEET ABOVE MAIN DECK Aft mounted Decca 1229 C Blind Arc 20 deg fwd.

Mobil

SEDCO 710

Owner:	SEDPEX
Transciever:	X Band ONE FWD ONE AFT
Radar Frequency:	9380 - 9440 MHz
Polarization:	HORIZONTAL
Peak Power:	25 K.W.
Pulse Length:	.05, .25, 1 u SEC.
PRF:	3300, 1650, 825
Antenna Gain:	30 db
Antenna Vert Beam Width:	20 DEG
Antenna Horz Beam Width:	1.2 DEG
Antenna Height:	160 FEET (FWD), 140 FEET (AFT) APROX.
Antenna Rotation:	28 RPM
Rx Noise Factor:	BETTER 10 db
Transciever:	S Band ONE FWD ONE AFT
Radar Frequency:	3040-3060 MHz
Polarization:	HORIZONTAL
Peak Power:	30 KW
Pulse Length:	.05, .25, 1 u sec.
PRF:	33-0, 1650, 825
Antenna Gain:	27 db
Antenna Vert. Beam Width:	25 DEG
Antenna Horz. Beam Width:	2 DEG
Antenna Height:	160 FEET (FWD), 140 FEET (AFT) APROX.
Antenna Rotation:	22 RPM
RX Noise Factor:	BETTER 10 db

All four transcievers switchable to the ARPA 1630 Display.
Two Aft transcievers switchable to the A/C 1629 Display.

November 3, 1983

Husky/Bow Valley
Box 37, 215 Water Street
St. John's, Nfld.
A1C 6C9

Attention: Mr. E. Ratke

Dear Sir:

In answer to your correspondence of 2nd November 1983, I have listed the following answers as requested by Newfoundland and Labrador Petroleum Directorate winter drilling requirements.

SEDCO 706

Owner:	Sedco
Model:	DECCA RM 1229 C
Radar Frequency:	9380 - 9440 MHz
Polarization:	HORIZONTAL
Peak Power:	25 K.W.
Pulse Length:	.05, .25, 1 µ SEC.
PRF:	3300, 1650, 825
Antenna Gain:	30 db
Antenna Vert Beam Width:	20 DEG
Antenna Horz Beam Width:	1.2 DEG
Antenna Height:	120 FEET
Antenna Rotation:	28 RPM
Rx noise factor:	BETTER 10db
Signal processing:	CLEAR SCAN V.P.I.
Display:	12 INCH
Antenna location:	30 FEET ABOVE HELIDECK. ABOUT 300 DEG COVERAGE BLIND ARC IMMEDIATELY AFT.

SEDCO 706

Owner:	Sedco
Model:	DECCA RMS 1230
Radar Frequency:	3040-3060 MHz

Polarization:	HORIZONTAL
Peak Power:	30 KW
Pulse Length:	.05, .25, 1 μ SEC.
PRF:	3300, 1650, 825
Antenna Gain:	27 db
Antenna Vert. Beam Width:	25 DEG
Antenna Horz. Beam Width:	2 DEG
Antenna Height:	110 FEET
Antenna Rotation:	22 RPM
RX Noise factor:	BETTER 10db
Signal Processing:	CLEAR SCAN VP2
Display:	12 INCH
Antenna Location:	20 FEET ABOVE HELIDECK. ABOUT 320 DEG COVERAGE BLIND ARC STARBOARD AFT QUADRANT.

SEDCO 706

Owner:	MOBIL
Model:	DECCA 2459 F/I A.R.P.A.
Radar Frequency:	F 3040-3060 I 9380-9440
Polarization:	HORIZONTAL BOTH
Peak Power:	F-30KW I-25KW
Pulse Length:	.05, .25, 1μ SEC
PRF:	3300, 1650, 825
Antenna Gain:	F-26 db I-32db
Antenna Vert Beam Width:	F-38Deg I-20Deg
Antenna Horz. Beam Width:	F-2Deg I-0.8Deg
Antenna Height:	280 FEET APPROX.
Antenna Rotation:	22 RPM
Rx noise factor:	F4DB I-7db.
Signal processing:	A.R.P.A.
Antenna Location:	Derrick Top 360 deg coverage.

JOHN SHAW

Owner:	Sonat
Model:	RAYTHEON RM 1625/9X
Radar Frequency:	9345 - 9405 MHz
Polarization:	HORIZONTAL
Peak Power:	25 KW
Pulse Length:	0.06, 0.5 1 μ SEC.
PRF:	3600 1800 900
Antenna Gain:	30 db
Antenna Vert Beam Width:	23 DEG
Antenna Horz. Beam Width:	0.9 DEG
Antenna Height:	79 FEET
Antenna Rotation:	33 RPM
Rx noise factor:	BETTER THAN 10 db
Antenna Location:	Starboard forward. THREE FEET OFF DECK. BLIND ARC FROM 35 to 195 Deg.

JOHN SHAW

Owner:	SONAT
Model:	FURUNO FRJ-100
Radar Frequency:	9375 - 9445 MHz
Polarization:	HORIZONTAL
Peak Power:	25 KW
Pulse Length:	0.05, 0.3, 1.3 μ SEC
PRF:	3200, 1600, 600
Antenna Gain:	28 db
Antenna Vert. Beam Width:	25 DEG
Antenna Horz. Beam Width:	0.95 DEG
Antenna Height:	79 FEET
Antenna Rotation:	24 RPM
Rx noise factor:	10 db
Antenna location:	Port Forward. 3 FEET OFF DECK BLIND ARC FROM 320 to 140 DEG.

JOHN SHAW

Owner:	MOBIL
Model:	DECCA 2459 F/I A.R.P.A.
Radar Frequency:	F 3040 - 3060 I 9380 - 9440
Polarization:	HORIZONTAL BOTH
Peak Power:	F-30KW I-25KW
Pulse Length:	.05, .25, 1 μ SEC
PRF:	3300, 1650, 825
Antenna Gain:	F/26db I/32db
Antenna Vert Beam Width:	F-38 deg I- 20 Deg
Antenna Horz. Beam Width:	F-2 deg I- 0.8 deg.
Antenna Height:	280 FEET APPROXIMATELY
Antenna Rotation:	22 RPM
Rx noise factor	F 4 DB I 7db
Signal Processing:	A.R.P.A.
Antenna Location:	DERRICK TOP. 360 DEG COVERAGE

Regards

Brian Garner.

APPENDIX 2

Radar Data Recording

APPENDIX 2
RADAR DATA RECORDING

The recording of radar video data poses a great problem whether the data is recorded in an analog or digital form. This is due to the large signal bandwidths and dynamic range encountered which may be typically anywhere from 2 to 20 Megahertz and 60 to 70 dB respectively.

Studio video recorders are capable of recording analog signals having bandwidths up to about 8 MHz. These units are quite expensive and are not known for having a large dynamic range.

Several analog systems are presently in use for the collection and display of radar data. McMaster University's Communications Research Laboratory operates a wide bandwidth ($\simeq$ 6 MHz), dual-channel analog recorder which is capable of reproducing a signal dynamic range of about 36-38 dB. This recorder is also capable of recording all radar ancillary signals such as trigger and antenna synchro. This allows the recorded data to be played back into a normal PPI radar display.

A similar system owned by Petro-Canada was used to collect iceberg radar data in the Arctic in 1980. The Petro-Canada systems (2) have about a four Megahertz bandwidth with close to a 50 dB dynamic range.

McGill University's Weather Radar Observatory has developed a digital recording system which permits more flexibility in data recording than either of these aforementioned systems.

McGill's approach is to digitize the incoming radar signals at a high sampling rate and buffer this digital data onto a magnetic tape through a minicomputer. Presently, the digitizer quantizes the peak signal value in a particular aperture time to 6 bits. This sampling is carried out at a 6 MHz rate. Ideally, it would be preferable to quantize the signal to 8 bits and sample at about 10 MHz (signal bandwidth for medium pulse is about 4 MHz), however, the buffering circuitry may not be able to handle this data rate. Efforts are presently being directed towards increasing this sampling rate. The digital system, while being more complex than the analog systems, permits the flexibility of storing only specific portions of the radar scan rather than having to store the complete scan as the analog systems do. This is an important feature from the point of view of both the field program length and ease of data reduction. Data need only be collected for areas of the antenna scan that are of interest.

As the data is immediately put into a computer compatible format, it will be possible to ship the tapes to shore-based facilities long before the program is complete. The recorded data may be also played back through the system for verification before they are sent to shore.

These features make the system to be used probably the best choice for the type of field program to be undertaken.

APPENDIX 3

Radar Propagation Model

APPENDIX 3
RADAR PROPAGATION MODEL

This experimental program has demonstrated that the most efficient way to predict radar performance in the offshore environment is to use the data collected on this and other field programs to validate mathematical models. These models may then be used with some confidence to predict radar performance in situations for which data is not available. Such a model has been developed. This model is based on the work of Blake (1980). Blake is responsible for much of the early work in radar range-performance analysis which was carried out at the Naval Research Laboratories, Washington, USA.

The power received from a target using a pulsed-radar is given by,

$$P_r = \frac{P_t G^2 \lambda^2 F^4}{(4\pi)^3 R^4 L} \qquad (1.0)$$

where P_r = received power, watts
P_t = peak transmitter power, watts
R = range to target, m
λ = radar wavelength, m
G = antenna gain
F = propagation factor
L = system losses

Blake formulates an expression for the propagation factor, F, in equation 1.0 which takes into account the earth's curvature, roughness and the atmospheric refractive index. Blake presents a formulation suitable for the calculation of the propagation factor in the interference, the intermediate and the diffraction regions. This formulation is based on the work of Fishback as described in Kerr (1951).

In the interference region, the electric field at some target point distant from the radar is the sum of the field which would be present in free space plus the field due to the reflection of the source (radar) by the ocean surface. At microwave frequencies, these are the dominant field components. The reflected energy arrives at the target point with some phase lag proportioal to the path length difference between direct and reflected paths. The propagation factor is the ratio of the electric field present at the target point, due to the sum of these

direct and reflected fields to the field that would be present if the earth or ocean was not there (i.e. free space). The formulae presented by Blake take into account the effects of a rough spherical earth on the path length difference, the ocean reflection coefficient, as well as the divergence or spreading effect. There are no restrictions on the antenna heights.

His method for calculation of the field in the diffraction region is derived from the work of Fishback, in Kerr (1951). Blake presents convenient empirical relationships for the propagation factor which are easily implemented in a computer model. The method used for calculating the propagation factor in the intermediate region was first suggested by Kerr (1951), that of interpolation between the interference and diffraction regions. A linear interpolation method was chosen for both its ease in implementation and well-behaved characteristics. The problem mentioned by Blake of discontinuities in the slope of the curves joining the interference and diffraction regions have been imperceptible. To generalize the model to consider targets which extend over some height, the propagation factor for points at regular intervals up the target face from some base height to the top of the target are calculated. Assuming an even distribution of scatters with height, it is permissible to take the average value of F over the height of the target. This is equivalent to numerically integrating F over the height and normalizing F to the height.

Combining equation 1.0 with a similar equation for clutter sources and an expression for the noise power at the detector input permits the calculation of signal to (noise + clutter) ratios as a function of range.

The output of the model is presently signal to noise or signal to (noise + clutter) ratios for a specific target and set of environmental conditions. These may be directly related to a specific probability of detection by the use of standard curves produced for that purpose, Blake (1980), Skolnik (1970). Alternatively, the probability of detection may be calculated using the expressions given by Brooks in Blake (1980).

APPENDIX 4

Probability of Detection Versus Signal-to-Noise Ratio

APPENDIX 4
PROBABILITY OF DETECTION VERSUS SIGNAL-TO-NOISE RATIO

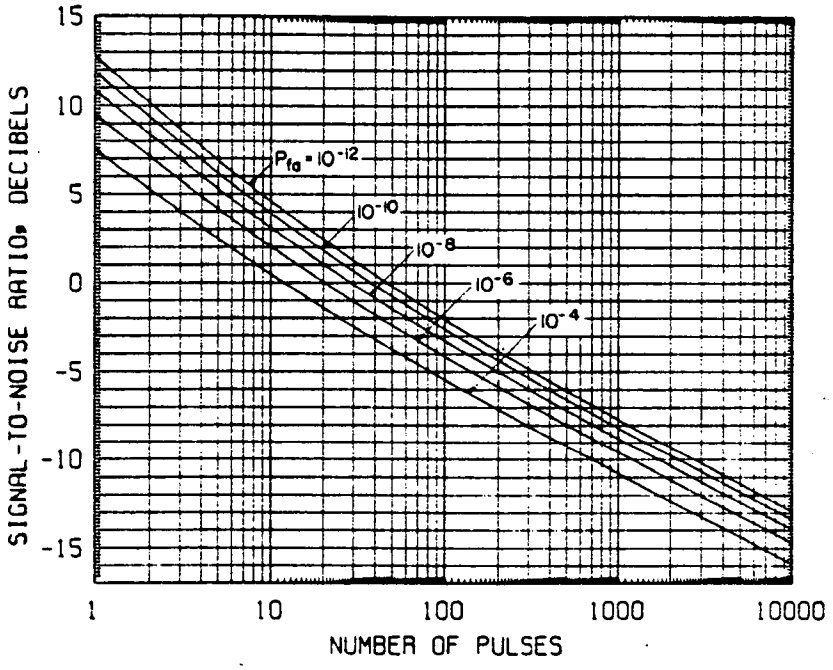

Source: Blake, "A Guide to Basic Pulse-Radar Calculation."

Required Signal-to-Noise Ratio for Detection with Noncoherent Integration of Pulses; Square-Law Detector, Swerling Case 1 Fluctuation, $P_d = 0.25$

Fig. A4-1. After Blake 1980.

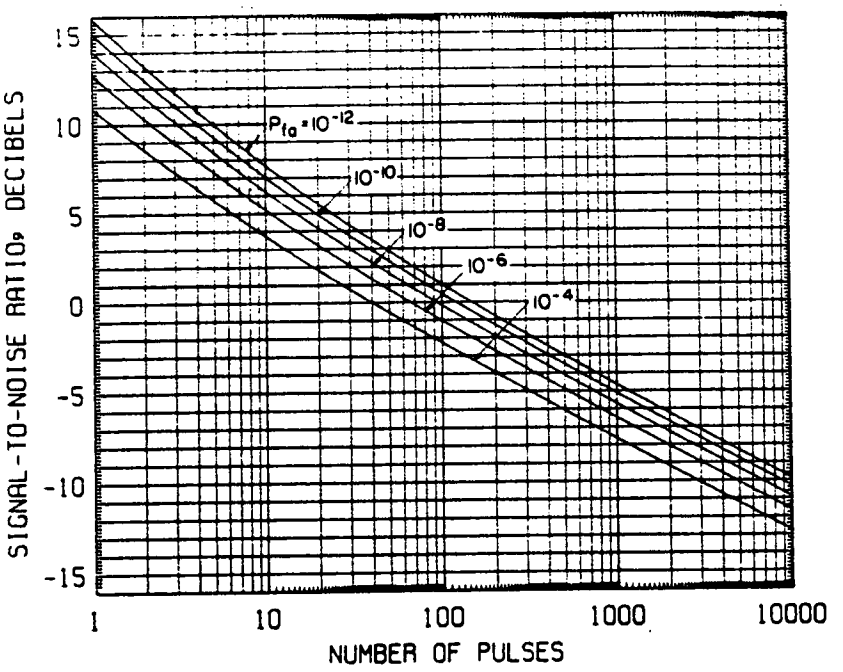

Source: Blake, "A Guide to Basic Pulse-Radar Calculation."

Required Signal-to-Noise Ratio for Detection with Noncoherent Integration of Pulses; Square-Law Detector, Swerling Case 1 Fluctuation, $P_d = 0.50$

Fig. A4-2. After Blake 1980.

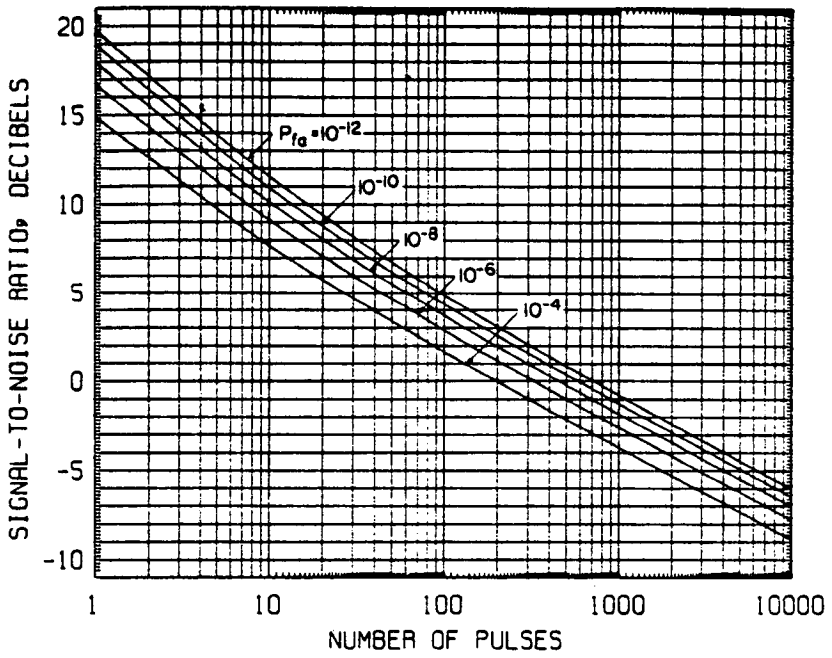

Source: Blake, "A Guide to Basic Pulse-Radar Calculation."

Required Signal-to-Noise Ratio for Detection with Noncoherent Integration of Pulses; Square-Law Detector, Swerling Case 1 Fluctuation, $P_d = 0.75$

Fig. A4-3. After Blake 1980.

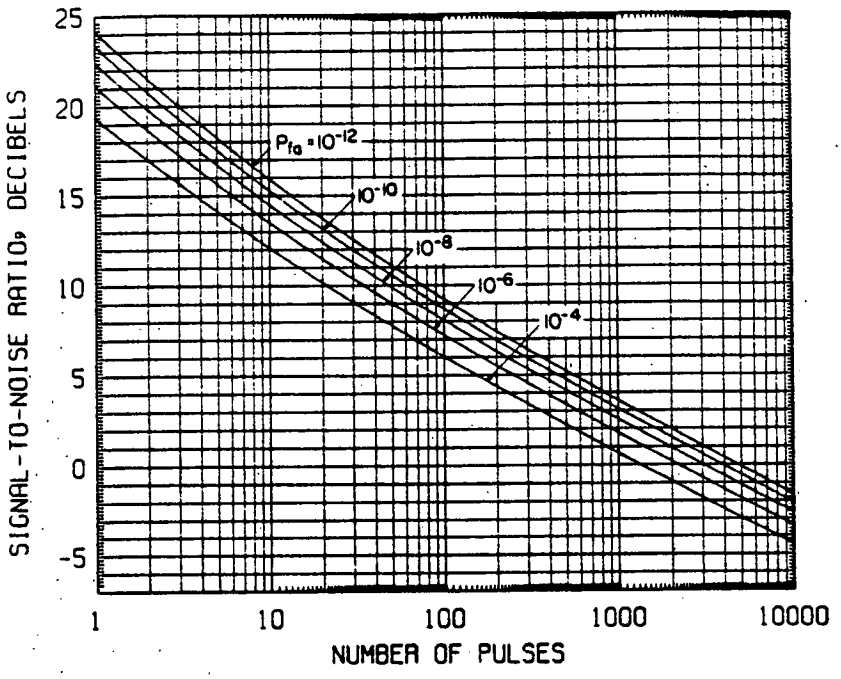

Source: Blake, "A Guide to Basic Pulse-Radar Calculation."

Required Signal-to-Noise Ratio for Detection with Noncoherent Integration of Pulses; Square-Law Detector, Swerling Case 1 Fluctuation, $P_d = 0.90$

Fig. A4-4. After Blake 1980.

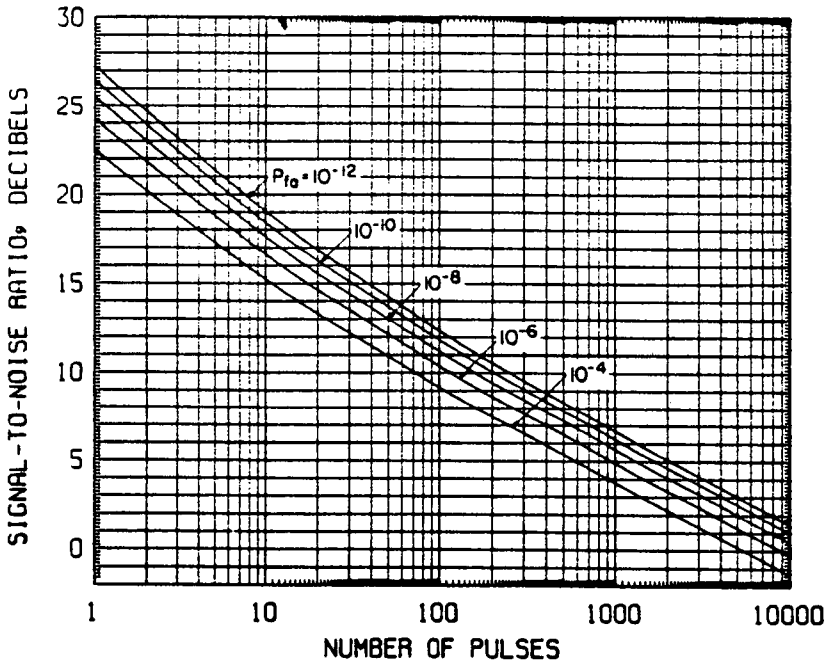

Source: Blake, "A Guide to Basic Pulse-Radar Calculation."

Required Signal-to-Noise Ratio for Detection with Noncoherent Integration of Pulses; Square-Law Detector, Swerling Case 1 Fluctuation, $P_d = 0.95$

Fig. A4-5. After Blake 1980.

APPENDIX 5

Photographs of Iceberg Targets

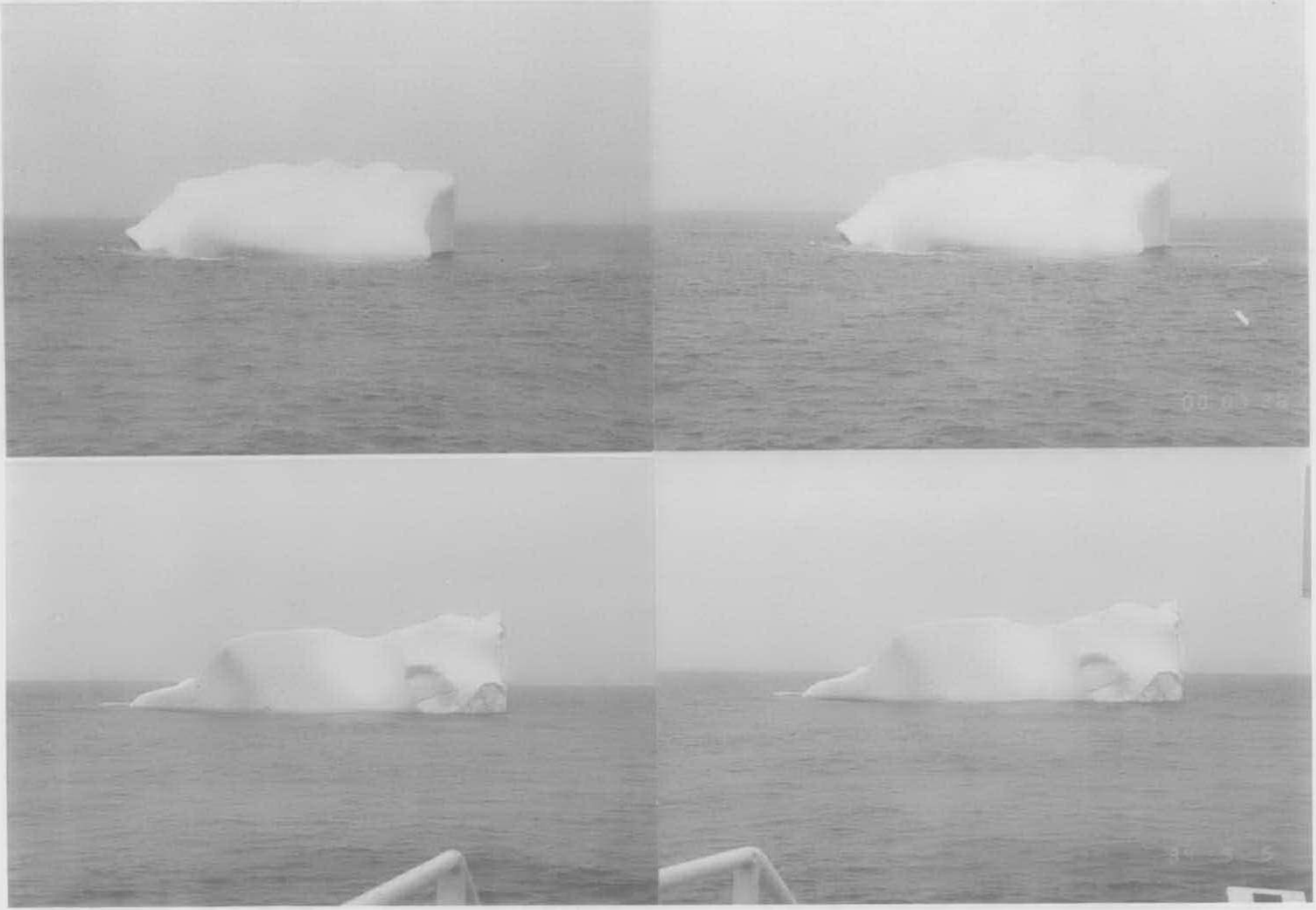

Fig. A5-1. T168 (N1242).

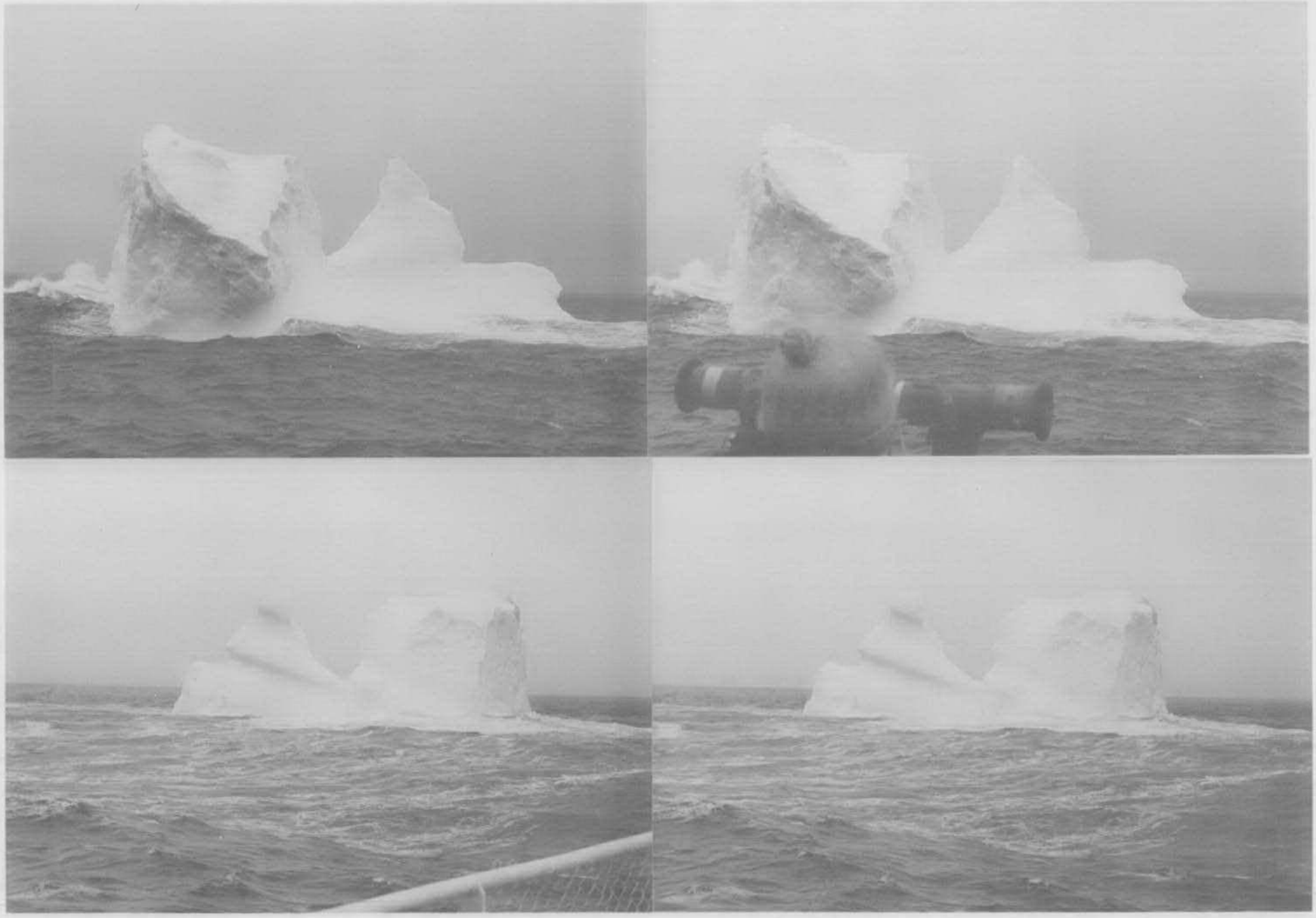

Fig. A5-2. T166 (Front and Back).

Fig. A5-3. T166 (Left and Right Sides).


BERG # T-178 @ 0858 Z / MAY 5 1984:
0.09 Nmi @ 155°T
0.15 Nmi @ 237°T
0.17 Nmi @ 350°T
0.17 Nmi @ 065°T
BERG # T-178 @ 1535 Z / MAY 6 / 1984:
0.17 Nmi @ 075°T
0.14 Nmi @ 345°T
0.14 Nmi @ 255°T
0.16 Nmi @ 165°T
BERG # T-166 @ 2015 Z / MAY 8 1984:
0.06 Nmi @ 145°T
0.10 Nmi @ 055°T
0.10 Nmi @ 295°T
0.10 Nmi @ 230°T

Fig. A5-4.


BERG # T-180 @ 1518 Z / MAY 9 1984
0.08 Nmi @ 285°T
0.08 Nmi @ 195°T
0.08 Nmi @ 105°T
0.09 Nmi @ 015°T
BERG T-184 @ 1858 Z / MAY 9 / 1984
0.17 Nmi @ 310°T
0.09 Nmi @ 220°T
0.12 Nmi @ 130°T
0.12 Nmi @ 040°T
BERG T-185 @ 1949 Z / MAY 9 1984
0.11 Nmi @ 280°T
0.14 Nmi @ 100°T
0.15 Nmi @ 010°T
0.11 Nmi @ 190°T

Fig. A5-5.

BERG # T-166 @ 1727 Z / MAY 3 / 1984

0.09 Nmi @ 130°T 0.12 Nmi @ 220°T 0.13 Nmi @ 310°T 0.08 Nmi @ 040°T

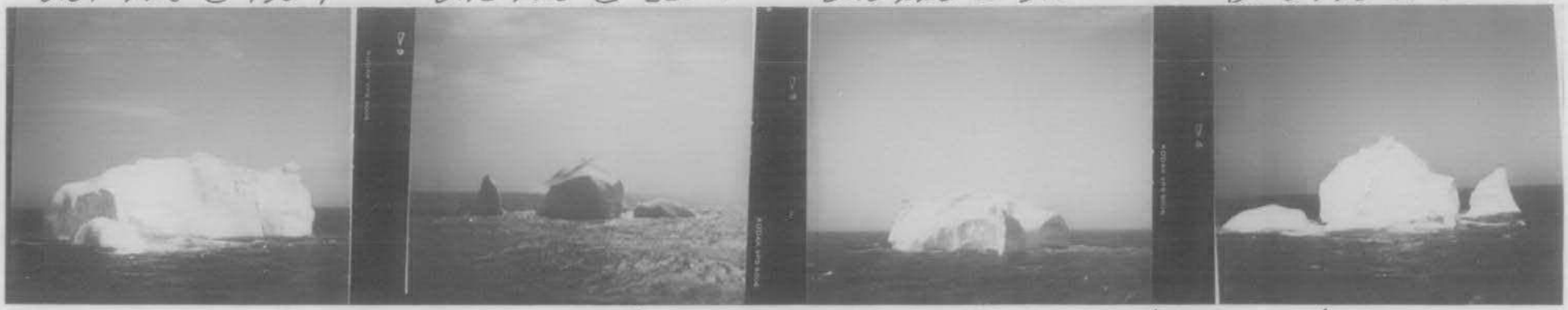

BERG # T-175 @ 1832 Z / MAY 3 / 1984

0.08 Nmi @ 060°T 0.10 Nmi @ 150°T 0.09 Nmi @ 240°T 0.10 Nmi @ 330°T

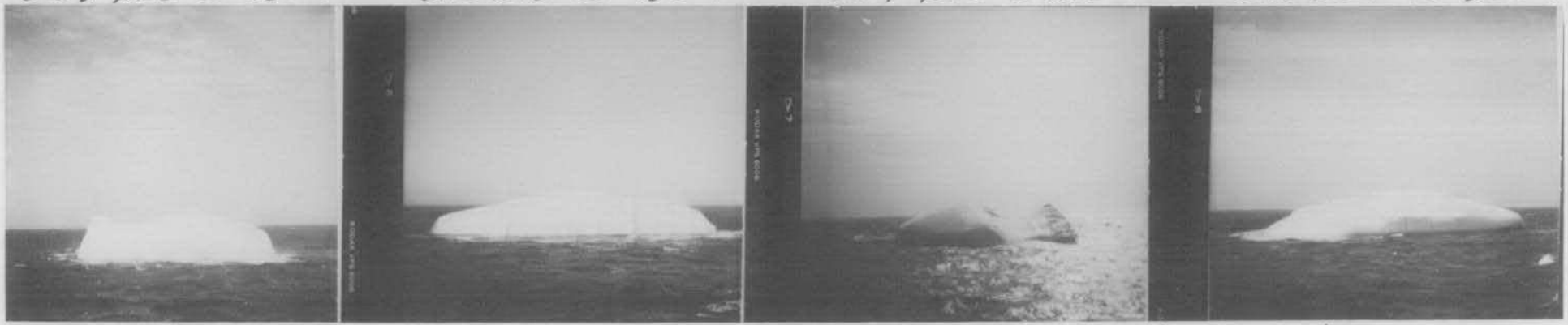

BERG # T-176 @ 2006 Z / MAY 3 / 1984

0.05 Nmi @ 090°T 0.09 Nmi @ 360°T 0.07 Nmi @ 270°T 0.12 Nmi @ 180°T

Fig. A5-6.


BERG T-185 @ 1231Z / MAY 10/ 1984
0.10 Nmi @ 320°T
0.07 Nmi @ 090°T
0.07 Nmi @ 180°T
BERG # T-197 @ 2226Z / MAY 12 1984
0.17 Nmi @ 288°T
0.16 Nmi @ 105°T
0.18 Nmi @ 195°T
0.22 Nmi @ 015°T
BERG # T-188 @ 1140Z / MAY 13 1984
0.03 Nmi @ 115°T
0.03 Nmi @ 295°T
0.03 Nmi @ 200°T
0.03 Nmi @ 025°T

Fig. A5-7.


BERG # T-199
0.06 Nmi @ 185°T
0.03 Nmi @ 005°T
0.04 Nmi @ 265°T
0.06 Nmi @ 095°T
BERG # T-196
0.06 Nmi @ 120°T
0.04 Nmi @ 300°T
0.04 Nmi @ 210°T
0.04 Nmi @ 030°T
BERG # T-199
0.09 Nmi @ 202°T
0.07 Nmi @ 014°T
0.04 Nmi @ 291°T
0.07 Nmi @ 111°T

Fig. A5-8.


BERG T - 197
0.06 Nmi @ 163°T
0.05 Nmi @ 344°T
0.15 Nmi @ 068°T
0.07 Nmi @ 254°T
BERG # T-203
0.04 Nmi @ 198°T
0.03 Nmi @ 020°T
0.03 Nmi @ 108°T
0.05 Nmi @ 288°T
BERG # T-206
0.07 Nmi @ 252°T
0.08 Nmi @ 056°T
0.08 Nmi @ 148°T
0.06 Nmi @ 340°T

Fig. A5-9.

APPENDIX 6

Calibration Curves

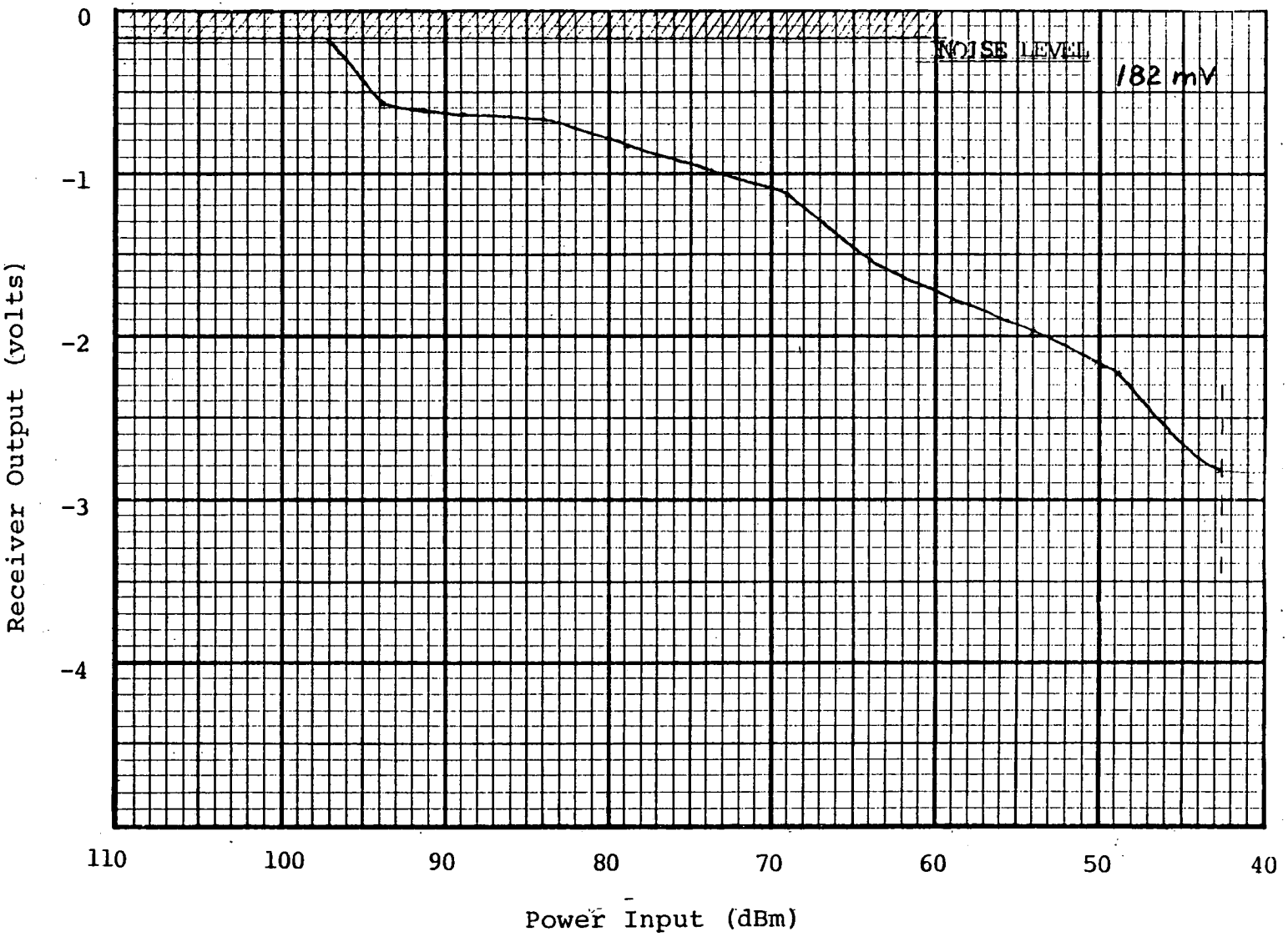

Fig. A6-1. Receiver characteristic for derrick-mounted X-band radar, X1.

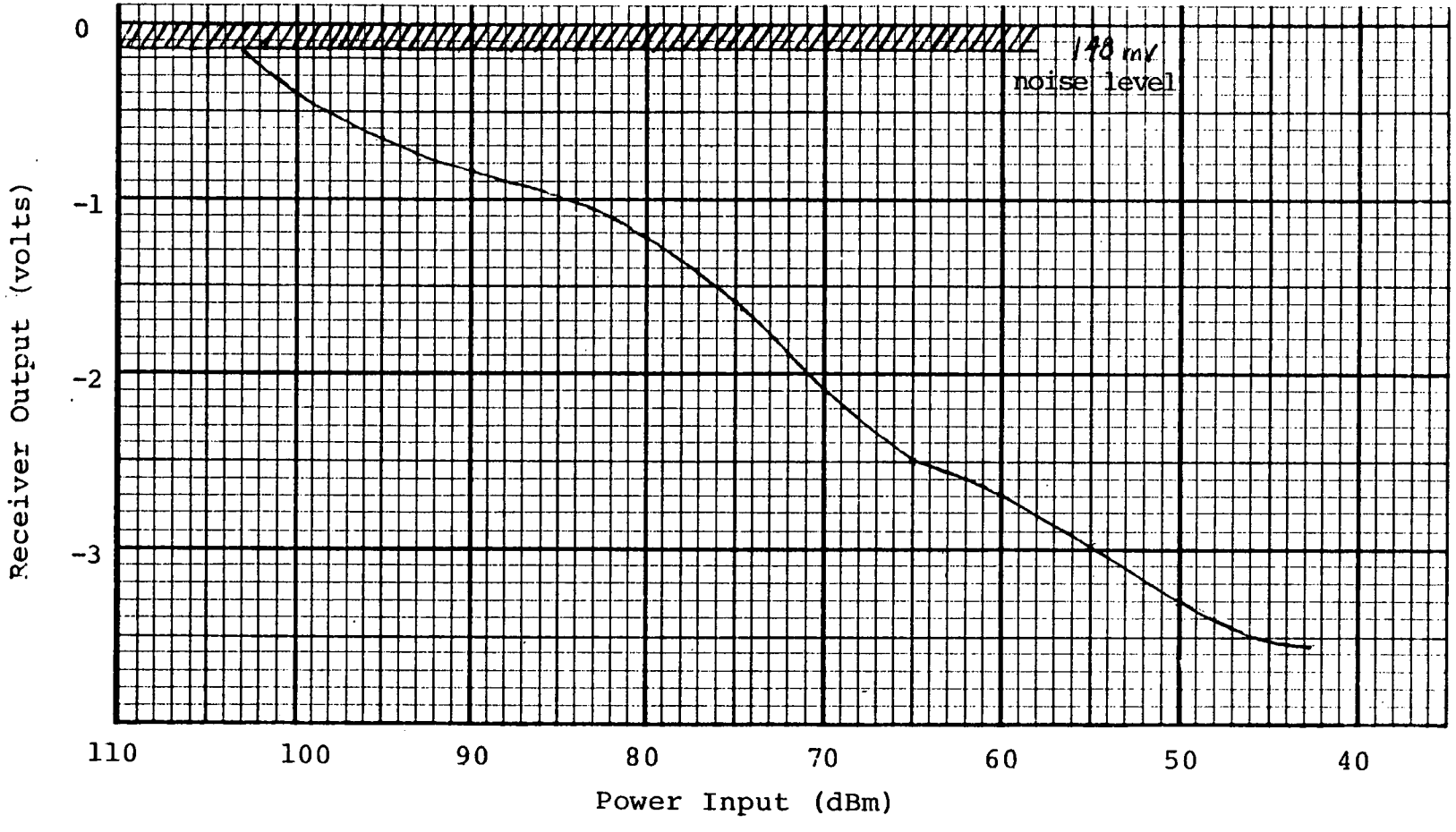

Fig. A6-2. Receiver characteristic for derrick-mounted S-band radar, S1.

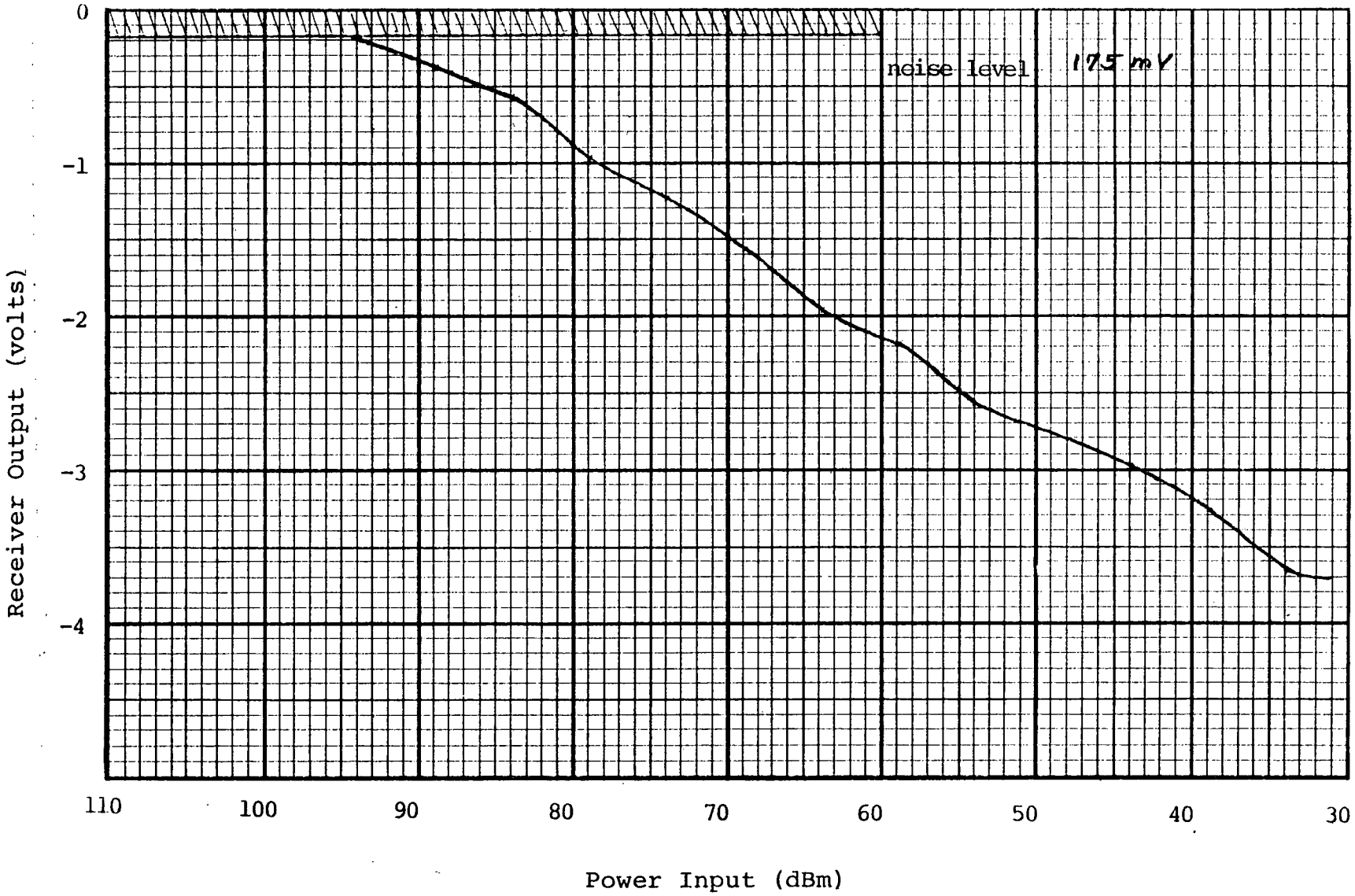

Fig. A6-3. Receiver characteristic for deck-mounted X-band radar, X2.

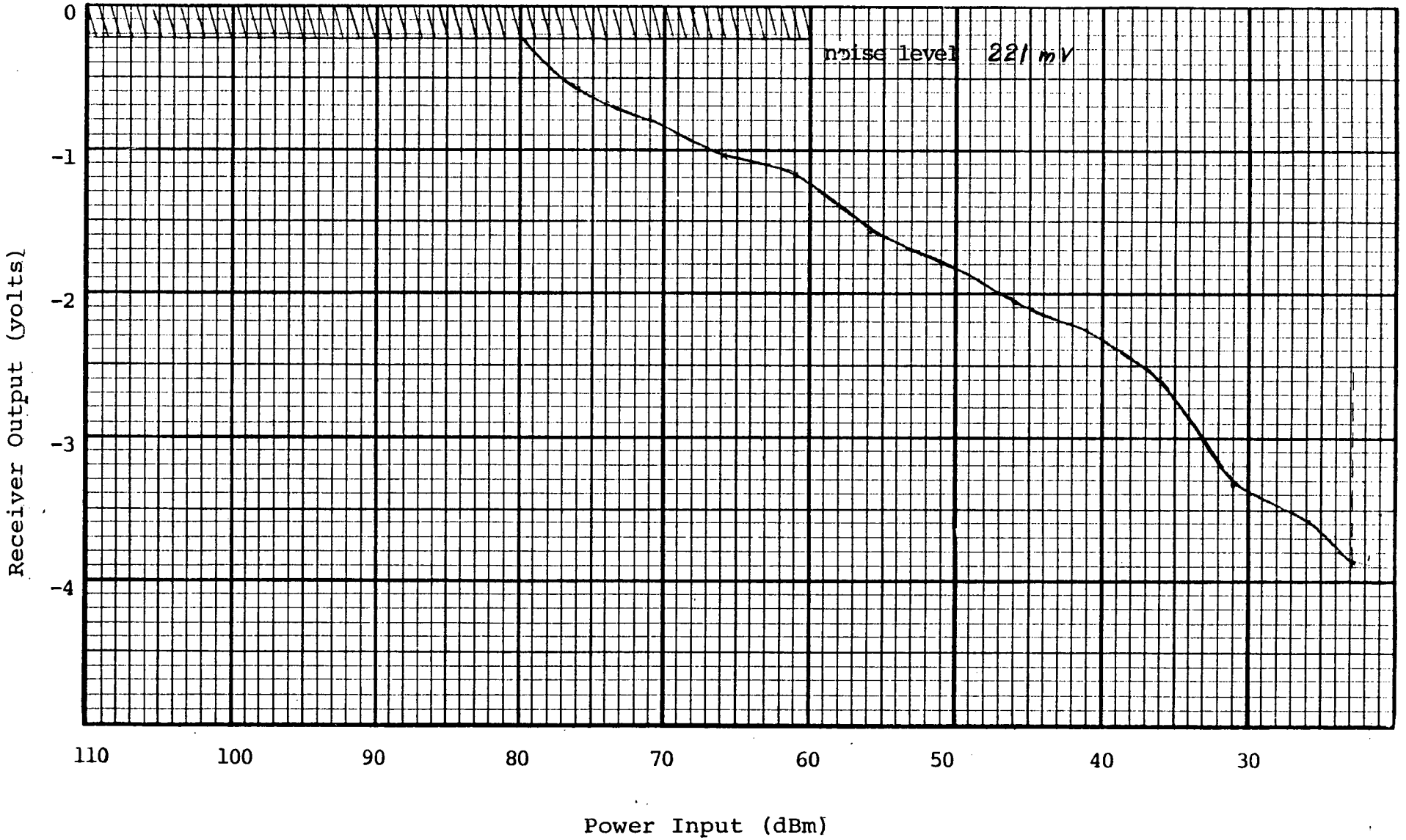

Fig. A6-4. Receiver characteristic for deck-mounted S-band radar, S2.

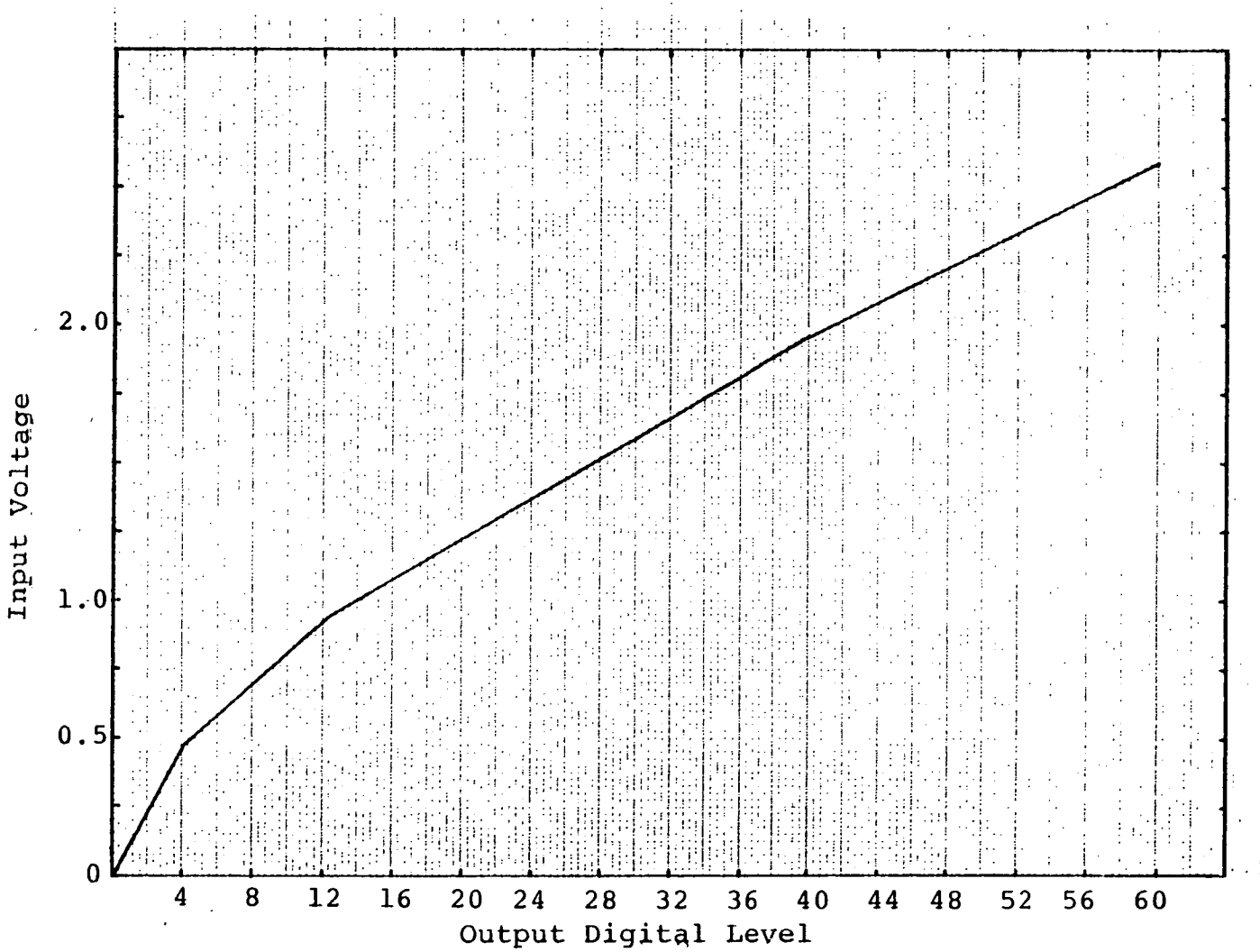

Fig. A6-5. Radar interface calibration.

APPENDIX 7

Discussion of Equipment Problems

APPENDIX 7
DISCUSSION OF EQUIPMENT PROBLEMS

The problems encountered with the radar equipment used for the data acquisition program concerned both the radar systems and the recording system. The radar systems' problems included:

a) Uncertain tuning on X1. The tuning meter on the X-band unit did not seem to work properly. This unit was serviced several times during the period of the field program and the magnetron was replaced in mid-April, however, its performance was still less than expected. During the data analysis, it was determined that the problem was probably in the front end of the radar system. It is probable that there was a mismatch between the low noise, front-end receiver and the main receiver or possibly the tuning of the receiver mixer was not functioning properly over the frequency band of the transmitter.

b) The radar units S2 and X2 were marine radars usually installed on drilling rigs. They were owned and maintained by Sedco Inc. These radars had been in operation for a number of years with only a minimum of servicing. The transmitted power for X2, measured 4.4 m from the antenna (total waveguide length was approximately 16 m), was only 11.5 kW. From inspection of the waveguide at the measurement point it appeared that water had penetrated the waveguide seals and that the waveguide was bent.

c) The performance of the lower S-band radar, S2, was the worst of all the radar systems used. Without a proper adaptor it was not possible to measure the transmitter power, however, from the data analysis it appears that the radar required servicing.

The problems associated with the recording system were of a more subtle nature. They included:

a) The nonlinearity of the radar interface characteristic. The nonlinearity was most severe in the low voltage range from 0 to 0.75 volts. Alone it would not cause problems but when combined with the fact that the input is from a logarithmic amplifier, the situation occurred in which one digital level change on the output may have represented up to a 10 dB change in the received signal power. This case is the worst that occurred,

and it was for the X-band radar on the derrick top (X1) which had an abnormally steep receiver characteristic (see Appendix 6, Fig. A6-1) in the low voltage range. The worst case for S1 was one digital level for a 3 dB change in received power level at the received power level range from -85 to -92 dBm. For all the radars, except X1, a change in digital level represented about a 1 dB change in power received for received power greater than -80 dBm.

b) Limited coverage of the radar dynamic range. The dynamic range, DR, of an n-bit analog to digital (A/D) converter is given by Oppenheim and Shafer (1975), as

$$DR = 6.02(n) \text{ dB}$$

or 36.12 dB for the six-bit unit used. This is a theoretical maximum dynamic range and in practice the effective dynamic range may be less. If, for example, the analog signal to be digitized is not matched level-wise to the input range of the A/D converter, some loss of lower or higher signal levels may occur. The A/D converter in the radar interface was set up to take video levels from -0.11 volts for the least significant bit to -2.70 volts. The only target signal observed to exceed this range was a supply vessel at 0.4 naut mi. Sea clutter was never observed exceeding this limit. It is believed, therefore, that the A/D converter as it was set up covered as much of the video dynamic range as possible. This coverage, however, is sparse at some points on the receiver characteristic curve, as was pointed out in the previous discussion. The maximum observed signal corresponded to a received power of -45 dBm for X1, so when compared to the receiver noise level for X1 (i.e., -97 dBm) it was necessary to cover a 52 dB dynamic range with the 36 dB dynamic range digitizer. This resulted in sparse coverage in the lower signal range. To recover this dynamic range more accurately, it would be necessary to increase the resolution in the digitizer. An eight-bit digitizer preceeded by a linear amplifier would provide a 1 dB resolution over its 48 dB dynamic range, thereby providing a solution to both of these problems. Alternatively, an anti-log circuit and eight-bit digitizer could have been used. Most of the iceberg data collected was within the range of

the system characteristics for which a 1 dB resolution was available, however, some of the smaller targets of primary interest (i.e., bergy bits) were located in a region of the characteristic where the resolution was not quite as good.

c) The instability of the drill-rig power system. Several interruptions in recording occurred due to voltage spikes and momentary power outages. One power line conditioner was destroyed, which saved the computer system. Future programs of this sort will require an uninterruptible power supply to ensure that no damage occurs to the recording system.

APPENDIX 8

Summary of Radar Modifications

APPENDIX 8
SUMMARY OF RADAR MODIFICATIONS

1. Temporary Modifications

At the beginning and at the end of the field program the radar receiving system will be calibrated.

Procedure:

(i) disconnect transmitter power

(ii) disconnect waveguide from transmitter/receiver receiver port

(iii) connect output of calibrated power source to the transmitter/receiver port

(iv) connect calibrated power source external trigger to trigger output of radar trigger board.

(v) apply incremental power to receiving system and record receiver output for all three radar pulse lengths.

(vi) disconnect calibration equipment and reconnect waveguide and transmitter power.

It is expected this procedure will take four hours per radar. Other than the four hours required to perform this calibration, normal radar operation will not be affected.

2. Semi-Permanent Modifications

The following modifications will be permanent for the period of the field program. Once the field program is complete, these modifications will be reversed.

(i) Radar Signal Recording Connections

Radar video, trigger and snychro will be recorded from each of four radars. These signals will be made available at the recording system by running coaxial cables to the signal sources. All signal cables will be run according to rig requirements. The signals will be buffered by Decca equipment such that a recording system malfunction will not influence normal radar operation. Four hours downtime per radar.

(ii) Radar Power Measurement Modifications

The radar transmitted power will be measured by the use of directional couplers installed in the waveguide of each radar. Signals from the directional couplers will be run from the radar site (derrick) to the vicinity of the radar recording equipment.

All approved cable will be routed to the certification standard of the rig (i.e armored cable and stainless steel straps to be used on the derrick mounted installation).

These modifications will not affect normal operation of the radar. The added benefit of this modification is that the rig operator will have accurate information on radar transmitter performance. These modifications will take four hours downtime per radar.

APPENDIX 9

Propagation Model used in Analysis

AC/243(Panel III)D/160
AC/141(IEG/1)D/130

PART II

TECHNICAL REPORT
MTR.77/37

MARCONI RESEARCH LABORATOR
SECTION 211

RADIOWAVE RANGE PREDICTION OVER THE SEA IN EVAPORATION DUCTING CONDITIONS

by

S. Rotheram

Propagation and System Studies Group

NOVEMBER, 1977

ABSTRACT

A method is described for predicting radiowave ranges over the sea in evaporation ducting conditions. The method can be used for radar and one way transmission paths in operational conditions. It can also be used non-operationally for system planning and evaluation. A step by step guide to using the method is given in an appendix.

KEYWORDS: Propagation prediction, radar range anomalous propagation, maritime evaporation duct.

APPENDIX 1 - Step by step guide

In this appendix a step by step guide is given to using the methods described in this report. The numbers after variable names refer to the step in which the value of that variable can be found. It is assumed that the user has a hand calculator available to do the arithmetical calculations. Steps 1 to 10 below are the input data which the user has to supply.

Input data

1.	Measurement height	h_1	=	_____	metres
2.	Wind speed at h_1	u_1	=	_____	metres/second
3.	Air temperature at h_1	T_1	=	_____	^oC
4.	Water vapour pressure at h_1	e_1	=	_____	m b.
5.	Sea temperature	T_o	=	_____	^oC
6.	R.m.s. roughness height	σ	=	_____	metres
7.	Transmitter (radar) height	h_t	=	_____	metres
8.	Receiver (target) height	h_r	=	_____	metres
9.	Free space range	R_f	=	_____	kilometres
10.	Frequency	f	=	_____	GHz.

Calculation of duct parameters

11. Find e_o from figure 1 using T_o(5) or use the formula

$$e_o = 6.1 \times 10^{7.5\, T_o/(237 + T_o)} = \text{_____} \text{ mb}$$

12. From T_1(3), T_o(5), e_1(4) and e_o(11) find ΔT and Δe from

$$\Delta T = T_1 - T_o = \text{_____} \ ^oC$$

$$\Delta e = e_1 - e_o = \text{_____} \text{ m b}$$

13. From ΔT(12), Δe(12) and u_1(2) find $1/L_e$ and ΔN from

$$\frac{1}{L_e} = \frac{.38\Delta T + .04\Delta e}{u_1^2} = \text{_____} \text{ metres}^{-1}$$

$$\Delta N = -4.7\, \Delta e + .98\Delta T = \text{_____}$$

14. From h_1(1) and $1/L_e$(13) find x_e from

$$x_e = \frac{h_1}{L_e} = \text{_____}$$

15. From x_e(14) and figure 2 read off x. For small x_e (say $|x_e| < .1$) use $x = x_e$
Note the separate curves for negative or positive x and x_e.

x = _____

16. From h_1(1) and x(15) find 1/L from

$$\frac{1}{L} = \frac{x}{h_1} = \_\_\_\_\_ \text{ metres}^{-1}$$

If $|\Delta N/L| < .01$ go to stage 21. If $1/L > .1$ the results are suspect. If $1/L > 1$ they are probably wrong. If $1/L < -1$ the results may be inaccurate.

17. From x(15) and figure 3 read off y. For small x (say $|x| < .1$) use $y = x$. Note the separate curves for negative or positive x and y.

$$y = \_\_\_\_\_$$

18. From h_1(1), ΔN(13) and y(17) find z from

$$z = \frac{.7\, y\, \Delta N}{h_1} = \_\_\_\_\_$$

19. From z(18) and figure 4 read off ρ. For $|x| < .01$ use $\rho = z$. Note the separate graphs for negative or positive ρ and z.

$$\rho = \_\_\_\_\_$$

20. From 1/L(16) and ρ(19) find h_d from

$$h_d = \rho L = \_\_\_\_\_ \text{ metres}$$

Proceed to stage 22.

21. If $|\Delta N/L| < .01$ one may use ΔN(13) and 1/L(16) to find

$$h_d = .7\Delta N = \_\_\_\_\_ \text{ metres}$$

$$\rho = \frac{h_d}{L} = \_\_\_\_\_$$

22. Assign a value to K, usually 1.205.

$$K = \_\_\_\_\_$$

23. From ρ(19 or 21) and figure 5 read off β. For $|\rho| < .01$ use $\beta = 1$. Note the separate graphs for negative and positive ρ.

24. From K(22) and β(23) find K_s and γ from

$$K_s = K\beta = \_\_\_\_\_$$

$$\gamma = \frac{K_s}{1.205} = \_\_\_\_\_$$

AC/243(Panel III)D/160
AC/141(IEG/1)D/130

9½" = 6" Square 1/10 inches

REPORT No. MTR 77/37

PLATE No.

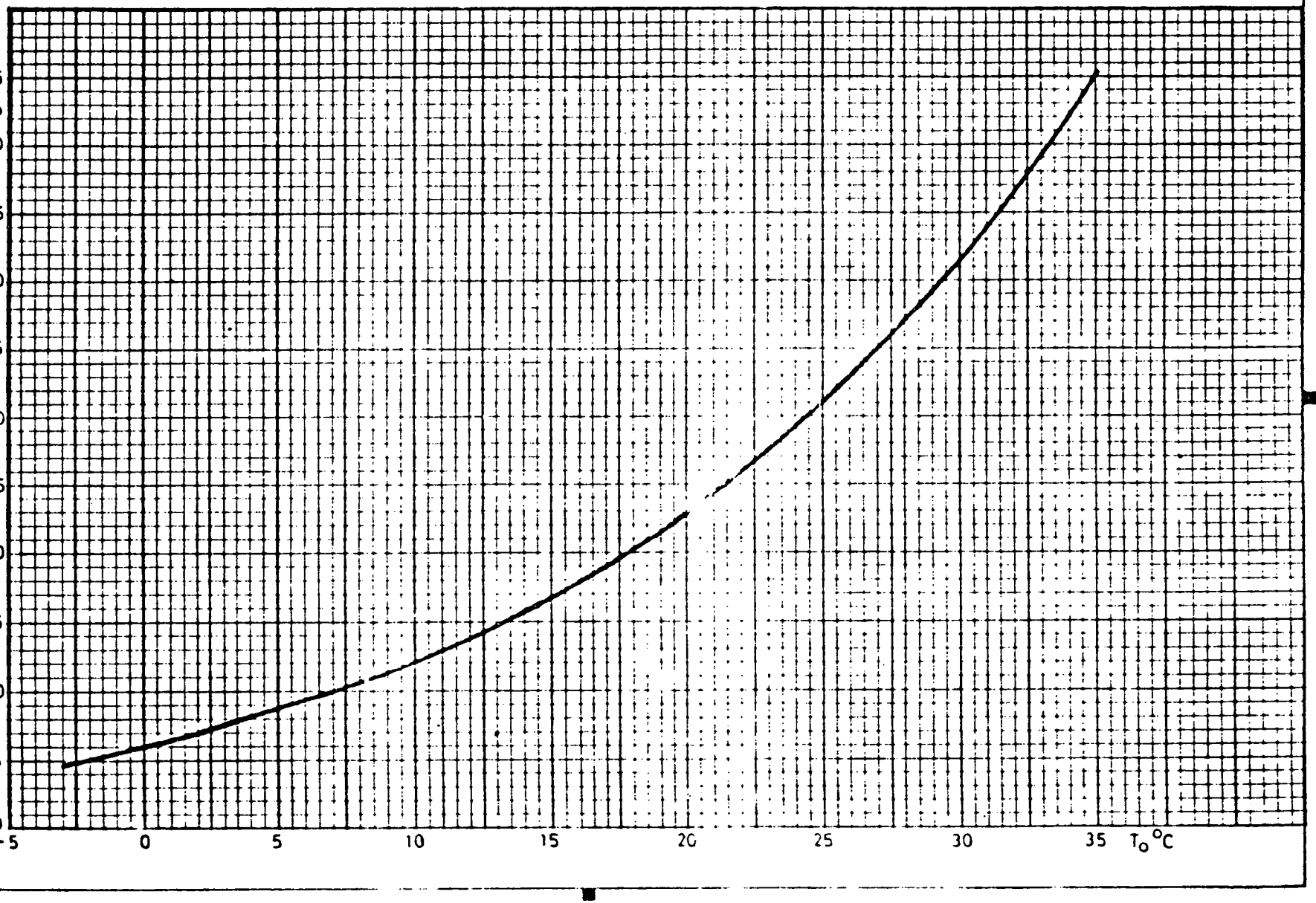

APPROVED

TITLE SATURATION VAPOUR PRESSURE OF AIR e_o mb AT A TOTAL AIR PRESSURE OF 1013·3 IN CONTACT WITH SEA WATER AT A TEMPERATURE OF T_o °C AND A SALINITY OF 35‰ (ie. 35 PARTS PER THOUSAND)

119

SH.No. FIG.1

A 4

AC/243(Panel III)D/160
AC/141(IEG/1)D/130

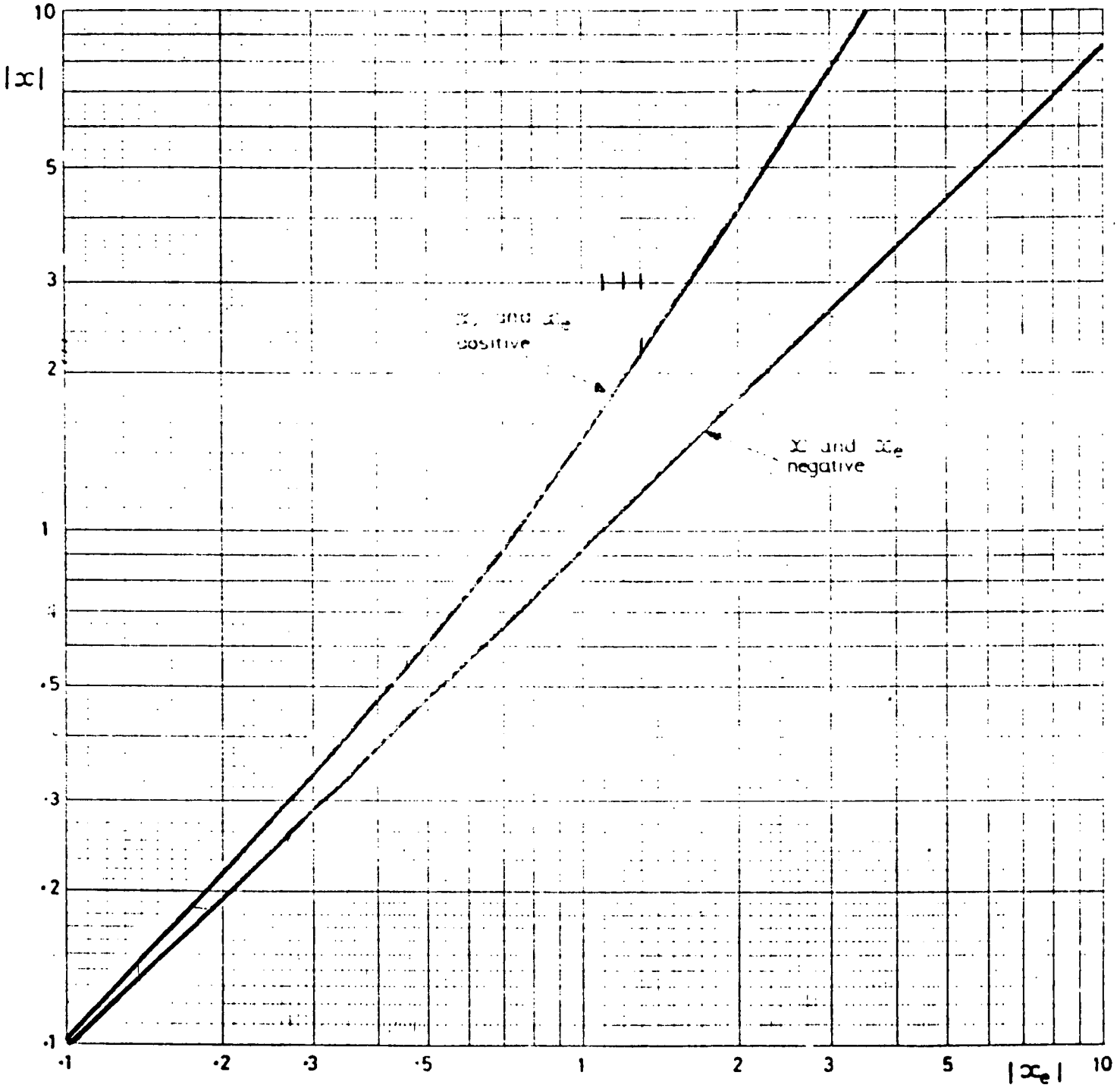

GRAPH OF χ AGAINST χ_e. NOTE THE SEPARATE CURVES FOR POSITIVE OR NEGATIVE χ AND χ_e
FOR $|\chi_e| < .1$ USE $\chi = \chi_e$

FIG. 2

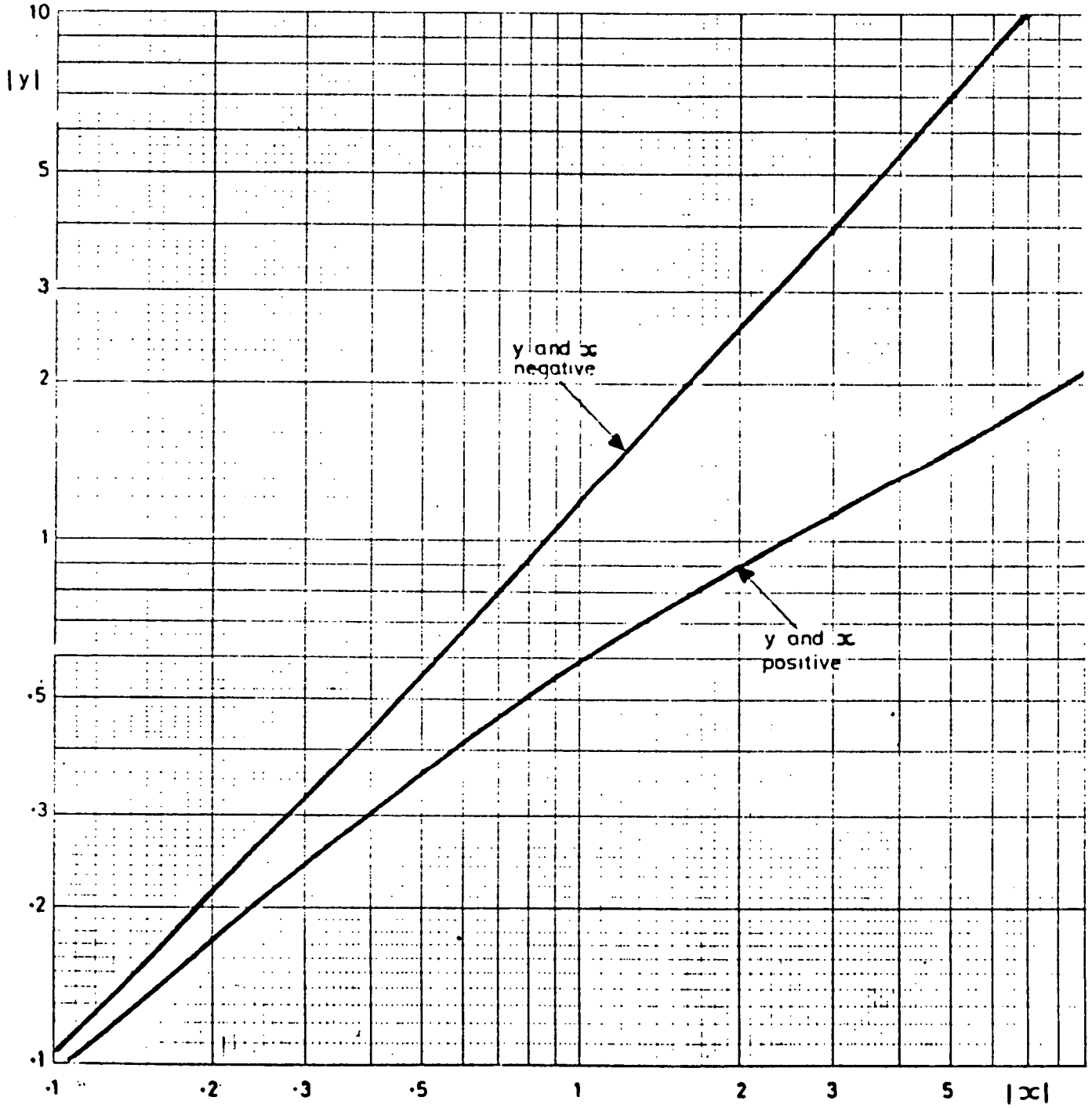

GRAPH OF y AGAINST x. NOTE THE SEPARATE CURVES FOR POSITIVE OR NEGATIVE x AND y.
FOR $|x| < \cdot 1$ USE $y = x$

FIG. 3

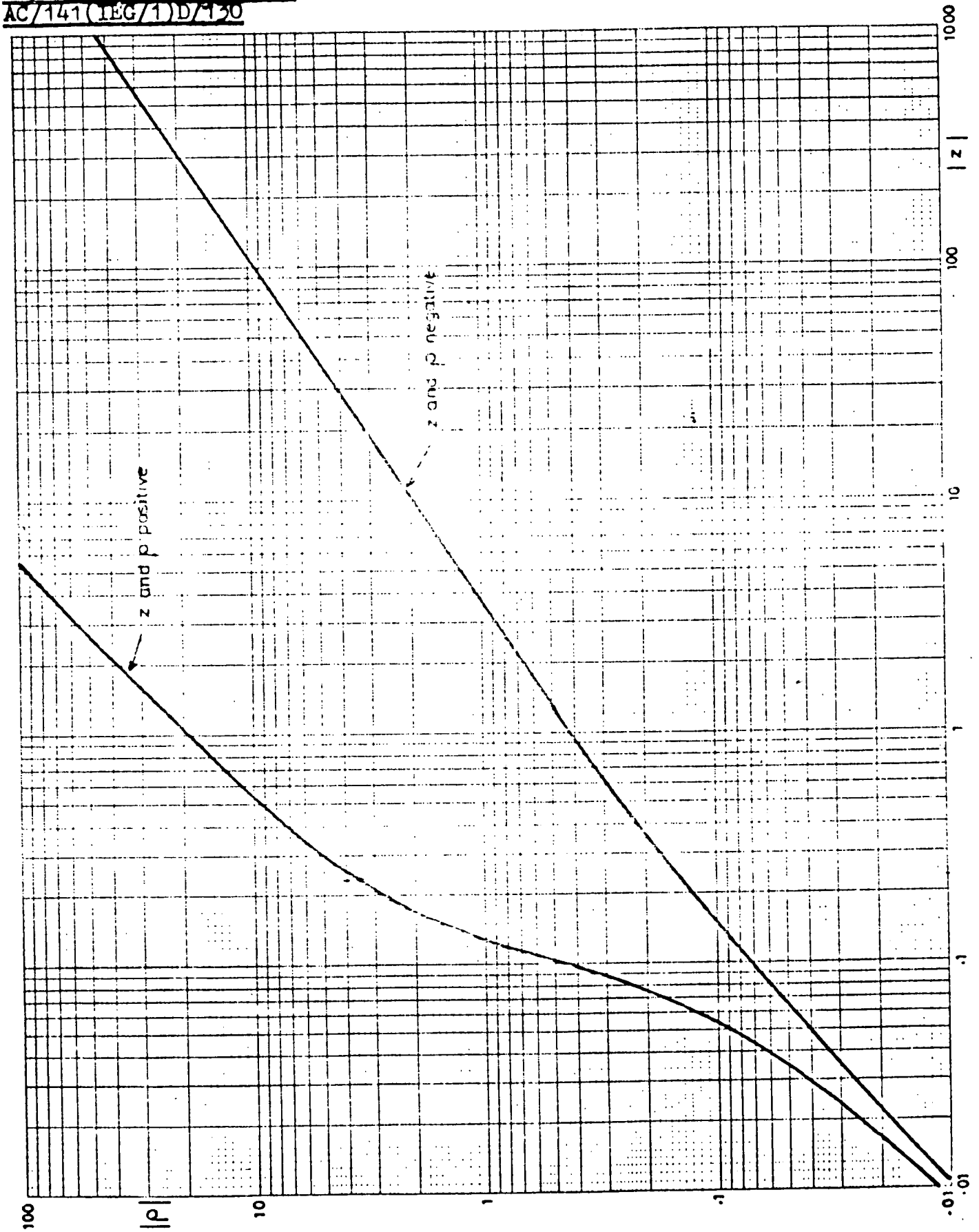

GRAPH OF ρ AGAINST z NOTE THE SEPARATE CURVES FOR POSITIVE AND NEGATIVE ρ AND z. FOR SMALL z, ρ → z.

REPORT No. MTR 77/37 PLATE No.

3 Cycle Log x mm

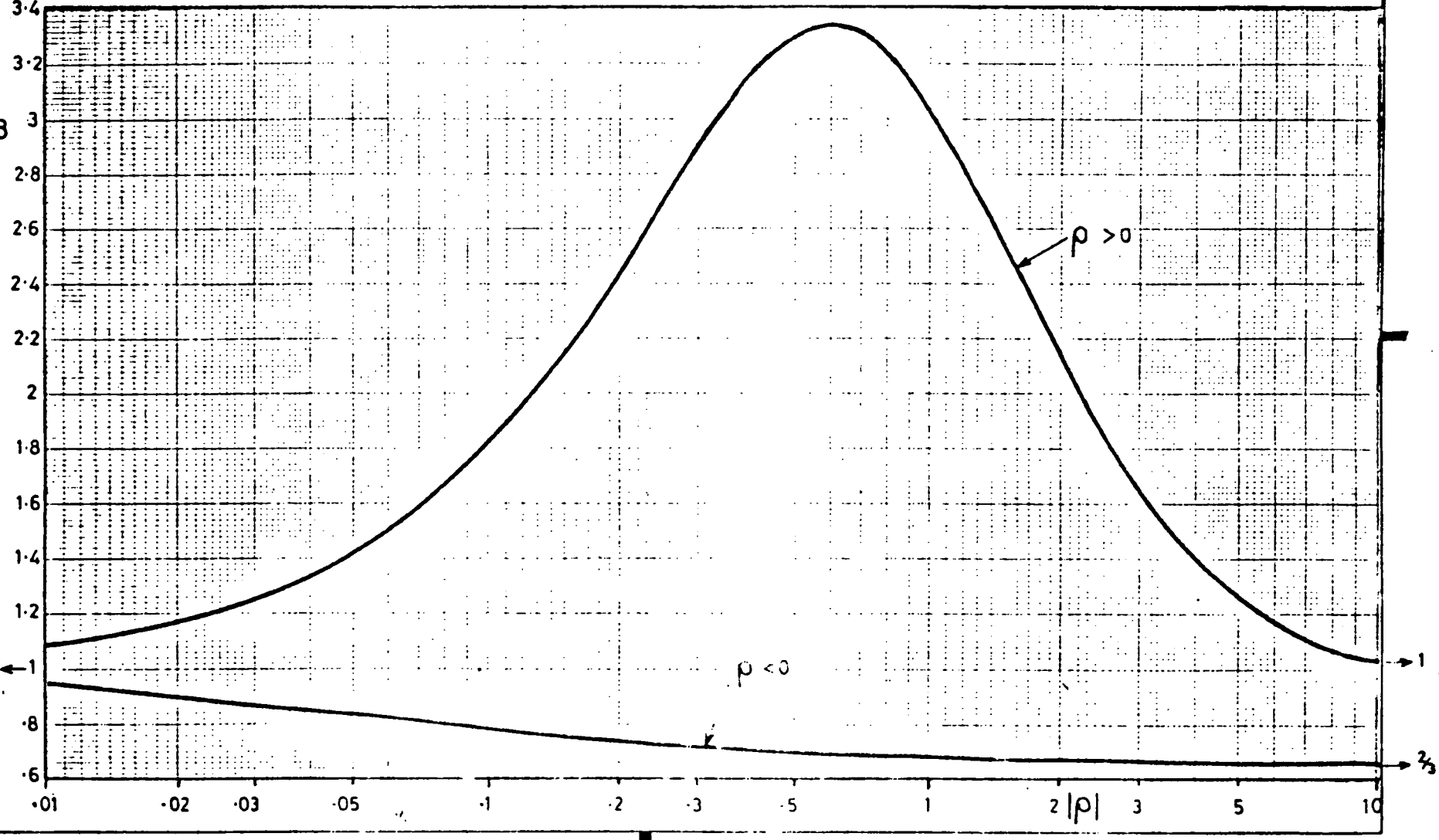

TITLE GRAPH OF β AGAINST ρ. NOTE THE SEPARATE CURVES FOR POSITIVE AND NEGATIVE ρ. THE SYMBOL $\longrightarrow \frac{2}{3}$ MEANS "TENDS TO $\frac{2}{3}$" SO THAT THIS VALUE CAN BE TAKEN BEYOND THE END OF THE GRAPH

APPROVED

SH.No. FIG. 5

123

A 4

Form No. 150/101/02926F

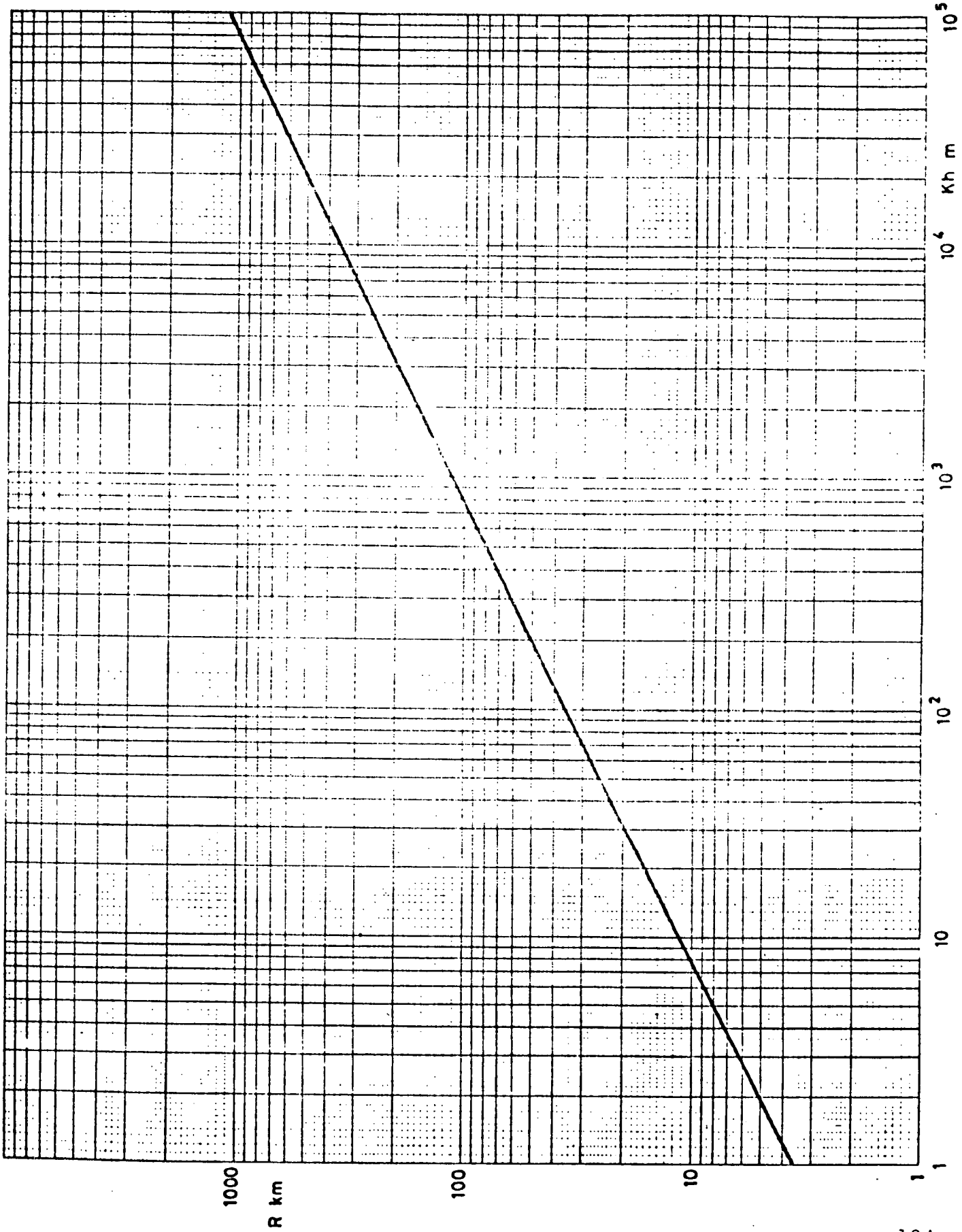

HORIZON DISTANCE R IN KILOMETRES AGAINST Kh WHERE K IS AN

14. LIMITATIONS

The method given here has a number of limitations of which we may mention the following :-

i) The model of the refractive index only takes detailed account of the evaporation duct so that the possible influence of other surface ducts, such as advection ducts, and elevated ducts is entirely ignored. This can be a serious limitation in some parts of the world where such layers are frequently present. They are more common in coastal regions when the wind is blowing from land to sea and in tropical regions. Stable conditions ($1/L > 0$) also promote their occurrence.

ii) The effects of horizontal inhomogeneity are ignored. These may be important in coastal areas when the wind blows from land to sea under stable conditions so that advection ducts are formed.

iii) The boundary layer theory on which section 6 is based starts to become suspect when $1/L > .1$ and deteriorates as $1/L$ increases. It has probably completely broken down when $1/L > 1$. Note that points (i), (ii) and (iii) are interrelated.

iv) The boundary layer theory may be inaccurate in strongly unstable conditions, say, $1/L < -1$.

v) To simplify the method, the stability dependence of the field strength was approximated as in section 7.

vi) To simplify the method the height-gain function was approximated as in section 10.

vii) Water vapour absorption, which can be serious above 20 GHz, and scattering from atmospheric turbulence have been ignored.

viii) The part of the theory which takes account of the rough sea is not very soundly based.

ix) Only three modes may be included in the method as described in section 13.

x) It is assumed that the path is transhorizon so that the free space range should be larger than the horizon range, i.e. $R_f > R_t + R_r$.

In spite of the aforementioned limitations and possibly others it is thought that the method will afford significant improvements on previous methods.

REFERENCES

Blake, L.V. 1980. Radar range performance analysis. D.C. Heath and Company.

Budinger, T.F. 1960. Iceberg detection by radar. International Ice Patrol Bulletin No. 45, United States Coast Guard.

Croney, J. 1956. Clutter on radar displays. Wireless Engineer.

Croney, J. 1966. Improved radar visibility of small targets in sea clutter. The Radio and Electronic Engineer.

Croney, J. 1975. Further observations on the detection of small targets in sea clutter. The Radio and Electronic Engineer 45:3.

Cross, F.R. and J.R. Lewis. 1974. CRC radar experiment, Norpoly '73, Phase I (u). CRC Technical Note No. 664, Communications Research Centre, Ottawa.

Currie, B. and S. Haykin. 1984. Iceberg detection using marine radar. Communications Research Laboratory, Faculty of Engineering, McMaster University, Ontario, CRL Report No. 122.

Kerr, D.E., editor. 1951. Propagation of short radio waves. Massachusetts Institute of Technology, Radiation Laboratory Series, 13, McGraw-Hill, New York.

LePage, L.S. and A.L.P. Milwright. 1953. Radar and ice. Journal of the Institute of Navigation, London VI(2).

Nathanson, F.E. 1969. Radar design principles. McGraw-Hill, New York.

North, D.D. 1963. An analysis of the factors which determine signal/noise discrimination in pulsed-carrier systems. Proceedings of the Institute of Technical and Electronic Engineers 7:1016-27.

Oppenheim, A.V. and R.W. Shafer. 1975. Digital signal processing. Prentice-Hall, New Jersey, 585 p.

Petro-Canada Exploration Inc. 1983. Field evaluation of sensors for development of ship-mounted ice hazard detection system. Report for Transport Canada, Ottawa. Report No. TP3506E.

Rotherham, S. 1978. Radiowave range prediction over the sea in evaporation ducting conditions. Report for the Defence Research Group, NATO, Naval Armaments Group, Panel on Physics and Electronics, AC/253 (Panel III) D/160.

Ryan, J. 1983. Iceberg detection capability. Technical Report for the Newfoundland Petroleum Directorate, Government of Newfoundland and Labrador, St. John's, Newfoundland.

Selwyn, D. 1981. Detection of Arctic ice by ground-based radar, spring 1980. Draft of Report for Department of Fisheries and Oceans, Ocean Science and Surveys, Burlington, Ontario.

Sittrop, M. 1977. On the sea - clutter dependency on wind speed. Radar-77, International Conference, London, England, October 25-28, 1977.

Skolnik, M.I. 1970. Radar handbook. McGraw-Hill, New York.

Swerling, P. 1957. Detection of fluctuating pulsed signals in the presence of noise. Institute of Radio Engineers, Transactions on Information Theory.

Williams, P.D.L. 1975. Limitations of radar techniques for the detection of small surface targets in clutter. The Radio and Electronic Engineer 45(8).

Williams, P.D.L. 1979. The detection of ice at sea by radar. The Radio and Electronic Engineer 49(6):275-287.

Williams, P.D.L. 1980. Medium fading of radar targets at sea with special reference to operation at 3 cm and 10 cm. Proceedings of Institute of Electrical and Electronic Engineers 127(F)(3).

Williams, P.D.L. 1981. Results from an experimental dual-band search radar. The Radio and Electronic Engineer 51(11/12):541-552.